# NANOCELLULOSE FROM WASTEWATER SOLIDS

*A biorefinery perspective*

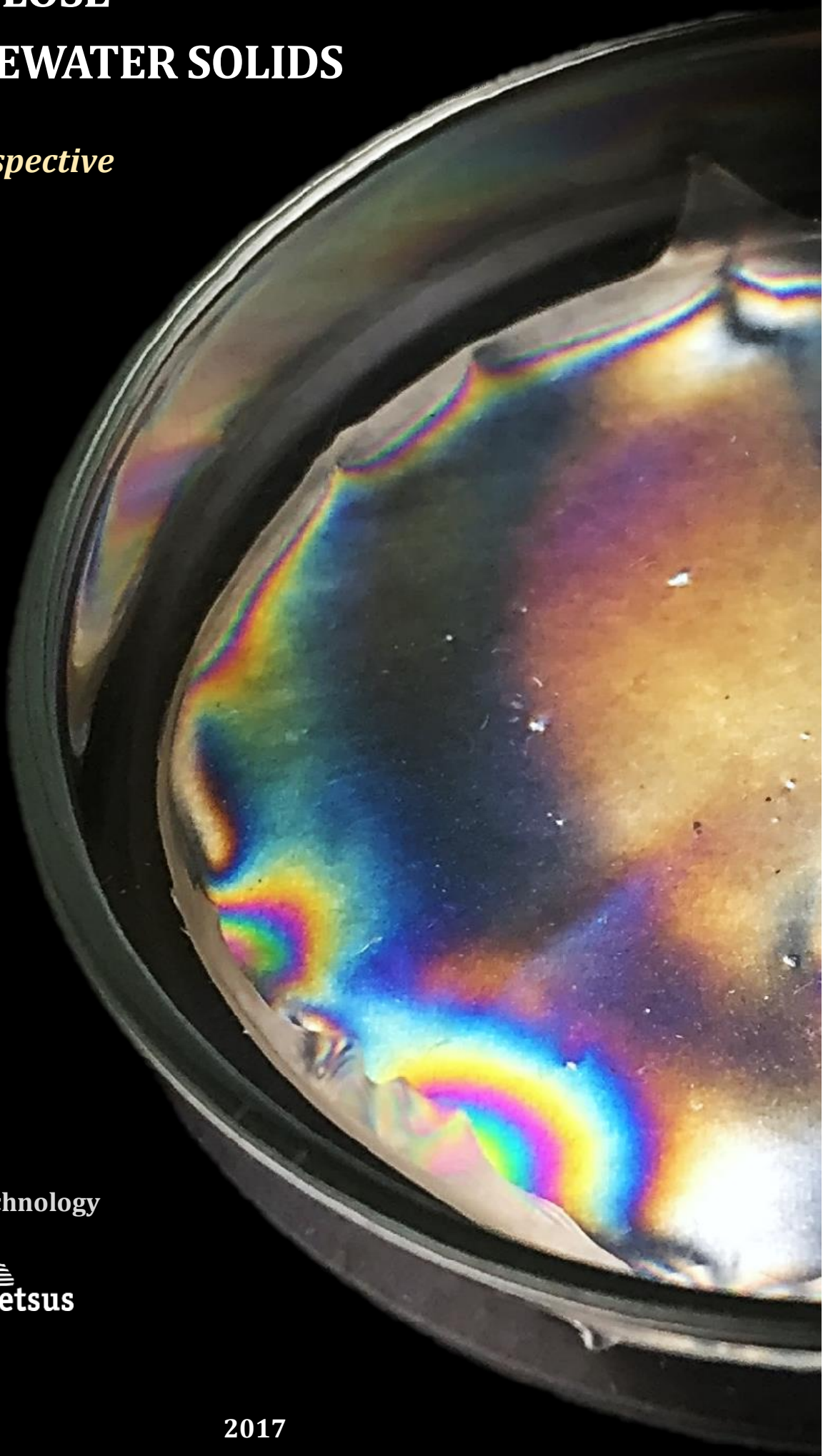

**S. P. Espindola**

**MSc. Thesis**

**Delft University of Technology**

TU Delft wetsus

**2017**

*"In science...*

*we can inspire something...*

*every discovery, however small, is a permanent gain."*

*Pierre Curie to Marie, 1894*

| | |
|---|---|
| **Title** | Nanocellulose from Wastewater Solids: A biorefinery perspective |
| **Author** | Suellen Pereira Espindola |
| **Student number** | 4640306 |
| **Daily Supervisor** | Dr Mario Pronk, Applied Sciences |
| **Chair Assessment Committee** | Prof. Dr Ir. Mark C. M. van Loosdrecht, Applied Sciences |
| **Assessment Committee** | Prof. Dr Stephen J. Picken, Applied Sciences |
| | Ir. Jure Zlopasa, Applied Sciences |
| **Project** | Master of Science Thesis Project (LM3901) |
| **Host University** | Delft University of Technology |
| **Faculty, Specialisation** | Applied Sciences, Life Science and Technology |
| **Defence Date** | Tuesday 25th April 2017, 4:00 PM |
| **Location** | Kronigzaal, Applied Science, van der Maasweg 9, Delft |

**Nanocellulose from Wastewater Solids: A biorefinery perspective**

By

**Suellen Pereira Espindola**

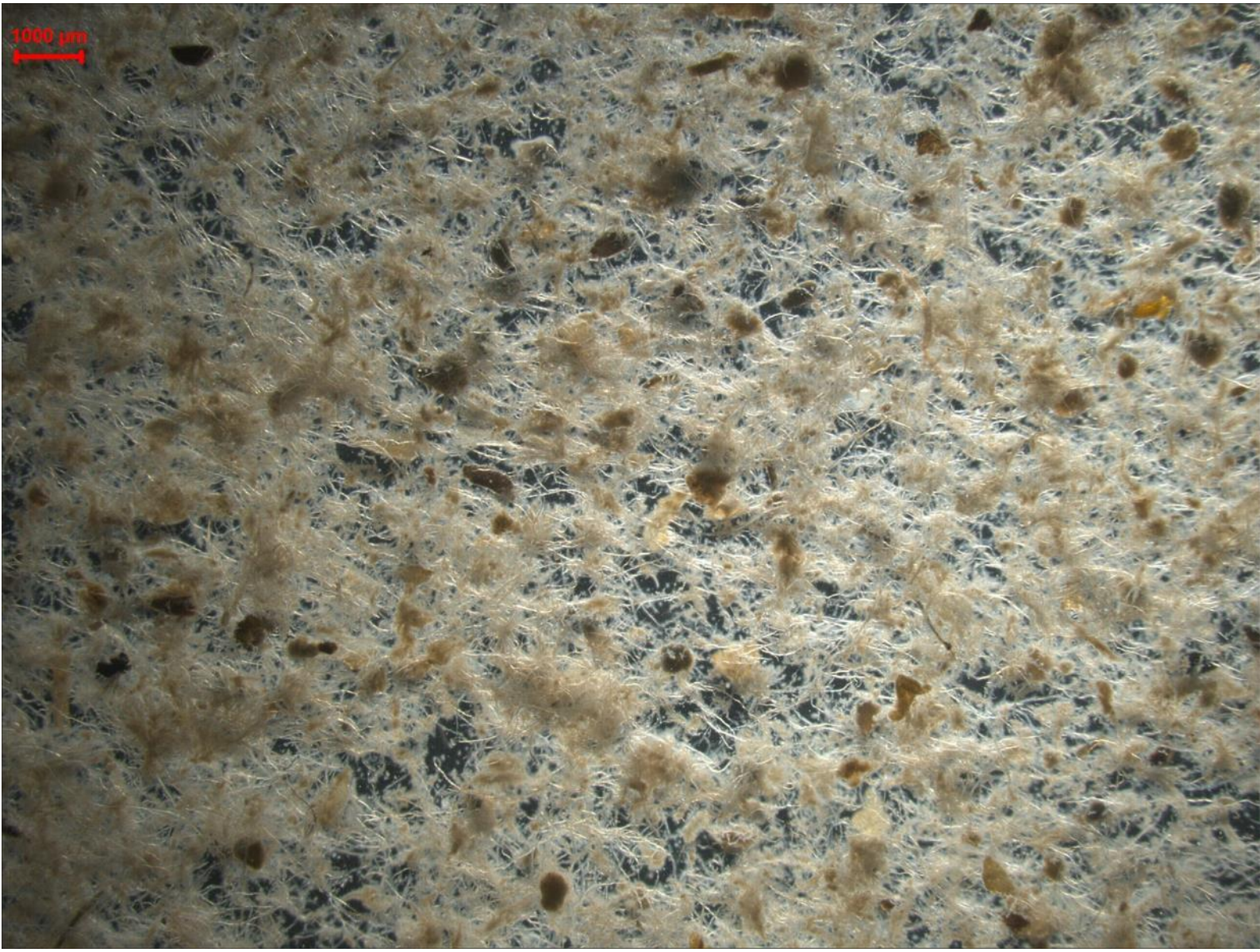


**Solids of sieved and washed Nereda® Excess Sludge**

Utrecht STP

Photo: Mario Pronk, 2016

# SUMMARY

Cellulose is a biopolymer commonly used as a renewable constituent in the production of green materials. Wastewater solids can be an attractive source of cellulose, mainly originating from toilet paper. Cellulosic solids can be recovered (i) through sieving before the sewage treatment - resulting in a Fine Sieve Fraction (FSF), or (ii) after biological treatment in the waste sludge – such as in Nereda® Excess Sludge (NES). Its recovery and valorisation into high-end bio-based products, such as crystalline nanocellulose, could improve the techno-economic feasibility of cellulose recovery from wastewater. A cellulose extraction method from wastewater solids was developed during this project. Reference materials (microcrystalline cellulose and toilet paper) and wastewater-extracted cellulosic pulps were studied for the production of cellulose nanocrystals (CNCs). CNCs were prepared by controlled acid hydrolysis followed by centrifugation, filtration, dialysis, neutralisation and ultrasonication. A detailed protocol for CNCs isolation from toilet paper and wastewater-recovered pulps can be found in the appendix section. CNCs could be extracted at around 30 % yield (g g $pulp^{-1}$). FSF showed to be an attractive source of nanocellulose since the yield per g FSF was 22 %, while for NES it was only 4 %. The wastewater-CNCs presented rod-like morphology with high aspect ratio (10 – 14), crystallinity (62 – 68 %), and chemical structure very similar to commercially available CNCs. However, there is still great extent for improvements since impurities might be still present and the isolation process needs reproducibility and optimization. Bionanocomposites consisting of CNCs (commercial and lab-made) and alginate materials were investigated by measuring the stiffness of freestanding films. A 50 % loading of commercial-CNCs reinforced alginate films by a factor of 1.6 (19 GPa). For the same loading, CNCs isolated from toilet paper and FSF reinforced alginate by a factor of 1.8 and 1.5 (22 – 18 GPa) respectively. Both characterisation results and reinforcement efficiency of CNCs isolated from toilet paper and wastewater-recovered pulps confirm the good quality of this potential product. Furthermore, we have observed changes in the nematic-isotropic phase diagram of CNCs in alginate suspensions. We developed a model hypothesizing that an alginate-shell decorates the CNCs rods increasing its volume fraction and allowing the nematic phase to appear at lower concentrations. The model was highly representative to the experimental data. Lastly, the market relevance of wastewater-CNCs is discussed together with a research outlook.

*Keywords*: Toilet Paper, Wastewater solids, Cellulose NanoCrystals, Alginate, Bionanocomposites.

# TABLE OF CONTENTS

# 1. INTRODUCTION

## 1.1 Wastewater Solids with High Cellulosic Content

Cellulose is the core building block of trees and plants being the most abundant natural biopolymer on Earth. Since thousands of years, men process plants' cellulose in the production of pulp, paper and derivatives. With the adoption of toilet paper in modern societies, cellulose fibres became a major insoluble substrate entering sewage treatment plants (STPs). They now compose 30-50% of the solids in the sewage of western countries (Ghasimi, 2016; STOWA, 2010). A large part of this cellulosic material is recalcitrant to most applied physicochemical and biological technologies. Therefore, the presence of these incoming fibres enhances costs to treatment plants since more chemicals, aeration and post-treatments to dispose of cellulose are required. Although limited research has been conducted on the fate and recovery of cellulose in wastewaters, the topic has lately gained attention within the wastewater authorities (Honda et al., 2002; STOWA, 2016, 2013, 2010).

The recovery of cellulosic material is considered a future trend in wastewater and sludge treatment technologies. Recent reports have shown the feasibility of using fine sieves on influents as a replacement for primary clarifiers, improving the wastewater treatment, and yielding cellulose (Ruiken et al., 2013; STOWA, 2016, 2010). In the last decade, a few sites have adopted this technology, mainly in Europe and North America (Paulsrud et al., 2014; Ruiken et al., 2013; Rusten and Odegaard, 2006). Fine sieving before the biological treatment results in a fibrous mass called Fine Sieve Fraction (FSF), which contains around 70% cellulose (Figure 1) (Ruiken et al., 2013).

Other common wastewater solids are believed to have high cellulose content, such as primary and waste sludge (Honda et al., 2002). That is the case with Nereda® Excess Sludge (NES). Nereda® is a novel aerobic granular sludge technology (AGS) that complies with strict effluent requirements (Pronk et al., 2015). Due to its unique granule design and short cycles, it is hypothesised that - after Nereda® treatment - most of the cellulose fibres input is removed with the excess sludge (Figure 1) (Pronk, 2016). This AGS characteristic could be advantageous for harvesting concentrated cellulose material in the waste sludge after granular settling, and thus, should be investigated.

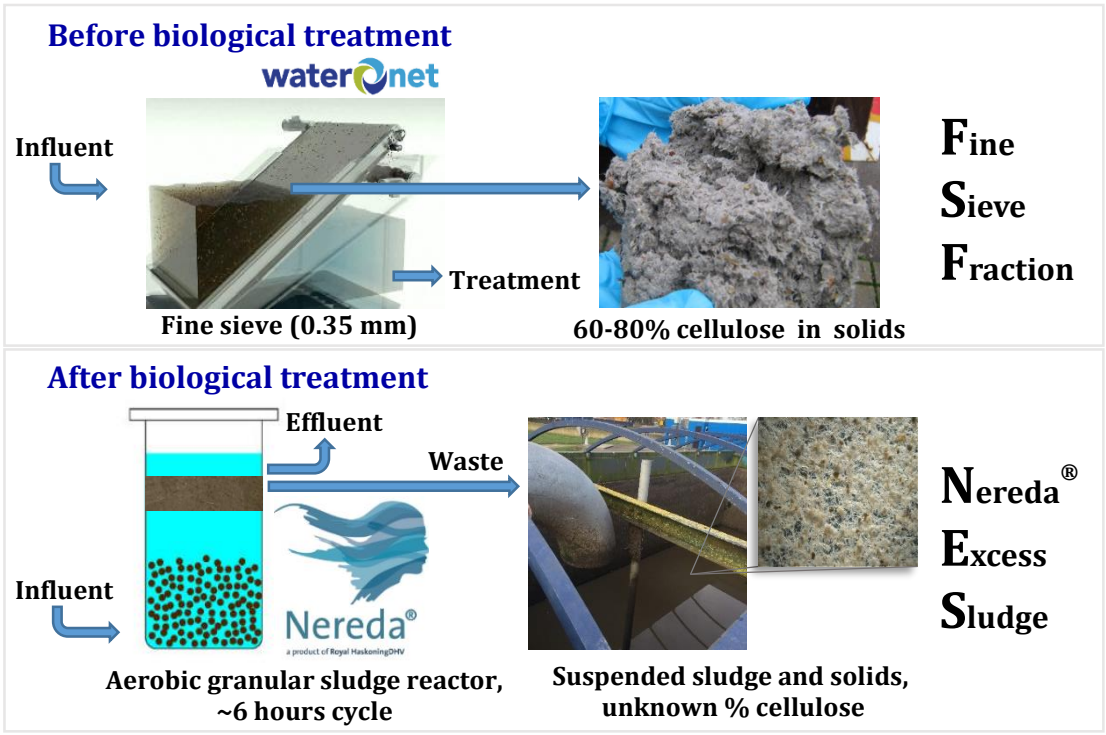


**Figure 1. The generation of cellulosic wastewater solids Fine Sieve Fraction and Nereda® Excess Sludge before and after biological treatment respectively. The top picture shows the fibrous material harvested by the company Waternet, with 20 – 30 % total solids of which around 60 – 80 % is cellulose. The bottom figure indicates that the suspended sludge and solids produced at the end of a Nereda® treatment cycle (~6 hours) are potentially rich in cellulose fibres.**

The production of bio-based materials from sewage and sludge can improve the economy of the wastewater sector (Römgens and Kruizinga, 2013). In the Netherlands solely, around 180,000 tonnes of cellulose per year could be harvested (Holland Trade and Invest, 2016). Cellulose is a well-known renewable constituent in the manufacture of green materials. Therefore, there are many possible valorization routes. Applications can be developed using the fibre itself - in the paper, construction, furniture, textile, and automotive industries; or as a base for producing valuable chemicals, such as bioethanol and bioplastics (Ghasimi, 2016; Ruiken et al., 2013; STOWA, 2016). In theory, cellulose recovered from wastewaters could also be modified into nanocellulose.

## 1.2 Nanocellulose from Wastewater

A microfibril of cellulose is composed of highly ordered cellobiose chains gathered by several strong intermolecular hydrogen bonds. Hence, the cellulose fibre exhibits highly ordered crystalline domains separated by less ordered ones called amorphous regions (Figure 2). Owing to this structure nanoparticles can be extracted from cellulosic pulps (i) mechanically, to produce Cellulose NanoFibres (CNFs) and (ii) chemically, via controlled acid hydrolysis, to produce Cellulose NanoCrystals (CNCs) (García et al., 2016). These nanocelluloses[1] are considered new super-materials due to exceptional strength properties - on a par with Kevlar -, high aspect ratio, low density, low thermal

[1] For a review of the key features of nanocellulose and CNCs, the reader is referred to *Appendix I*.

## Nomenclature

| | |
|---|---|
| **AFM** | Atomic Force Microscopy |
| **AGS** | Aerobic Granular Sludge |
| **ALE** | Alginate-Like Exopolysaccharides |
| **AS** | Activated Sludge |
| **CNCs** | Cellulose NanoCrystals |
| **CNFs** | Cellulose NanoFibers |
| **DMA** | Dynamic Mechanical Analysis |
| **EPS** | Extracellular Polymeric Substances |
| **FP** | Filter Paper |
| **FSF** | Fine Sieve Fraction |
| **FTIR** | Fourier Transform-InfraRed Spectroscopy |
| **I** | Isotropic |
| **LC** | Liquid Crystal |
| **MCC** | MicroCrystalline Cellulose |
| **N** | Nematic |
| **NES** | Nereda® Excess Sludge |
| **RTP** | Recycled pulp Toilet Paper |
| **TS** | Total Solids |
| **TSS** | Total Suspended Solids |
| **STP** | Sewage Treatment Plant |
| **VS** | Volatile Solids |
| **VSS** | Volatile Suspended Solids |
| **XRD** | X-Ray Diffraction |

expansion, uncomplicated surface chemical modification, and low toxicity (Börjesson and Westman, 2015; Koskinen et al., 2013; Lagerwall et al., 2014; Liu et al., 2016). Such properties, together with its renewable and biodegradable intrinsic features, make nanocellulose an ideal reinforcement agent in composites. At the same time, other numerous applications are also listed in the paper, food, biomedical, automotive, and cosmetic industries (Börjesson and Westman, 2015). As new products and patents are being developed, the attention over nanometre-sized cellulose has increased exponentially in the past decade (García et al., 2016).

Nanocellulose as a new bio-based material has got momentum, and its production is now beyond scientific curiosity with growing interest in research and development. Large-scale production is already a reality and there is increasing interest in commercialization (García et al., 2016; Oksman et al., 2011; Reid et al., 2016). During the past decade, the production of cellulose nanoparticles from lignocellulosic biomass, bacterial cellulose, paper and pulp industrial wastes have been extensively published (García et al., 2016; Silvério et al., 2013a). However, to the best of our knowledge, the production of cellulosic nanomaterial from toilet paper or wastewater solids has not been reported. Cellulose from wastewater may be a cleaner source of fibres for CNCs production in comparison with the often-studied agricultural wastes, as several bleaching steps might be avoided. Thus, CNCs are hereby explored as a new bio-based material for the valorisation of wastewater-recovered cellulosic material.

### 1.3 Alginate-Like Exopolysaccharides from Wastewater

Wastewater has great potential in the biobased economy as a source of raw

materials. Not only cellulose but also other valuable resources, such as alginate-like exopolysaccharides (ALE), polyhydroxyalkanoates (bioplastics), phosphates, nitrogen, sulphur, carbon dioxide, algal biomass, energy and clean water can be mined from wastewater streams all over the world. An example of such idea is the wastewater biorefinery concept of the Dutch organisation Energy and Raw Materials Factory (EFGF, www.efgf.nl). The project created by Dutch water authorities benefits the transition into a circular economy by transforming STPs into biorefineries. Currently, 8 STPs were turned into energy factories, and phosphorus recovery occurs in 7 sites.

Among the wastewater-recovered compounds, ALE is exceptionally interesting due to possible high-end applications in different industries (www.efgf.nl/producten/alginaat). ALE can be found in high concentrations in AGS biomass (Giesen et al., 2017; Lin et al., 2015; Van Der Roest et al., 2015). AGS produces polymers with similar characteristics as alginate, a mannyronate and guluronate polysaccharide, often harvested from brown seaweed (Zlopasa et al., 2015). The potential yield of extractable ALE can be as high as 350 mg/gVS granule (Felz et al., 2016; Lin et al., 2010). Furthermore, there are several on-going projects for large-scale extracting and characterising ALE.

CNCs exhibit remarkable reinforcing properties and have been tested with many polymeric matrixes (Kim et al., 2015; Lagerwall et al., 2014; Reddy and Rhim, 2014). Bionanocomposites comprising alginate and CNCs have been shown before, with increasing stiffness by CNCs addition (Markstedt et al., 2015; Ureña-Benavides et al., 2010). Nevertheless, bionanocomposites containing wastewater-derived CNCs or ALE were never investigated. This study investigates the quality of wastewater-CNCs through the production of bionanocomposites from alginate and CNCs materials. In a broad perspective, this serves the purpose of the wastewater biorefinery concept with novel, green, added-value products being developed from wastewater.

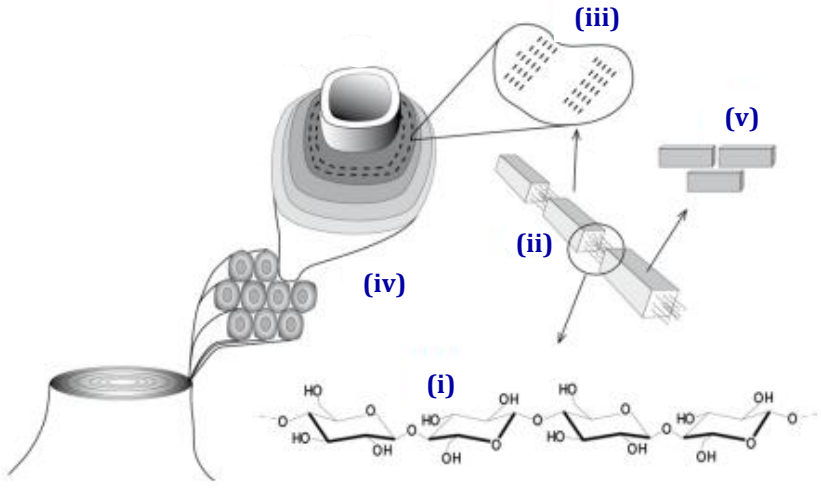


**Figure 2. The various levels of the cellulose structure: (i) molecule, (ii) polymers ordering into microfibrils with crystalline and amorphous regions, (iii) several microfibrils assembled to form a macrofibril, and (iv) cell wall layers. Numbers (ii) and (v) show cellulose microfibrils and cellulose nanocrystals (CNCs), respectively. Figure adapted from Börjesson and Westman (2015).**

# 2. OBJECTIVES

The main goal of this study was to investigate ***the lab-scale production of CNCs from wastewater solids of Dutch treatment plants.***

Additional objectives were to assess the yield and quality of the wastewater-CNCs, discuss the feasibility of producing wastewater-CNCs in the Netherlands, and to manufacture bionanocomposites with CNCs and alginate material. The latter had a two-fold purpose: measuring the stiffness of commercial and lab-made CNCs for a quality comparison and as a conceptual application of wastewater-CNCs.

To meet these objectives, the focus of this thesis is on:

1) Extracting cellulosic pulps from wastewater solids (FSF and NES);
2) Investigating the isolation of CNCs from cellulosic pulps deriving from wastewater;
3) Characterising the main properties of wastewater-CNCs;

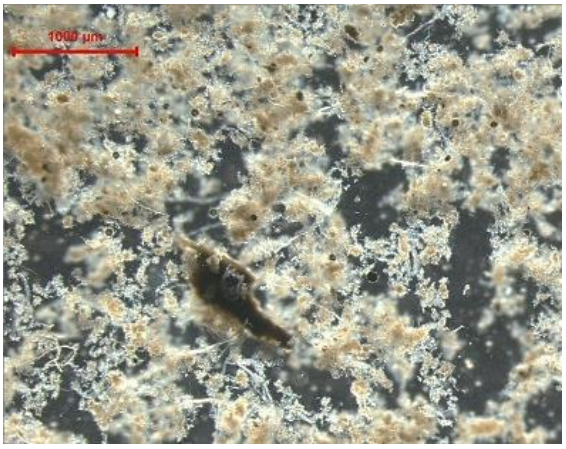


**Figure 3. Microscopic picture of untreated Nereda® Excess Sludge collected at Garmerwolde STP, showing mainly sludge, fibres and other debris (scale bar 1000 µm).**

The approach of this thesis was to:

1) Develop a methodology for extraction of cellulosic materials from wastewater solids (FSF and NES), that could also serve as an estimation of total cellulose in wastewaters. The development can be done by first creating reference samples with known concentrations of cellulose submerged in activated sludge and, after that, testing different extraction protocols for these ideal samples. Finally, the obtained protocol is once again adapted for real FSF and NES samples.

2) Investigate the conditions for CNCs isolation from the resulting cellulosic pulps. First, by applying what is commonly reported for other cellulose sources (such as paper waste, agro-wastes and microcrystalline cellulose) to recycled pulp toilet paper (RTP) as a reference material. After obtaining RTP feasible hydrolysis conditions, an adaptation of these is performed to the studied cellulosic pulps from wastewater.

3) Characterize the dispersity, surface morphology, dimensions, chemical composition and crystallinity of wastewater-CNCs.

4) Test and analyse the mechanical properties of the isolated CNCs through the production of bionanocomposites with CNCs and alginate materials. These bionanocomposites are initially produced with commercially available chemicals. Lastly, novel bionanocomposites are created by mixing commercial CNCs and wastewater-based CNCs with alginate materials.

# 3. MATERIALS & METHODS

## 3.1 Wastewater Sampling

The activities of this MSc thesis were carried out in cooperation with the Dutch companies Royal HaskoningDHV and Waternet who provided samples of wastewater solids.

### *3.1.1 Fine Sieve Fraction*

Screened wastewater (mesh size 6 mm) was finely sieved by a rotating belt filter equipped with a <0.35 mm pore size sieve (Salsnes Filter, Norway) at the STP Blaricum, the Netherlands, operated by Waternet (www.waternet.nl). Plant size was of 30,000 pe and maximum hydraulic capacity 1600 $m^3$ $h^{-1}$. The retained fine sieve fraction (FSF) was collected in December 2016 and stored at 4 °C before analysis. The FSF was composed of mainly toilet paper fibres, some sand, hair, leaves and undefined materials. The solids content of FSF is listed in Table 1. Total solids (TS) and volatile solids (VS) were measured on weight base (g $kg^{-1}$) according to standard methods (APHA/AWWA/WEF, 2012). Further information on fine sieving, FSF and microscopic images of fibres from this material can be found in previous reports (Balkom, 2012; Ghasimi, 2016; Ruiken et al., 2013).

### *3.1.2 Nereda® Excess Sludge*

***Nereda® Garmerwolde STP***: A Nereda® Excess Sludge (NES) sample was collected in November 2016 from the sludge buffer tank (400 $m^3$) where this material is commonly discharged (Figure 3). It was kept at 4 °C until further analysis. The full-scale Nereda® Aerobic Granular Sludge (AGS) installation in Garmerwolde, the Netherlands, is operated by Royal HaskoningDHV (www.royalhaskoningdhv.com) since June 2013 with a hydraulic capacity of 4,200 $m^3$ $h^{-1}$ (Pronk et al., 2015). Wastewater entered the installation, through coarse screens (6 mm) and via the grit removal, in the influent buffer (4,000 $m^3$). Two AGS reactors (height 7.5 m and 9,600 $m^3$ volume each) were operated simultaneously with half a cycle time-difference (Pronk et al. 2015). A dried portion of the NES sample was sent for Van Soest analysis (NDF/ADF/ADL) described in section 3.2.4.

***Prototype Nereda® Utrecht***: Excess sludge was sampled from a buffer tank in January and March 2017 from the AGS Nereda® prototype plant operated by Royal HaskoningDHV in Utrecht, the Netherlands. The AGS treatment was under start-up phase which initiated on 19th December 2016. During the first sampling time, cellulose fibres seemed to be building up in the reactor (Figure 4). The prototype plant had a maximum hydraulic capacity of 125 $m^3h^{-1}$ and volume of 1,000 $m^3$. The reactor was fed with screened (6 mm) municipal wastewater. A conventional activated sludge treatment system was operated in parallel next to the AGS, and the excess sludge was usually transported to the on-site sewer system.

***Nereda® Dinxperlo STP:*** Excess sludge was sampled in March 2017 from the buffer tank of the AGS Nereda® plant operated by Royal HaskoningDHV in Dinxperlo, the Netherlands. This STP has a hydraulic capacity of 129 $m^3h^{-1}$. The Nereda® reactors were fed with screened (3 mm) wastewater.

***Nereda® Vroomshoop STP:*** Excess sludge was sampled in March 2017 from the waste sludge line of the AGS Nereda® plant operated by Royal HaskoningDHV in Vroomshoop, the Netherlands. This STP consists of a hybrid system with a conventional Activated Sludge treatment with a capacity of 2,400 $m^3$ and a Nereda® reactor (1,350 $m^3$). The reactor received 50% of the influent and was fed with screened (3mm) wastewater. NES samples from this installation, Garmwerwolde and Dinxperlo STPs should be more

representative of long-term operating Nereda® treatments.

Each Nereda® reactor was operated in sequencing batch mode, with process cycles of ± 6 hours. Within these hours, one was of anaerobic feeding in upwards plug-flow with simultaneous effluent withdrawal, followed by 15 min of excess sludge discharge (Figure 1), four hours of aeration/reaction, depending on the applied removal targets, and one hour for settling (Giesen et al., 2013). During rainy weather, the cycle was shortened to a 3 hours minimum. More operational details can be found in Pronk et al. 2016. During start-up, biomass concentration in the reactor is increasing over time. Total suspended solids (TSS) and volatile suspended solids (VSS) of regular and concentrated excess sludge samples (by settling and decanting off clear supernatant) were measured on weight/volume base (g $L^{-1}$) according to standard methods (APHA/AWWA/WEF, 2012) (Table 1). Except for NES from Vroomshoop STP, which came directly from the waste sludge line, the used excess sludge was mainly a mixture of (i) unsettling solids that remain on top of the reactor after the aeration phase and (ii) eventual granular sludge that is periodically removed to achieve the targeted biological phosphorus removal.

**Table 1. Characterization of the wastewater solids (FSF, NES) used in this study in comparison with available literature when applicable.**

| Sample | Components | Unit | This study | Literature | Reference |
|---|---|---|---|---|---|
| **FSF** | Total solids | g $kg^{-1}$ | 162 ± 8 | 100-250 | Ghasimi et al., (2015) |
| | Volatile solids | g $kg^{-1}$ | 150 ± 9 | 90-225 | |
| | VS/TS ratio | % | 93 ± 1 | ~90 | |
| **NES Garmerwolde** | Total suspended solids | g $L^{-1}$ | 2.0 ± 0.2 | - | - |
| | Volatile suspended solids | g $L^{-1}$ | 1.4 ± 0.0 | - | |
| | VSS/TSS ratio | % | 70 ± 0.1 | - | |
| **Concentrated NES Utrecht*** | Total suspended solids | g $L^{-1}$ | 13.0 ± 0.2 | - | - |
| | Volatile suspended solids | g $L^{-1}$ | 11.7 ± 0.4 | - | |
| | VSS/TSS ratio | % | 91 ± 2 | - | |
| **Concentrated NES Utrecht**** | Total suspended solids | g $L^{-1}$ | 14.0 ± 0.1 | - | - |
| | Volatile suspended solids | g $L^{-1}$ | 12.5 ± 0.3 | - | |
| | VSS/TSS ratio | % | 86 ± 1 | - | |
| **Concentrated NES Dinxperlo** | Total suspended solids | g $L^{-1}$ | 5.8 ± 0.3 | - | - |
| | Volatile suspended solids | g $L^{-1}$ | 4.6 ± 0.2 | - | |
| | VSS/TSS ratio | % | 79 ± 2 | - | |
| **NES Vroomshoop** | Total suspended solids | g $L^{-1}$ | 1.5 ± 0.1 | - | - |
| | Volatile suspended solids | g $L^{-1}$ | 1.2 ± 0.1 | - | |
| | VSS/TSS ratio | % | 81 ± 1 | - | |

*: Sample from January 2017; **: Sample from March 2017.

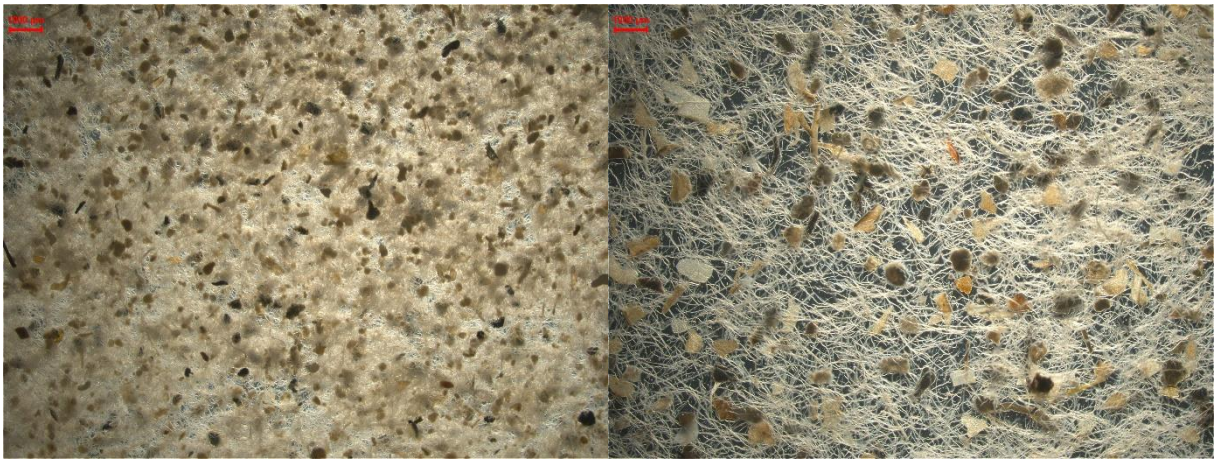

**Figure 4. Sieved and water-washed Nereda® Excess Sludge obtained from Utrecht STP during the start-up phase. (A) shows material retained on a sieve of 0.2 mm, and (B) of 0.4 mm (scale bar: 1000 µm).**

### *3.1.3 Activated Sludge and Nereda® Aerobic Granular Sludge*

The activated sludge (AS) used in this study was collected in December 2016 in the return waste sludge line from a full-scale domestic wastewater treatment plant in Harnaschpolder, The Netherlands. TSS was 4.7 ± 0.1 g $L^{-1}$ and VSS was 4.0 ± 0.1 g $L^{-1}$. In addition, the Nereda® AGS used was collected at the end of an aerobic cycle in March 2016 from the STP in Utrecht. The granular sludge had a TS of 89.2 ± 1.9 g $L^{-1}$ and VS of 79.9 ± 1.8 g $L^{-1}$. AGS had a sludge volume index (SVI) of 59.5 mL g $VSS^{-1}$ and was stored under -20 °C until further use.

## 3.2 Cellulosic Pulp Extraction

Several attempts have been made to extract and measure cellulose fibres from wastewater solids during this thesis. The report will present only the most interesting findings. A protocol was developed based on blending treatment(s) in combination with removal of water-, alkaline-soluble compounds, and a final bleaching treatment. The protocol is described in detail in *Appendix II*.

### *3.2.1 Extraction Scheme*

A scheme illustrates the complete standard cellulose extraction procedure (Figure 5). Briefly, the sample was dried, cut into small pieces and blended with demi water until forming a homogeneous fibrous suspension. This suspension was heated on a hot plate to 50 °C while stirring for removing water-soluble compounds. Next, the residue of filtration was placed in a beaker with an alkaline solution and heated to 80 °C. The mixture was filtrated and washed thoroughly with demi water for removing alkaline-extracted compounds. This alkaline step was performed at least twice. Finally, the remaining residue was bleached with a sodium chlorite ($NaClO_2$) solution in slightly acidic buffer. After a final filtration and washing step until obtaining pH neutral, the resultant pulp was dried at 60 °C, and the cellulose yield could be calculated based on the initial solids content of the sample (initial grammes or TS, TSS values). All reagents were of analytical grade and used without further processing.

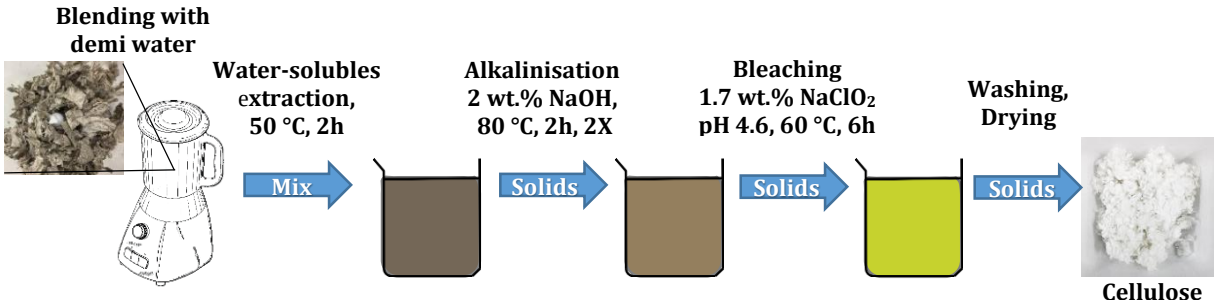


**Figure 5. Standard scheme with protocol steps for cellulose extraction from wastewater solids. Pictures at first and last steps show, respectively, dried recycled pulp toilet paper that was submerged in activated sludge and cellulose extracted from this recycled pulp toilet paper.**

### *3.2.2 Alkaline Treatment Tests*

To validate the above-described method (3.2.1), reference samples were first created. These were composed of around 10 g Whatman® filter paper (FP) or recycled pulp toilet paper (RTP, brand CWS, obtained at TU Delft bathrooms) submerged in 500 mL of activated sludge at room temperature (RT) for at least four days. The samples were tested using a 2 wt.% or 0.5 M sodium hydroxide (NaOH) solution in the alkalization step. Later, FSF samples collected at Blaricum STP were also tested using the same NaOH treatment. Cellulose fibres present in the AS source were first neglected.

Furthermore, two types of alkaline treatments were tested for NES due to its expected high sludge and extracellular polymeric substances (EPS) content when compared to FSF. One test using NaOH and another with concentrated urea (8 M).

### *3.2.3 Bleaching Tests*

Bleaching steps were performed by using a bleaching solution composed of equal parts of 1.7 wt.% $NaClO_2$ and acetate buffer (27 g NaOH and 75 mL glacial acetic acid in 1 L, pH 4.6). The minimum reaction time for each bleaching step was around 6-7 hours (often overnight) in a heating environment of 60-70 °C. More than one bleaching step was sometimes tested to ensure the samples were free of pigments and lignin-like compounds. Tests with sodium hypochlorite (NaClO) were also performed but not included due to relatively low efficiency (more extraction steps required) when compared to $NaClO_2$.

### *3.2.4 Van Soest Analysis (NDF, ADF, ADL)*

The method of Van Soest and Wine (1967), initially developed for estimating dietary fibre fractions, was used to obtain the fractions of lignin, hemicellulose and cellulose of samples. The method is based on the combined activity of detergents (in neutral and acidic extraction conditions). With the assay, three fibre residues were obtained: neutral detergent fibre (NDF), acid detergent fibre (ADF) and acid detergent lignin (ADL), from which it is possible to evaluate the lignins (ADL), celluloses (ADF–ADL) and hemicelluloses (NDF–ADF). The technique was applied on the final cellulosic pulps extracted from both FSF and NES (NaOH was used) to check for the validity of the extraction method.

## 3.3 Cellulose NanoCrystals Isolation

### *3.3.1 Materials*

Sulphuric acid 95 – 98 % was obtained from Sigma-Aldrich. For dialysis, cellulose acetate bags with 3,500 Da molecular weight cut off (MWCO) were purchased. Avicel PH101 Eur. microcrystalline cellulose (MCC) was purchased from Sigma-Aldrich. RTP (brand CWS, obtained at TU Delft bathrooms) was

first cleaned by the cellulosic pulp extraction method (sections 3.2.1 and 3.2.2).

A commercial CNCs sample was obtained via donation from a current industrial producer of sulphuric acid-extracted CNCs: CelluForce™ (Montreal, Canada). Afterwards, this product was compared to CNCs produced in our laboratory. CelluForce, the world's largest producer of CNCs with a 1 tonne day$^{-1}$ capacity, uses traditional 64 wt.% sulphuric acid hydrolysis to produce CNCs from bleached Kraft pulp (www.celluforce.com). Following hydrolysis, CNCs are commonly diluted, separated from residual acid, neutralised to sodium form and spray dried.

All chemicals were of analytical grade and used as received.

### *3.3.2 Isolation Scheme*

The CNCs isolation was tested via controlled acid hydrolysis with sulphuric acid (60 – 64 wt.% $H_2SO_4$) at 45 °C. Following hydrolysis, quenching, centrifugation and washing with water, glass fibre vacuum filtration, neutralisation with NaOH, dialysis (at least 4 days) and ultrasonication steps were performed (Figure 6). The specific method used varied per cellulose source and is described in detail in *Appendix III*. The yield of isolated CNCs from the treated cellulose sources was determined gravimetrically by freeze-drying the resultant precipitate after ultrasonication.

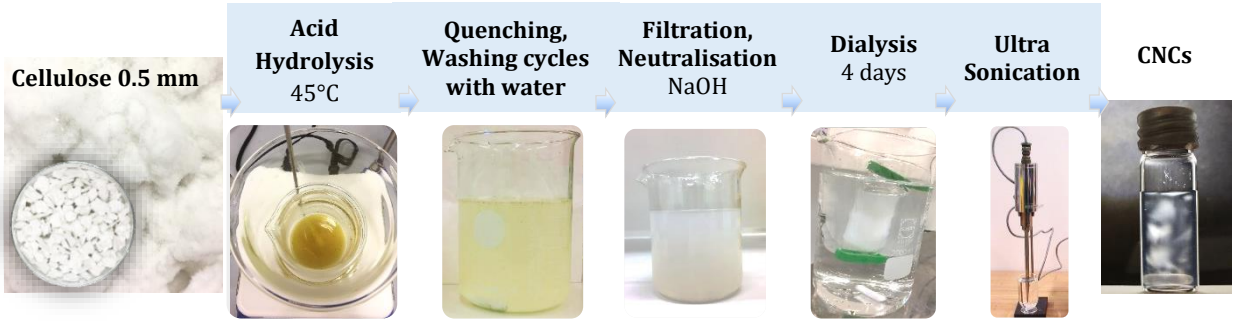


**Figure 6. Standard scheme of used protocol for CNCs isolation from cellulosic pulps.**

### *3.3.3 Cellulose Sources*

Several cellulose sources were tested for CNCs isolation. As reference materials, MCC and RTP were used first to obtain a baseline method. Then, FSF and NES pulps were used for CNCs production with this method as an initial reference.

The RTP, FSF, NES pulps were milled (mesh 0.5 mm, Fritsch mill D-55743, Germany) before hydrolysis to guarantee a homogenous fibre digestion. Further, key hydrolysis parameters were tested, such as acid to cellulose ratio, acid addition, temperature and time of reaction. Moreover, different conditions of centrifugation and washing steps, filtration and neutralisation were applied.

## 3.4 Cellulose NanoCrystals Characterization

### *3.4.1 Visual Observations: Birefringence and Opalescence*

Well-known optical properties of CNCs suspensions were used to detect for a significant presence of nanoparticles (Figure 6, last image). To assess wheter there was self-assembly of nanocrystals in suspension and dried films, the samples were observed between cross polarizers with a background source of light. For suspensions, this was done after shaking and standing for 5-10' to check for birefringent behaviour (double refraction of light manifested by orientation-

dependent differences in refractive index)[2]. The presence of this refractive property under shear indicated a biphasic behaviour with both isotropic (properties same in all directions) and nematic liquid crystal phases of CNCs. Upon displaying standing birefringence, the samples were considered in fully chiral nematic regime (N* critical concentration was achieved) (Habibi et al., 2010). Furthermore, due to anisotropy (properties different when measured along different axes); the presence of haziness or opalescence in samples was also used as a form of identification of an N* phase.

### *3.4.2 Polarized Optical Microscopy*

The self-assembly property of the commercial CNCs in suspension was also observed by polarised optical microscopy. A drop was placed on a glass surface to check for the appearance of fingerprint patterns as the dilute suspension dried.

### *3.4.3 Atomic Force Microscopy*

Atomic force microscopy (AFM) was performed to determine the morphology and dimensions of the isolated CNCs by using an Ntrega Prima NT-MDT scanning probe microscope (Moscow, Russia). Before the observations, a few drops of diluted aqueous suspension (mildly ultrasonicated) were placed on a Si wafer and allowed to dry for 20' at RT. The samples were scanned in tapping mode, using ETALON probes, at RT. The length and width of CNCs were measured using Nova Px software by manually obtaining the values from at least three different pictures from which 20 measurement values were averaged.

### *3.4.4 Fourier Transform-InfraRed Spectroscopy*

The surface chemistry and structural properties of CNCs were analysed by Fourier Transform-InfraRed spectroscopy (FTIR) spectra. A FTIR spectrometer (Nicolet 6700 from Thermo Fisher Inc., USA) was used from 400 to 4000 $cm^{-1}$ at a resolution of 2 $cm^{-1}$. To obtain the spectra, the samples were ground and mixed with KBr at a ratio of 1:100 (w/w) and pressed into thin pellets before analysis. The acquired spectra was an average of 32 scans.

### *3.4.5 X-ray Diffraction*

XRD measurements, to obtain the degree of crystallinity, were performed on cellulose sources and freeze-dried CNCs samples (commercial and isolated in laboratory). The XRD measurements were done with Bruker D8 Advance diffractometer in Bragg-Brentano geometry (λ = 1.78897 Å), with lynxeye position sensitive detector. A cobalt tube with iron filter scattered from 5° to 55° while the sample was spinning, using step size 0.05° and counting time 0.8 s per step. Si wafer blanks were subtracted from all sample measurements.

It is emphasised that a comparison between samples and laboratories is extremely challenging. As such, the crystallinity values presented here should be taken as relative (and comparable within this study), not absolute.

The crystallinity index (CrI) was determined empirically according to the following equation:

$$CrI(\%) = (I_{200} - I_{am})/I_{200} \times 100 \quad (1)$$

Where $I_{200}$ is referred to the maximum intensity of the 200 lattice diffraction peak at region around 2θ = 26.1° and $I_{am}$ is the intensity of diffraction for the amorphous part at around 2θ = 21.0° (Segal et al., 1959). The angle values were translated from Cu Kα values to Co-equivalent by using Bragg's

[2] A short definition of useful terms related to liquid crystals is present in *Appendix I*.

equation and d-spacing values for native cellulose (Poletto et al., 2014).

## 3.5 Bionanocomposites

Bionanocomposites with CNCs and alginate material were made to assess the quality of the isolated CNCs, specially from toilet paper or wastewater. The quality can be assessed by comparing the stiffness of lab-made and commercial material (the modulus of an alginate composite can be subtracted).

Bionanocomposites were prepared by testing different ratios of a 2% w/v stock suspension of CNCs and 2% w/v stock solution of alginate. The density of both materials was assumed as 1.5 g $cm^{-3}$. Both commercial and lab-made materials were used for making the materials (commercial CelluForce™ CNCs, lab-made CNCs (MCC, RTP, FSF), section 3.3; Sodium Alginate from Sigma-Aldrich; Alginate-like exopolysaccharides from Nereda® granules, section 3.5.4).

### *3.5.1 Commercial Cellulose NanoCrystals and Alginate*

Thin films (around 85 µm) of commercial CNCs (CelluForce™) and sodium alginate (Mannuronate/guluronate = 1.56, $M_w$ = 150 kg $mol^{-1}$, Sigma-Aldrich) were prepared in different ratios (20, 50, 80 % v/v final CNCs content). Reference material films were also made by drying dispersions of only commercial CNCs or sodium alginate. All mixtures were ultrasonicated for 5' on ice to avoid overheating (Brandson ultrasonicator, 40 % duty cycle, microtip limit 3) prior and after mixing. No remaining agglomerates were visible. The resulting dispersions were ambient-dried (20°C, 50 % RH) in Petri dishes of 6 cm for around two weeks. Freestanding films were obtained by peeling the film off a Petri dish. The storage modulus of the resulting bionanocomposites was assessed by Dynamic Mechanical Analysis (DMA) using vacuum-dried (40 °C) rectangular samples (around 0.25mm × 10mm × 85 µm) that were cut from the films (PerkinElmer Pyris Series DSC7, USA). Testing was done for 2 minutes in the frequency sweep mode using tensile clamps. Frequency and strain amplitude were kept at 1 Hz and 2 mm respectively. The applied static force was always 20 % higher than dynamic (linear elastic-viscous regime). The storage modulus was averaged from at least 3 samples from the same composite.

The estimated theoretical storage modulus ($E'_{theo}$) of these bionanocomposites was also estimated since the modulus of raw materials is can be easily obtained. Its dependency to the volume fraction of CNCs was determined according to the rule of mixtures equation for fibre-reinforced composites (Krenchel, 1964):

$$E'_{theo}\,(GPa) = (K\,\Phi_{CNCs}\;E'_{CNCs}) + (1 - \Phi_{CNCs})E'_{Alg} \qquad (2)$$

where $E'_{theo}$ is the theoretical storage modulus; K is the efficiency factor for UD (unidirectional) or completely aligned (=1), 2D random or isotropic (=3/8) or 3D random or isotropic (=1/5) distribution of nanofibres; E′ is the storage modulus of CNCs or Alginate; and $\Phi_{CNCs}$ is the volume fraction of CNCs in v/v.

### *3.5.2 Phase diagram of Cellulose NanoCrystals-Alginate Suspensions*

Based on detecting higher opalescence and birefringence (cross-polarized visualisation) of CNCs-Alginate suspensions, the critical concentrations for a nematic phase formation could also be determined. For that, dispersions with different final concentrations of commercial CNCs (0.01 – 5 % w/v) and sodium alginate (0.5 – 2 % w/v) were investigated after placing the suspensions in closed round glass vials of d = 1.2 cm. A phase diagram of CNCs-Alginate concentrations showing boundary

conditions of nematic, biphasic and isotropic phases was constructed.

### *3.5.3 Scanning Electron Microscopy*

The cross section of the alginate materials – CNCs (commercial) bionanocomposite films was also characterised by scanning electron microscopy (SEM). Images were obtained by a JEOL model JSM-6010LA equipment. The analysis of uncoated samples was performed in high vacuum mode with an accelerating voltage of 5 kV.

### *3.5.4 Alginate-Like Exopolysaccharides Extraction*

Alginate-like exopolysaccharides (ALE) were extracted from aerobic granular sludge collected at Utrecht STP using the high temperature – sodium carbonate extraction according to Felz et al. (2016). The hydrogel formation of the extracted ALE was verified by observing the formation of beads when adding small droplets of the extract to copious amounts of cold acetone. The yield of ALE was calculated in relation to the initial amount of gVS granules used for extraction.

### *3.5.5 Lab-made Cellulose NanoCrystals and Alginate-Like Exopolysaccharides*

Bionanocomposites were also made with the extracted reference CNCs or toilet paper-based CNCs (MCC, RTP, FSF) or ALE and in combination with equivalent commercial compounds. In this sense, thin films of commercial CNCs (0, 20 and 50 % v/v) with ALE and lab-made CNCs with sodium alginate (50 % CNCs v/v) were obtained. The storage modulus of these films was also measured by DMA (section 3.5.1).

**Fine Sieve Fraction cellulosic pulp**

# 4. RESULTS

## 4.1 Wastewater Solids Characterization

### *4.1.1 Fine Sieve Fraction*

FSF from Blaricum STP showed a high VS/TS ratio (~90), in agreement with the literature (Ghasimi, 2016). The sample was solid but quite moist, with TS of around 16 %. It contained mainly greyish fibres, which resembled papier-mâché (Figure 7A), some large coarse debris, small pieces of plastics, and remains of vegetable skins, seeds, and hairs, among others.

### *4.1.2 Nereda® Excess Sludge*

The Nereda® waste sludge collected from several STPs in the Netherlands was dark brownish in colour with apparent high sludge content (Figure 7B and C). Furthermore, in most cases, some fibrous material could be visualised with the naked eye. Granules were absent in these samples; on the other hand, it also contained seeds, sandy material, small pieces of plastics, among other debris. TSS of NES samples varied between 1.5 to 14 g $L^{-1}$ for regular and concentrated samples respectively. The samples from NES Utrecht showed higher solids content when compared to the other concentrated samples (Table 1) and apparent higher fibre content under microscopy (Figures 3, 4 and 7C). The VSS/TSS ratio of NES ranged from 70 to 91.

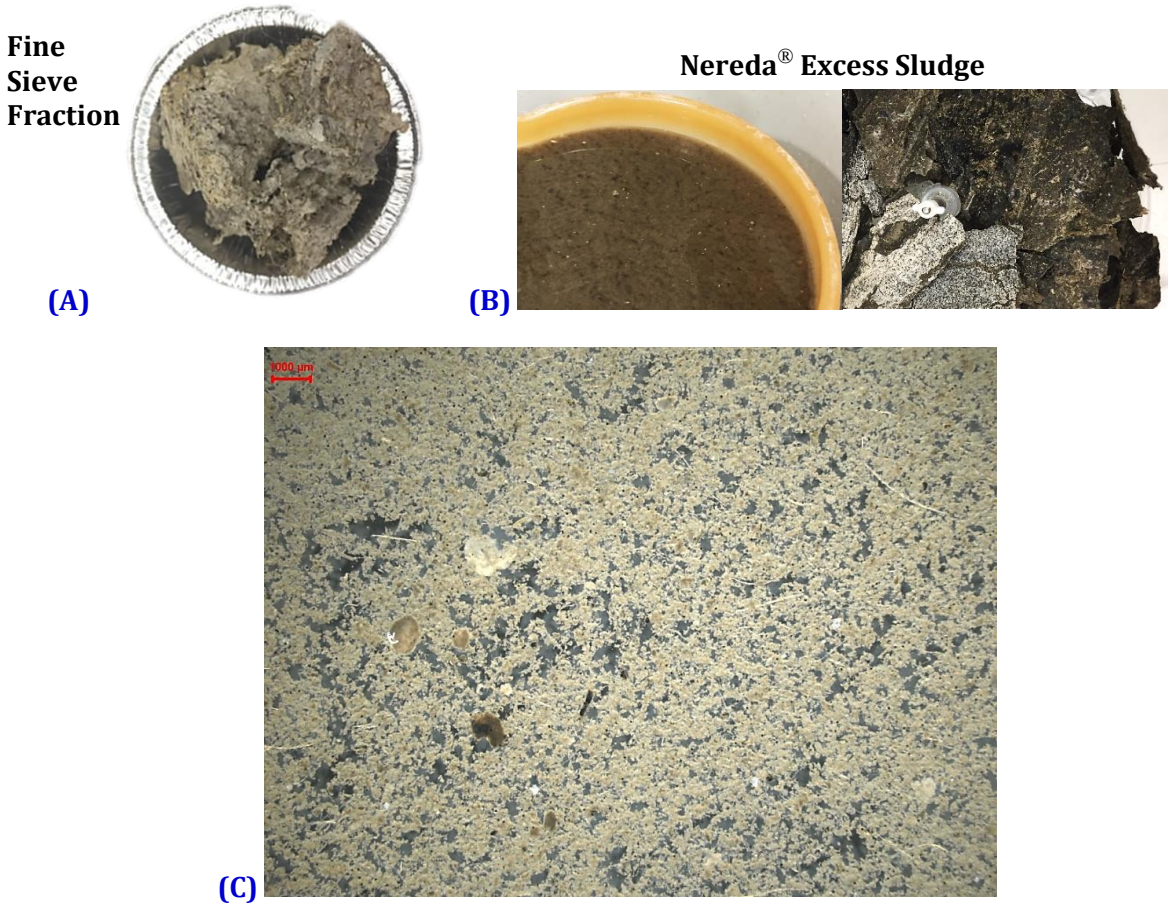


**Figure 7. Dry FSF sample (A); Top view of wet and dry NES sample from Utrecht STP (B); Microscopic picture of NES Garmerwolde STP, scale bar is 1000 µm (C).**

## 4.2 Cellulosic Pulp Extraction

### *4.2.1 Extraction of Reference Materials in Activated Sludge*

To test the proposed method for cellulose extraction, samples with reference materials were composed by submerging FP or RTP in activated sludge for at least four days (Figure 8). After this period, the paper pieces seemed to be disintegrating in the suspension and had acquired a dark colour. The standard extraction procedure with two NaOH extraction steps and one bleaching step (Figure 5) was sufficient to remove the activated sludge added and to obtain pulps with no apparent colour and resembling cellulose in the original material. Following the extraction, FP, which is almost pure cellulose (>95 % α-cellulose), could be almost entirely recovered from the sludge media (Table 2). Furthermore, RTP, here considered as main cellulose source in wastewater solids, was almost fully recovered from the sludge mixture (around 80 % according to Van Soest method, Table 3). The added AS was first neglected but might have contributed to only 1 % of the cellulose in this experiment (addition of 0.5 L of AS from Harnaschpolder STP, Table 2).

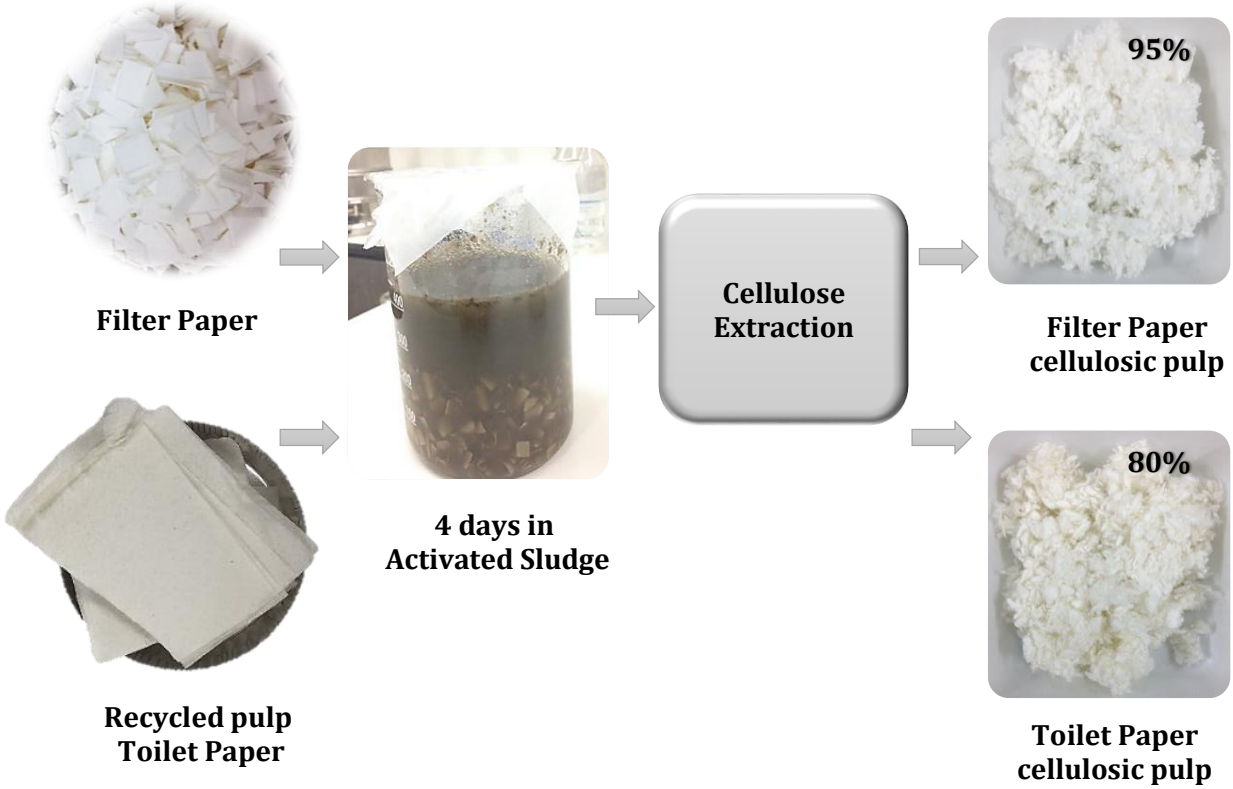


**Figure 8. Reference samples of cellulose sources (FP (~95 % cellulose) and RTP (~80 % cellulose), left): in activated sludge (middle) and final pulps after the tested extraction method (right). Fibres present in the added activated sludge were initially neglected.**

### *4.2.2 Alkaline treatment tests*

**Fine Sieve Fraction**

Before the alkaline extraction with NaOH, FSF samples were extracted with demi water under heating. During this extraction, several water-soluble impurities were already removed. A layer of scum could be observed on the top of the beaker after the 2 hours heating period. The resulting light brown filtrate was very turbid. For FSF extractions, two alkaline treatments with NaOH 2 wt.% were considered sufficient to remove most sludge, EPS, and some pigments (lignin-like compounds), resulting in a red-brownish filtrate (Figure 9A and B). The blending step was sometimes performed twice, with demi-water and after the first alkaline extraction, due to the presence of large debris. These materials could be distinguished from the cellulosic matrix during all the steps of extraction, and most became darker already with the alkaline treatment step.

**Nereda® Excess Sludge**

Alkaline treatments were crucial in the cellulose extraction from NES due to high sludge and EPS content of the source. Without these steps, the samples would always cause clogging, even in wider 350 µm sieves. After a first alkaline treatment with 2 wt.% NaOH, the samples were still viscous, and fibres presented a dark-brownish aspect (Figure 9A). This was solved with more successive alkaline treatments - two times or more depending on wastewater solids characteristics - or even treatments with increased NaOH concentration (4 – 8 wt.%). After three consecutive alkaline treatments with NaOH, the resulting pulp was similar to the one obtained from FSF, presenting a much-diluted red-brownish colour (Figure 9A).

As an alternative, a less harsh alkaline treatment with urea was also tested. Highly concentrated urea (8 M) was used for achieving chemical denaturation of proteins, and thus, partially dissolving sludge and EPS attached to the cellulose fibres from NES. The pH of the alkaline filtrate was around 9, what could promote the solubilisation of EPS of higher molecular weight in comparison with high pH of 13 in NaOH steps. Indeed, comparing the filtrates of NES extraction after NaOH and urea extractions, it can be observed that a significant amount of polymers might have precipitated in cold acetone using the same NES source (Figure 9B). The resultant pulp after the concentrated urea alkalinisation and bleaching can be seen in Figure 9C. Unfortunately, the final pulp was very grey in aspect, and this colouration did not fade even after successive bleaching steps. While with NaOH treatments, a gradual decolouration of the sample with the alkaline treatment occurs, leaving mainly cellulosic fibres, which can be identified by its snowy-white aspect.

### *4.2.3 Bleaching treatment tests*

The number of bleaching steps varied per wastewater solid investigated.

**Fine Sieve Fraction**

For fibrous material that has been in contact with wastewater/sludge for a low time, such as the reference samples and FSF, one bleaching step was sufficient to extract cellulose. The resulting fibres were very white with minor impurities, often darkened, depending on the source (Figures 8 and 9A).

**Nereda® Excess Sludge**

The bleaching step for NES also varied within the samples collected. For samples of NES from Utrecht STP, one bleaching step was sufficient after modifying the extraction method (Figure 9A). While for NES collected in Dinxperlo and Vroomshoop STPs, one and two extra bleaching steps were required respectively.

For waste sludges, including AS, the starting point of the bleaching step was crucial. Samples that were bleached when the pulp was still too dark (colour from sludge material and pigments) have acquired a light red-brownish colour (Figure 9D) that was impossible to remove with a few bleaching steps. To tackle this issue, the extraction was re-started with additional alkaline and bleaching steps until higher purity was reached.

From pictures 9D and E, it can be observed that, depending on the wastewater source, much other inert debris can be present and interfere in the measuring and extracting of cellulose. In addition, milling at 0.5 mm mesh size has shown to be a good alternative to further purify the extracted pulp, thus, releasing impurities attached to the cellulosic matrix to some extent.

After testing ideal alkaline and bleaching conditions required to obtain snowy-white pulps from wastewater and sludge sources, protocols could be defined for FSF and NES (*Appendix II*). With the standardisation of methods, the cellulosic content of the wastewater samples could be determined, which can be found in Table 2. Values for other reference cellulose sources, such as toilet paper, are also shown.

FSF cellulose content was high, around 65 % g g $TS^{-1}$. NES cellulose values varied from 4 to 15 % g g $TSS^{-1}$, or the same as 0.06 to 2 g L $NES^{-1}$, depending on sampling and location (STP).

### *4.2.4 Van Soest Analysis*

The method of Van Soest and Wine (1967), initially developed for estimating dietary fibre fractions, was applied to the extracted FSF and NES pulps. The technique fractionates lignocellulosic material into cellulose, hemicellulose and lignin. Both extracted pulps showed a high cellulosic content (above 86 %), and low hemicellulose and lignin values (Table 3).

In addition, it can be observed that a similar cellulose content, around 80 %, is obtained for the reference source toilet paper from both the developed and Van Soest methods (Tables 2 and 3).

Also from Table 3, it can be observed that, according to the Van Soest method, the cellulose content of the NES Garmerwolde sample is low, of only 4.7 % or 0.94 g $L^{-1}$. This low value is similar to what was obtained for AS samples, varying from 4 to 11 % cellulose (Reijken C., personal communication, 2017). Furthermore, the hemicellulose content of both waste sludges (AS and NES) was high (15 – 21 %) in comparison to cellulose percentages.

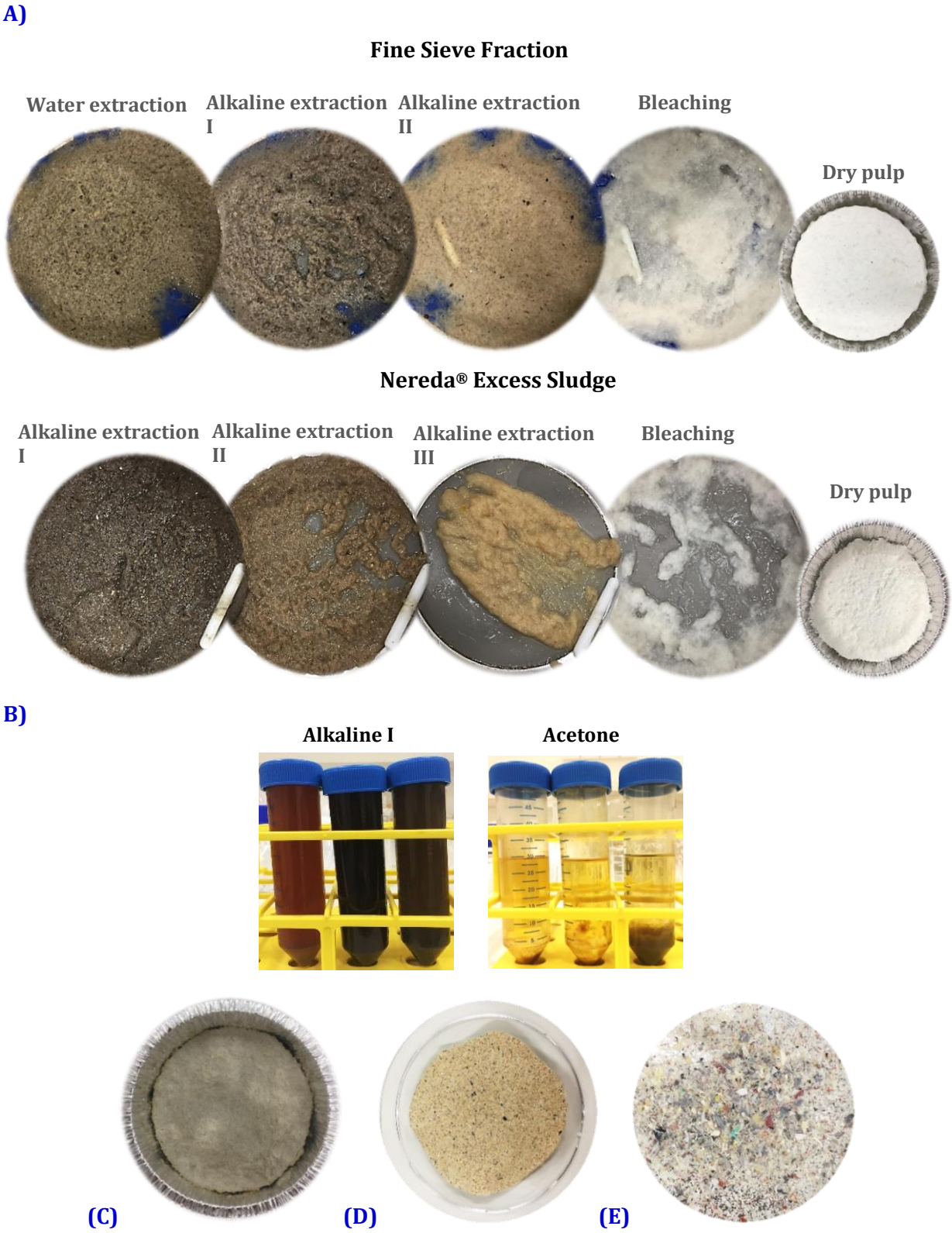


**Figure 9. (A) FSF (top) and NES (bottom) residues collected on sieve after each cellulose extraction step and dry pulp obtained at the end of the procedure. (B) Left: Filtrates of the first alkaline heating extractions for FSF, NES (NaOH) and NES (Urea), Right: Aliquots of the same filtrates diluted in copious amounts of cold acetone. (C) NES pulp after alkaline (Urea 8M) and bleaching steps. (D) NES Dinxperlo pulp resultant from incomplete alkaline and bleaching steps (pigments and coarse material are still present). (E) Inert impurities from NES samples that remain after the extraction treatment.**

**Table 2. The yield of cellulosic pulp after extraction for toilet paper, reference materials (FP, RTP) and wastewater solids from different STPs (FSF, NES).**

| Sample | Cellulosic pulp % (g 100g$^{-1}$) | Cellulose concentration | Literature (Cellulose %) | Reference |
|---|---|---|---|---|
| **Toilet Paper (brand Tork)** | 84.7 | - | - | (Reijken C., personal communication, 2017) |
| **AS (Harnaschpolder STP)** | 8.0 | 0.3 g L$^{-1}$ | - | - |
| **FP + AS** | 95.0 ± 2.6 | - | - | - |
| **RTP (brand CWS) + AS** | 80.1 ± 2.9 | - | - | - |
| **FSF** | 64.8 ± 6.6 | 105.1 ± 5.3 g kg$^{-1}$ | 60 – 80 | (Ghasimi et al., 2015b; Ruiken et al., 2013) |
| **Concentrated NES (Utrecht STP, Jan 17')** | 13.1 ± 0.4 | 1.7 ± 0.1 g L$^{-1}$ | - | - |
| **Concentrated NES (Utrecht STP, Mar 17')** | 15.3 ± 1.3 | 2.0 ± 0.0 g L$^{-1}$ | - | - |
| **Concentrated NES (Dinxperlo STP)** | 7.4 ± 0.4 | 0.43 ± 0.0 g L$^{-1}$ | - | - |
| **NES (Vroomshoop STP)** | 4.3 ± 0.2 | 0.06 ± 0.0 g L$^{-1}$ | - | - |

**Table 3. Van Soest analysis for toilet paper, wastewater solids and extracted cellulosic pulps.**

| Sample | Cellulose % (g 100g$^{-1}$) | Hemicellulose % (g 100g$^{-1}$) | Lignin % (g 100g$^{-1}$) | Reference |
|---|---|---|---|---|
| **Toilet Paper (brand Tork)** | As received: 80.3 | 9.2 | 4.2 | (Reijken C., personal communication, 2017) |
| **AS** | Raw sample: 4 –10.7 | 15 – 21.4 | 8 – 10 | (Reijken C., personal communication, 2017) |
| **NES (Garmerwolde STP)** | Raw sample: 4.7 (0.94 g L$^{-1}$) | 14.9 | 7.3 | - |
| **FSF cellulosic pulp** | Pulp: 87.4 | 4.2 | 0.8 | - |
| **NES cellulosic pulp (Utrecht STP)** | Pulp: 86.1 | 4.9 | 1.1 | - |

## 4.3 Cellulose NanoCrystals Isolation

### *4.3.1 Hydrolysis conditions*

A controlled strong acid hydrolysis treatment was applied to the cellulosic pulps to isolate CNCs in aqueous suspensions (Figure 10A). The isolation methods varied per cellulose source and are described in detail in *Appendix III*. Conditions of acid addition, cellulose to acid ratio, temperature and time of reaction, centrifugation, filtration and neutralisation steps were crucial to obtaining the CNCs.

Overall, a slightly higher acid to cellulose ratio and lower reaction times were more suitable for the isolation of RTP and wastewater-CNCs. The addition of cold 60 % acid instead of (dropwise) 96.5 % acid was also imperative. On the other hand, for MCC, a lower cellulose to acid ratio and harsh acid addition conditions were ideal. These settings resulted in a deep yellow transparent reaction mixture after hydrolysis (Figure 1, *Appendix III*). An increase in temperature from 45 to 50 °C also induced faster hydrolysis kinetics.

For RTP, part of the sample was also studied for longer reaction times, resulting in a dark hydrolysis liqueur. In this, yellow-brownish impurities were formed indicating over hydrolysis. Unwanted over hydrolysis of MCC was also observed after 150 minutes of reaction, with a light-brown colour being developed. For samples showing this aspect, longer centrifugation-washing and dialysis cycles were necessary. However, part of the colour developed during hydrolysis remained attached to nanocrystals in all isolated sources (Figure 11, RTP and FSF samples).

Due to impurities of the wastewater- derived pulps, several centrifugation-washing cycles and filtration steps were also required when obtaining CNCs from FSF and NES. These impurities were still present in the pulps, even after milling, and were visible again at the bottom of the reaction flask after hydrolysis (Figure 10B). In addition, for some samples, neutralisation with higher concentrations of NaOH was required due to inefficient dialysis.

The yield of isolated CNCs is shown in Table 4. The yield of CNCs from MCC was the highest observed, of 38 % g g $MCC^{-1}$. For RTP and wastewater-CNCs, this yield was also around 30 % on an extracted-pulp basis, with considerable variation.

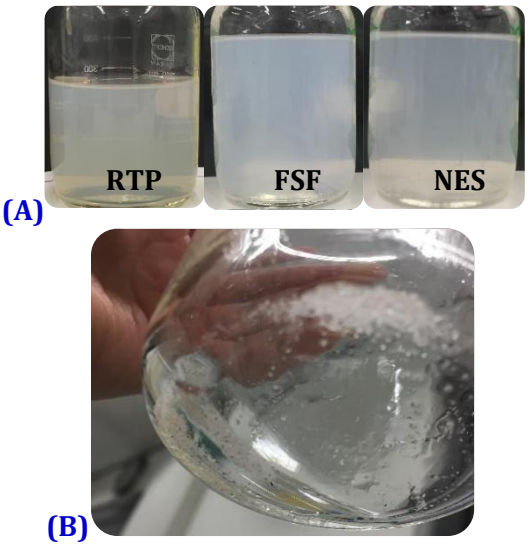


**Figure 10. (A) Suspensions of CNCs isolated from toilet paper (RTP), and wastewater solids (FSF, NES). (B) Remaining inert solids after acid hydrolysis of NES cellulosic pulp.**

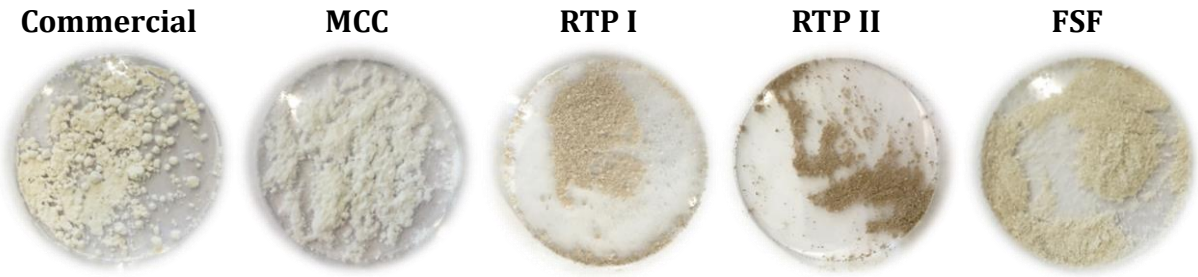


**Figure 11. Dried commercial and lab-made CNCs isolated from MCC, RTP and FSF. RTP I refers to the CNCs isolated in regular hydrolysis time, and RTP II to CNCs obtained after prolonged hydrolysis time. CNCs isolated from NES resembled the aspect of RTP I (not shown). The commercial sample was spray-dried whereas the lab-made samples were freeze-dried.**

**Table 4. The yield of isolated CNCs on pulp and original source basis. Duplicate values were performed only for wastewater-CNCs.**

| Cellulose | Yield of CNCs (g 100 g pulp$^{-1}$) | Yield of CNCs (g 100 g source$^{-1}$) |
|---|---|---|
| **MCC** | 38 % | 38 % |
| **RTP** | 32.8 % | 26.2 % |
| **FSF** | 33.4 ± 17.9 % | 21.7 ± 11.6 % |
| **NES** | 26.5 ± 8.2 % | 4.0 ± 1.2 % |

## 4.4 Cellulose NanoCrystals Characterisation

### *4.4.1 Visual Observations: Birefringence and Opalescence*

After obtaining the most suitable protocol for each cellulose source, CNCs could be observed in a macroscopic perspective via two visual aspects: opalescence and birefringence. When CNCs were successfully isolated, the suspensions showed a transparent but opalescent aspect (Figure 10A). The occurrence of shear birefringent domains in samples was observed between a cross polarisation setup (Figures 12 and 14A). This birefringence was more intense with higher CNCs concentration in suspension and longer ultrasonication periods, as can be observed for the sample of CNCs from MCC. The formation of an anisotropic liquid crystal (LC) phase at higher concentration of CNCs was also observed when drying, and structural solids could also be produced from the CNCs from MCC (Figure 14B). CNCs isolated from NES showed similar visual aspect to RTP samples (not shown). During dilute regimes, with almost no CNCs present (<0.15 %), the suspensions did not show haziness nor birefringence. In addition, the isolated CNCs showed good colloidal stability in water and thixotropic behaviour around 4 % CNCs (in static mode it behaves as a gel and immediately after agitation, it behaves more like a liquid).

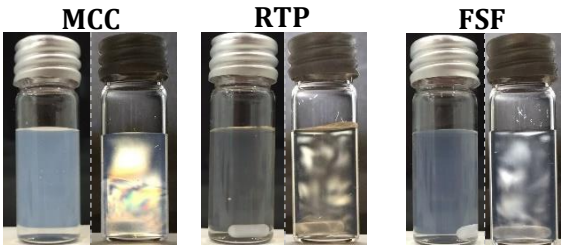


**Figure 12. Suspensions of CNCs isolated from different sources: MCC, RTP, and FSF. Left: under normal illumination. Right: under cross polarisation and shear. Concentrations are ~1 wt. % for MCC; and 0.15 wt. % for RTP and FSF. CNCs isolated from NES resembled the aspect of RTP (not shown).**

### *4.4.2 Atomic Force Microscopy*

AFM images of commercial and isolated CNCs are found in Figure 13. The rod-like morphology of CNCs is present in all images. Although not shown, high fibre densities, as observed in the pictures of CNCs from MCC and RTP, were observed even in much-diluted samples (0.1 % wt. CNCs) for all the investigated sources. Nanocrystals' lengths and diameters could also be estimated by AFM (Table 5). The aspect ratio of the isolated CNCs was similar to what was found for commercial CNCs, ranging from 10 – 14. The average dimensions of CNCs from MCC, and commercial were closely related, with fibres around 86 – 110 nm long and 7 nm wide. Interestingly, the CNCs isolated from RTP and wastewater-pulps showed more similarities, with lengths ranging from 111 to 134 nm and diameters from 10 – 14 nm.

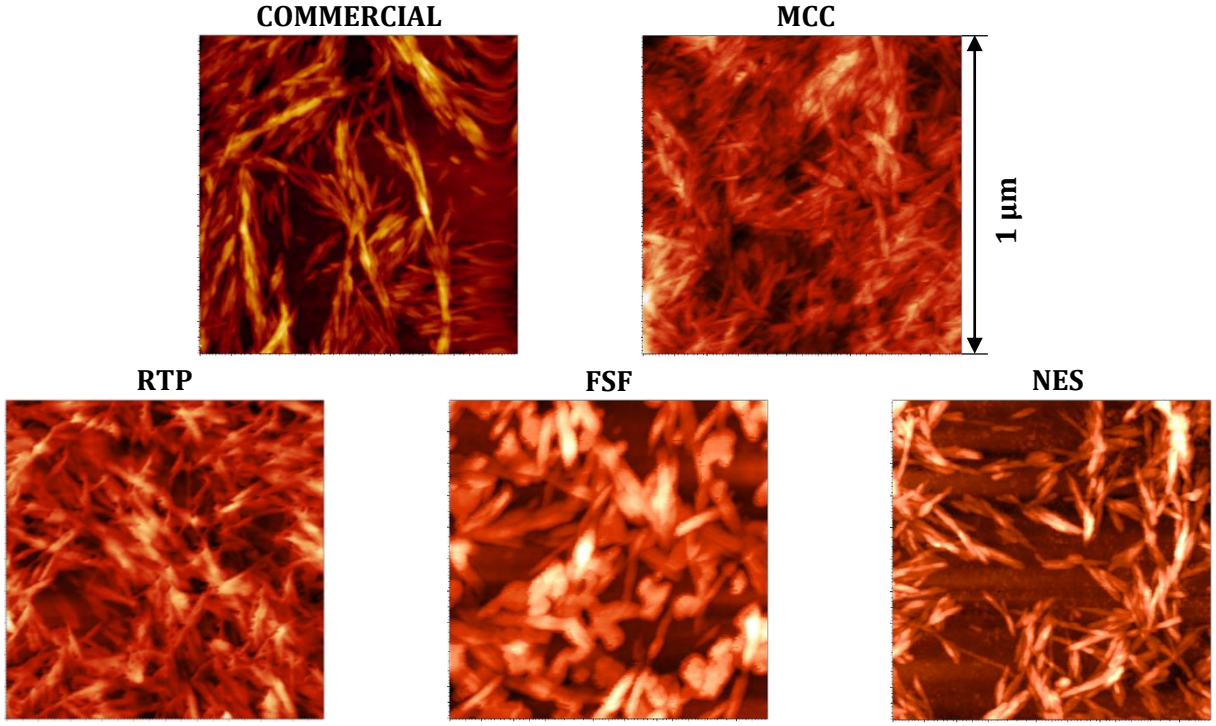


**Figure 13. AFM of CNCs from different sources: commercial and isolated from MCC, RTP, FSF, and NES celluloses. The area covered by the height images is 1 µm x 1 µm.**

**Table 5. Estimation of CNCs dimensions of commercial nanocrystals and isolated from MCC, RTP, FSF and NES cellulose sources.**

| Parameter | CNCs | | | | |
|---|---|---|---|---|---|
| | MCC | Commercial | RTP | FSF | NES |
| **L (nm)** | 86 ± 9 | 110 ± 21 | 134 ± 24 | 145 ± 32 | 111 ± 18 |
| **d (nm)** | 6.6 ± 1.3 | 7.5 ± 1 | 9.9 ± 2.2 | 14.4 ± 3.8 | 9.8 ± 1.5 |
| **L d$^{-1}$** | 13.2 ± 1.9 | 14.6 ± 1.2 | 13.6 ± 0.9 | 10.2 ± 0.6 | 11.3 ± 0.2 |

### *4.4.3 Fourier Transform-InfraRed Spectroscopy*

The FTIR spectra of pulp fibres and CNCs was obtained to assess changes in surface chemistry with cellulose extraction and CNCs isolation treatments. Because of their complexity, the FTIR spectra were separated into two regions, namely: the -OH and -CH stretching vibrations in the 4000 – 2600 $cm^{-1}$ region (Figure 15, left), and the 'fingerprint' region, which is assigned to various stretching vibrations of different groups in the 1800 – 700 $cm^{-1}$ region (Figure 15, right).

More specifically, absorption peaks could be identified near the 3400 $cm^{-1}$, 2900 $cm^{-1}$, 1640 $cm^{-1}$, 1530 $cm^{-1}$, 1428 $cm^{-1}$, 1371 $cm^{-1}$, 1315 $cm^{-1}$, 1245 $cm^{-1}$, 1160 $cm^{-1}$, 1100 $cm^{-1}$, 1050 $cm^{-1}$, 898 $cm^{-1}$ and 810 $cm^{-1}$ wavelengths, as depicted in Figure 15.

As a similarity, features representative to cellulose I at 1428, 1160, 1110 and 898 $cm^{-1}$ wavelengths (Chen et al., 2016) are present in all samples of both cellulose and nanocellulose.

Based on the obtained FTIR spectra, the patterns of cellulosic pulps from FSF and NES almost exactly matched with that of RTP (cellulose source in wastewaters). The spectra of these materials, in turn, were also closely comparable to commercially available α-cellulose and MCC. Moreover, there is the absence of an absorption peak at 1245 and 1530 $cm^{-1}$ in all extracted samples.

For nanocellulose, all the isolated CNCs showed strong similarities to results for commercial CNCs (Figure 15). Furthermore, there is a relevant narrowing of the peak 1640 $cm^{-1}$ after the CNCs isolation in comparison with the original polymer. At 3400 $cm^{-1}$ region, there is wrinkling in the spectra of the CNCs from MCC, RTP I and RTP II. Also, the appearance of a new peak at the spectra (810 $cm^{-1}$) occurred only for samples of nanocellulose.

**(A)** 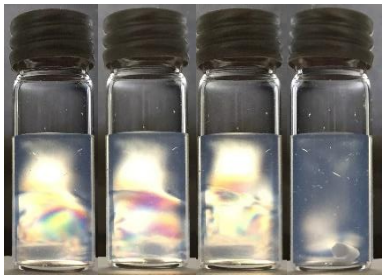 **(B)** 

**Figure 14. (A) Time lapse showing the dynamic birefringence in a suspension of isolated CNCs (MCC), between cross polarizers. (B) Thin film casted by air-drying CNCs from MCC after ultrasonication. The film shows light blue structural colour due to the ordering of CNCs (pitch was developed).**

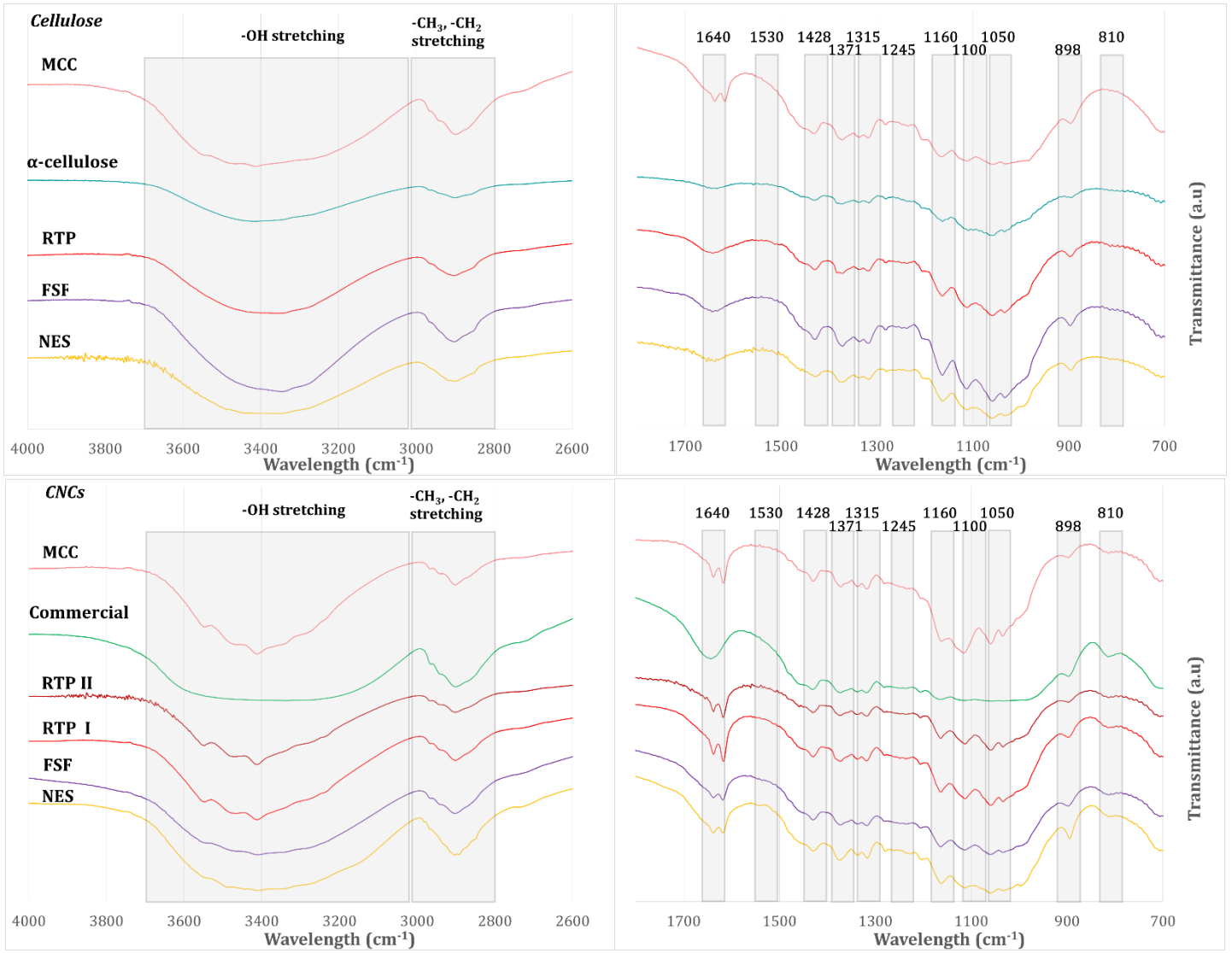


**Figure 15. FTIR of studied cellulose samples (MCC, FP (α-cellulose), RTP, FSF, NES; top image) and CNCs (MCC, Commercial, RTP I, RTP II, FSF, NES; bottom image).**

### *4.4.4 X-ray Diffraction*

XRD results show the intensity of diffraction peaks of the studied cellulose sources and CNCs (Figure 16). The method is useful for comparing relative differences between samples. As expected, all cellulose samples showed reflection peaks at 16.8 °, 18.6 °, 26.1 ° and 40.4 ° regions. These peaks are related to the crystal planes $1\bar{1}0$, 110, 200 and 040 respectively, which are commonly attributed to native cellulose I (here represented by filter paper, FP) (Poletto et al., 2014). The major peak at 26.1 ° corresponds to the crystalline structure of cellulose I.

The diffraction patterns of wastewater-extracted celluloses and CNCs are similar to reference samples - filter paper and commercial CNCs respectively. After CNCs isolation, there is also clear broadening of the all the equatorial peaks ($1\bar{1}0$, 110, 200, 040) for all studied sources.

However, for wastewater-CNCs, other extra peaks were observed at 13.6 °, 23.7 ° and 34 ° (unidentified). CNCs from MCC also showed many other interferences with a major peak at 37.2 °.

Based on the diffraction peak 200 and amorphous region, the crystallinity index of samples could be calculated (Table 6). The crystallinity index (CrI) was similar for both celluloses and CNCs, ranging from 60 – 71 % for toilet paper-based cellulose sources and from 62 – 68 % for the respective CNCs. Overall, the CrI for toilet paper-based sources is comparable to value obtained for the commercially available CNCs (73 %). Moreover, the crystallite size of CNCs samples was also estimated by using Scherrer's equation (Das et al., 2009). The crystallite values ranged from 4 to 8 nm for all the isolated-CNCs and had an average size 4.6 nm for the toilet paper-based CNCs.

**Table 6. Crystallinity index of studied celluloses and CNCs obtained in this study and from literature.**

| Celluloses | CrI (%) | CNCs | CrI (%) |
|---|---|---|---|
| **Filter Paper (Reference)** | 80 | **Commercial (Reference)** | 73 |
| **MCC** | 71 | **MCC** | 80* |
| **RTP** | 71 | **RTP I** | 65 |
| | | **RTP II** | 66 |
| **FSF** | 70 | **FSF** | 62 |
| **NES** | 60 | **NES** | 68 |

**: Peak shape not very well defined.*

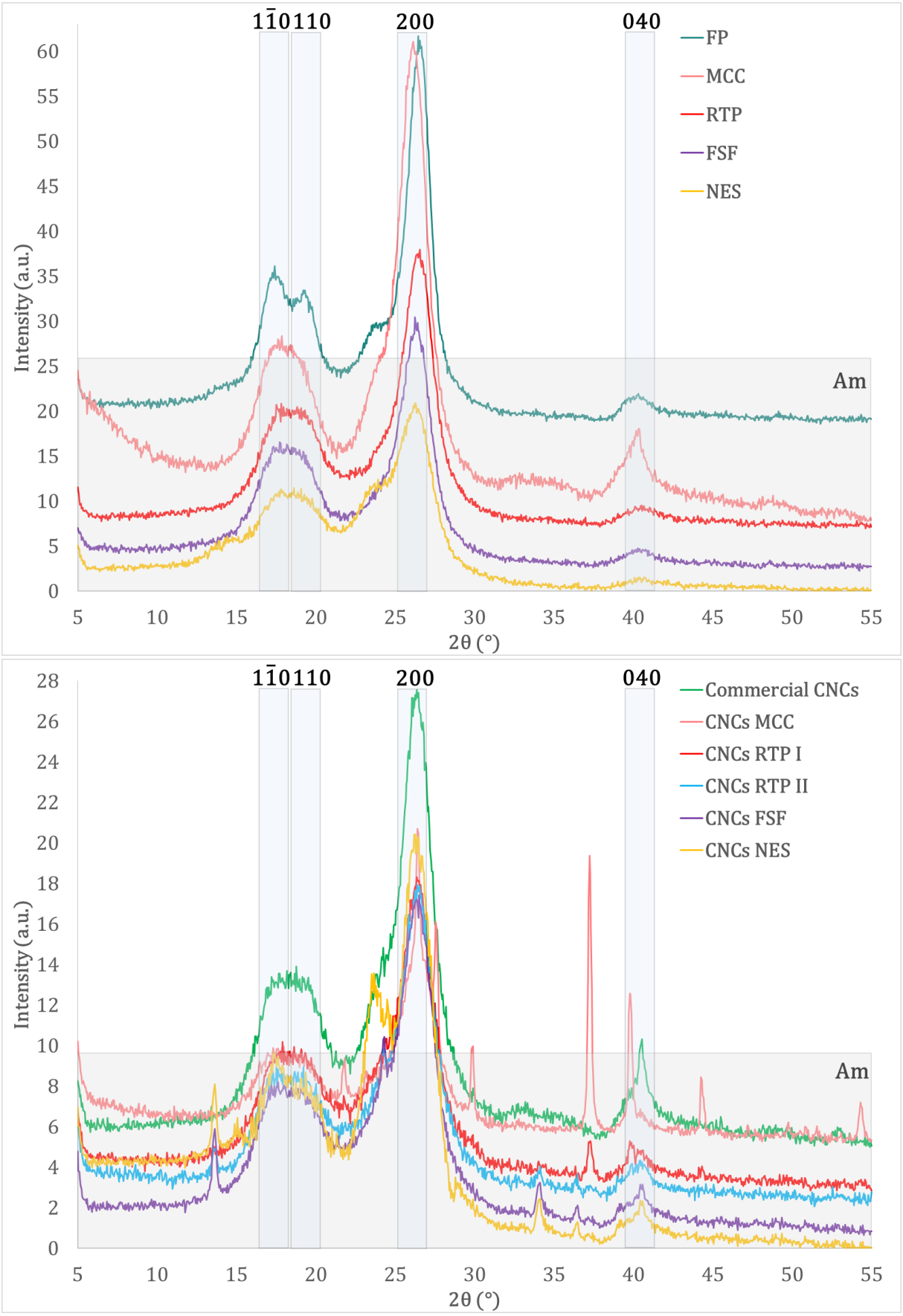


**Figure 16. X-ray diffraction of celluloses (FP (α-cellulose), MCC, RTP, FSF, NES; top image) and CNCs (Commercial, RTP I, RTP II, FSF, NES; bottom image) with evidence on the peaks and amorphous (Am) regions correspondent to the crystal lattice structure of native cellulose.**

## 4.5 Bionanocomposites

### *4.5.1 Commercial Cellulose NanoCrystals and Alginate*

Bionanocomposites were successfully produced from commercial CNCs and sodium alginate. Several volume fractions of CNCs in bionanocomposites were investigated, ranging from 20 to 80 % CNCs. The visual aspect of these composite films is seen in Figure 17. With increasing CNCs addition, the Alginate-CNCs bionanocomposites became more opaque but still were translucent. The films consisting of only commercial CNCs showed iridescence under ambient illumination only if ultrasonicated (difference between E and E*, Figure 17).

In between cross polarizers, the bionanocomposite films of Alginate-CNCs displayed birefringent domains typical of the nematic (N) phase of CNCs with sparse isotropic (I) regions.

**Dynamic Mechanical Analysis**

The mechanical properties of Alginate-CNCs bionanocomposites (and controls containing only alginate or CNCs) were measured by DMA. The resulting storage modulus for the produced films is shown in Figure 18.

For the correct plotting and interpretation of the DMA data, some assumptions were made.

If assuming a 2D-isotropic orientation of the system (K= 3/8 in equation 2), the experimental storage modulus value obtained for a film composed of 100% v/v CNCs was 23 GPa (Figure 18). Thus, it is obtained by the rule of mixtures that the intrinsic modulus of the studied CNCs ($E'_{CNC}$) is around 61.3 GPa (= (8/3)*23). This value is the lowest intrinsic stiffness of the material used.

However, the value of $E'_{CNC}$ is also recalculated with regards packing of the system. Considering a 2D isotropic ordering of the structure, an ideal hexagonal packing of CNCs cylinders in 100 % of the volume fraction would be unrealistic. It can be estimated that the corrected volume fraction of CNCs in the pure film is about 90.69 %, based on the surface area of hexagonally packed cylinders ($\Phi_{CNCs}$ = π/(4*0.866) = 0.9060). Assuming that, the studied CNCs intrinsic modulus is estimated to be 68 GPa (= ((8/3)*23)*0.9060 = 61.3/0.9060 GPa). The recalculated $E'_{CNC}$ was used to obtain theoretical values for the UD, 2D and 3D isotropic regimes as references (dashed lines in Figure 18).

This already quite high modulus value would increase even further if we would take the level of orientation into account, which, however, is not yet known. The reported theoretical intrinsic storage modulus of CNCs is in the order of 130 GPa (Dufresne, 2013).

More importantly, the stiffness *E'* of Alginate-CNCs bionanocomposites increased with the addition of the CNCs, following the estimated theoretical 2D Isotropic pattern. At 50% CNCs, the recinforcement efficiency was of 1.6 times.

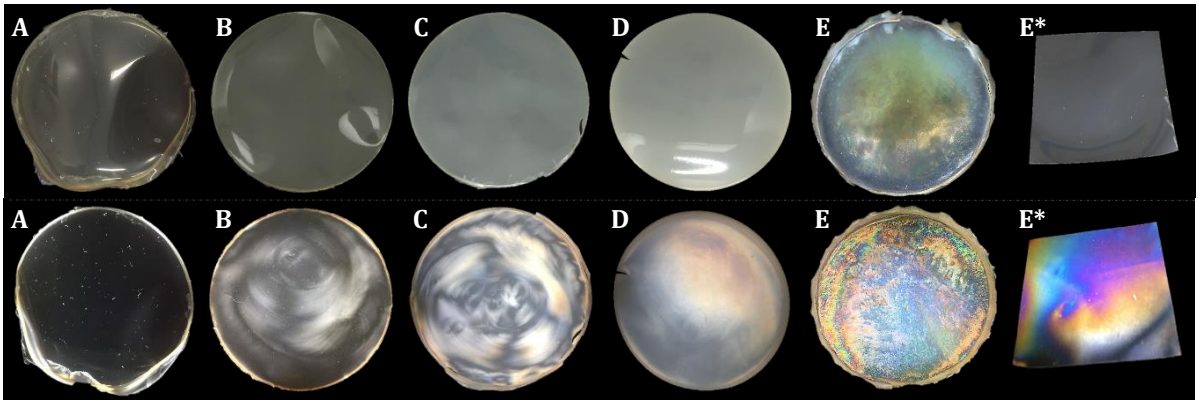


**Figure 17. Bionanocomposites: (A) alginate only; (B) 80 % alginate and 20 % CNCs; (C) 50 % alginate and 50 % CNCs; (D) 20 % alginate and 80 % CNCs; (E) CNCs only - ultrasonicated; (E*) CNCs only - not ultrasonicated. Upper figures are under normal illumination conditions and lower images are in between cross-polarisation.**

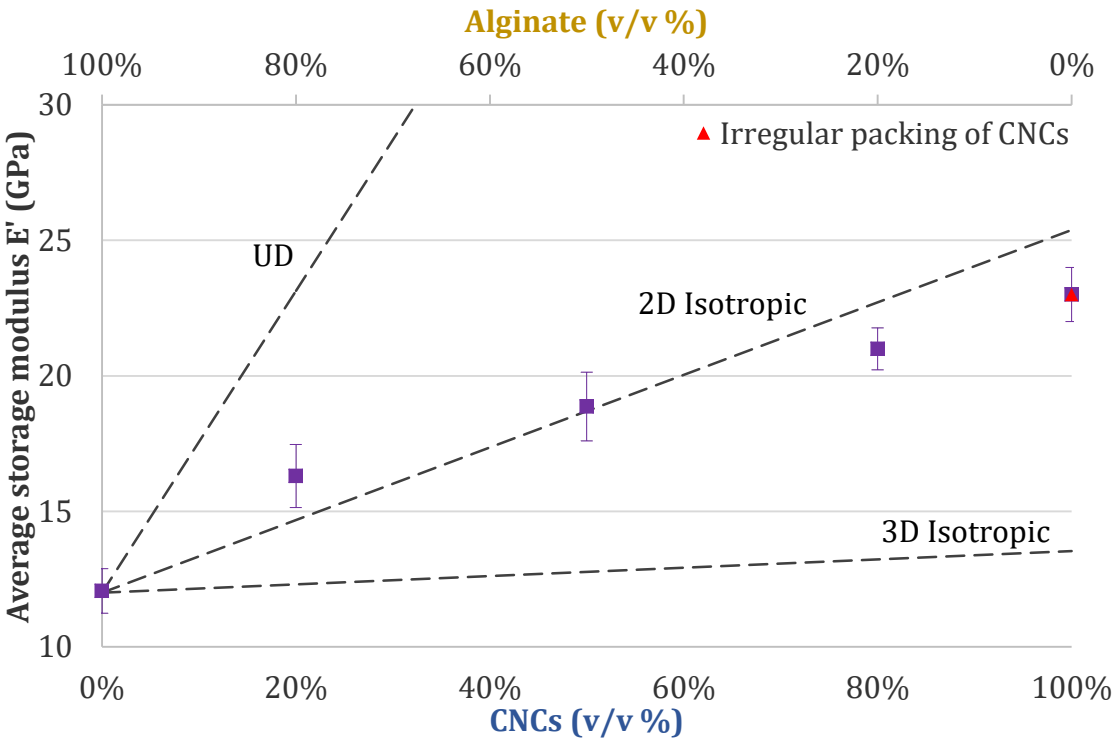


**Figure 18. Theoretical (3D Isotropic, 2D Isotropic, unidirectional UD) and experimental storage modulus E' of Alginate-CNCs bionanocomposites at different ratios of alginate and CNCs. The red triangle represents the $E'_{CNCs}$ value for the 2D-isotropic regime of a pure irregularly packed CNCs film.**

### *4.5.2 Phase Diagram of Cellulose NanoCrystals-Alginate suspensions*

Commercial CNCs´ rigid, rod-like particles formed a fully chiral nematic LC phase in water at relatively low concentrations (>3.5 % w/v) (Figure 19). This highly ordered chiral nematic regime of CNCs could also be observed by the fingerprint texture formed on a drying droplet, under POM (Figure 20). More dilute suspensions of CNCs in water were either biphasic (~3 %) or isotropic (<3 %) as can be seen in Figure 19.

However, during the preparation of bionanocomposites, the Alginate-CNCs suspensions showed the nematic-isotropic transition at lower CNC concentrations (Figure 21). As a proposed explanation for this phenomenon, an alginate-shell model was developed. More detail on this and a complete derivation of the alginate-shell model can be found in *Appendix IV*.

For assessing the alginate-shell model, a phase diagram with regards the Nematic (N) and Isotropic (I) regimes was constructed by varying final alginate and CNCs concentrations in dispersions (Figures 21 and 22). It can be observed that low CNCs concentrations (0.25 – 1% w/v) are required to induce a shift in the CNCs N critical concentration when suspended in alginate.

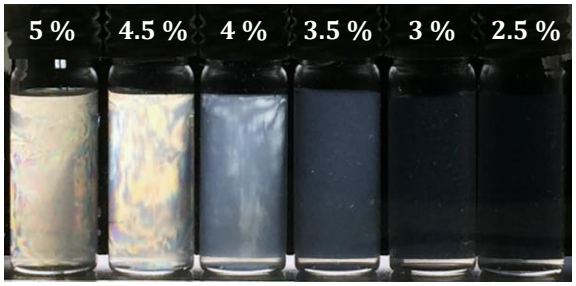


**Figure 19. Suspensions of commercial CNCs (from left to right: 5 %, 4.5 %, 4 %, 3.5 %, 3 %, 2.5 % w/v). The critical concentration for a static nematic liquid crystalline phase is >3.5 % w/v.**

Deriving from the alginate-shell model (*Appendix IV*), the following relation between the critical volume fraction for an N phase ($\Phi_{NI}$) and alginate ([Alg]) could be formulated:

$$\Phi_{NI\,([Alg])} = \Phi_{NI}\,\frac{1}{1+\alpha[Alg]}\left(\frac{1}{1+\beta[Alg]}\right)^2 \qquad (3)$$

where α, β are parameters related to aspect ratio and alginate-shell layer thickness (Δ).

Assuming a β value close to zero, the fitting of this simplified model to the experimental phase diagram data was good, with $R^2$ = 0.9969 (Figure 22). The α value obtained is 5.7 and is related to the aspect ratio of the alginate decorated CNC rods and the density of alginate. However, this is outside the scope of this work.

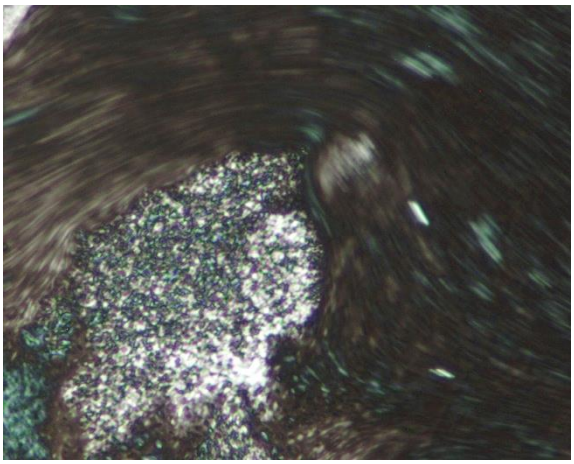

**Figure 20. POM images of the anisotropic phase of commercial CNCs. Upper region shows clear fingerprint texture indicating a chiral nematic LC organization.**

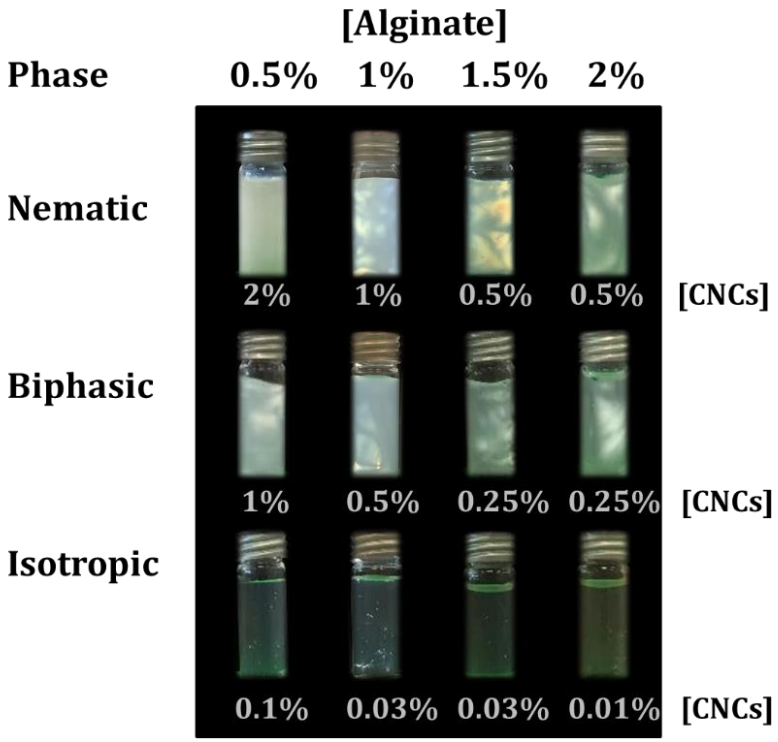


**Figure 21. Glass vials in between cross polarisers: the different Nematic, Biphasic and Isotropic phases of CNCs-Alginate dispersions with varying final concentrations of CNCs and Alginate (w/v).**

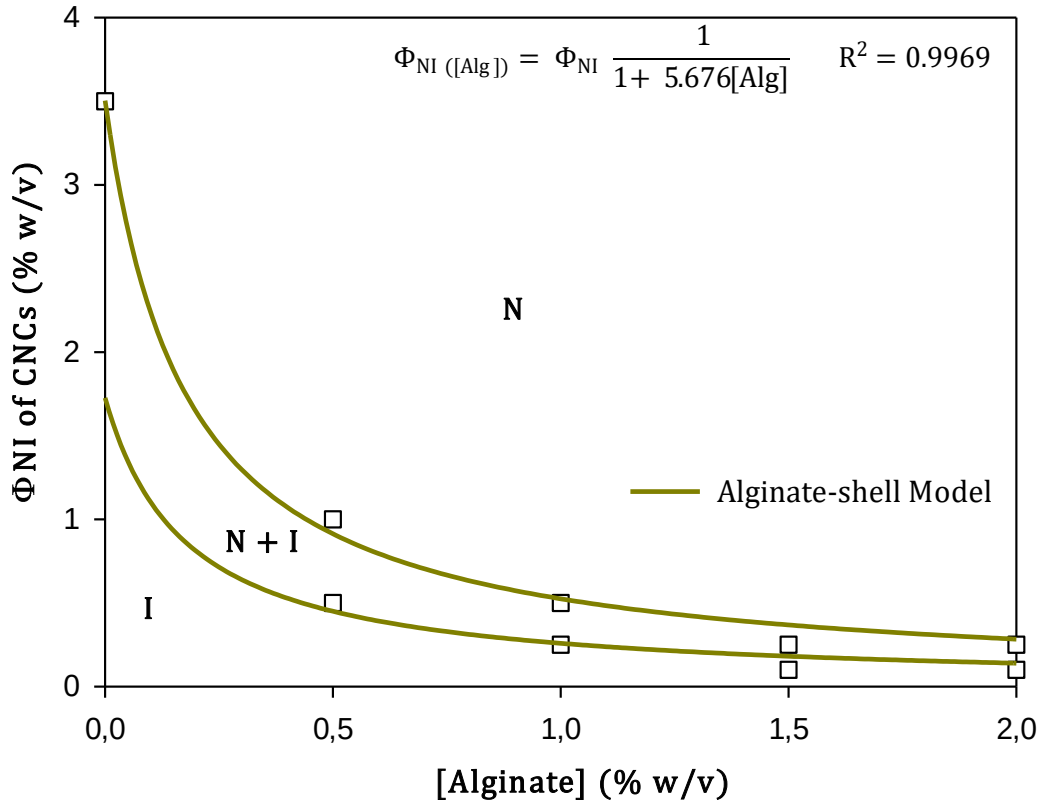


**Figure 22. Phase diagram CNCs-Alginate dispersions with varying volume fractions of CNCs and Alginate. N: Nematic regime, N+I: Nematic-Isotropic Biphasic regime, I: Isotropic regime.**

### *4.5.3 Alginate-Like Exopolysaccharides and Cellulose NanoCrystals*

Alginate was chosen as the matrix polymer of bionanocomposites because its stiffness can be measured and further subtracted to assess the reinforcement ability of CNCs. A bio-based product that is similar to sodium alginate extracted from brown seaweed can also be produced from wastewater (ALE). ALE was first successfully extracted from AGS, forming gel beads in copious amount of acetone, and with a yield of extraction of 344 mg $gVS^{-1}$ granule, in accordance with literature (Felz et al., 2016).

The resulting ALE-CNCs bionanocomposites are presented in Figure 23. It can be seen that the films were very brittle. Pristine ALE did not show any birefringence. While with the addition of 50 % CNCs to the volume fraction, a pattern could be observed under cross polarization.

DMA of ALE bionanocomposites with varying additions of CNCs was also performed (Figure 24). For comparison, the addition of CNCs to sodium alginate increased the stiffness of this material by 1.3 and 1.6 times for 20 and 50 % filler loading respectively. The addition of CNCs to ALE increased the storage modulus by 1.7 and 3.4 fold for 20 and 50 % filler loading respectively. The resultant stiffness for a 50 – 50 % bionanocomposite of Alginate materials-CNCs is around 18 to 19 GPa.

**Figure 23. Bionanocomposites with 50 % ALE and 50 % CNCs (C'). Left: normal illumination conditions. Right: in between cross-polarisation.**

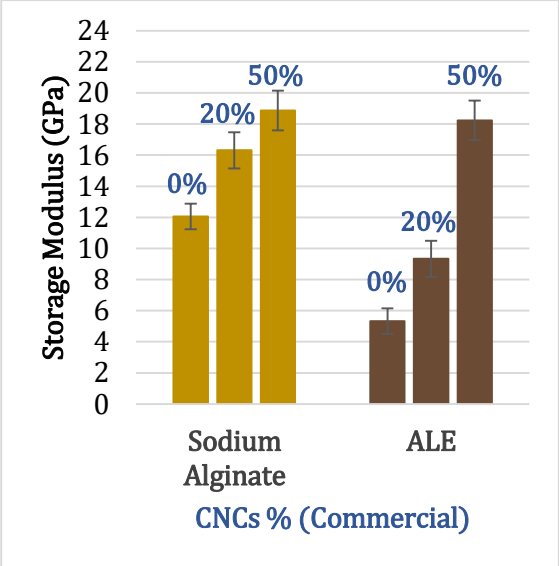


**Figure 24. Storage modulus of bionanocomposites with sodium alginate and ALE in combination with different volume fractions of CNCs (0, 20, 50 %).**

### *4.5.4 Scanning Electron Microscopy*

SEM images of the cross section of Alginate-commercial CNCs films are shown in Figure 25. The cross section of a pure CNCs film (composite E) was also observed. In the latter, a highly layered structure of the film is seen. The same pattern was found in bionanocomposites with alginate, with increasing intensity of this effect in the higher CNCs fractions. The height of pure CNCs layers is about 400 to 600 µm, which is in the range of the visible spectra. ALE composites also have shown dramatic ordering effects after the incorporation of 50 % loading of CNCs. In this, layers with heights similar to the ones observed for a commercial CNCs film were observed.

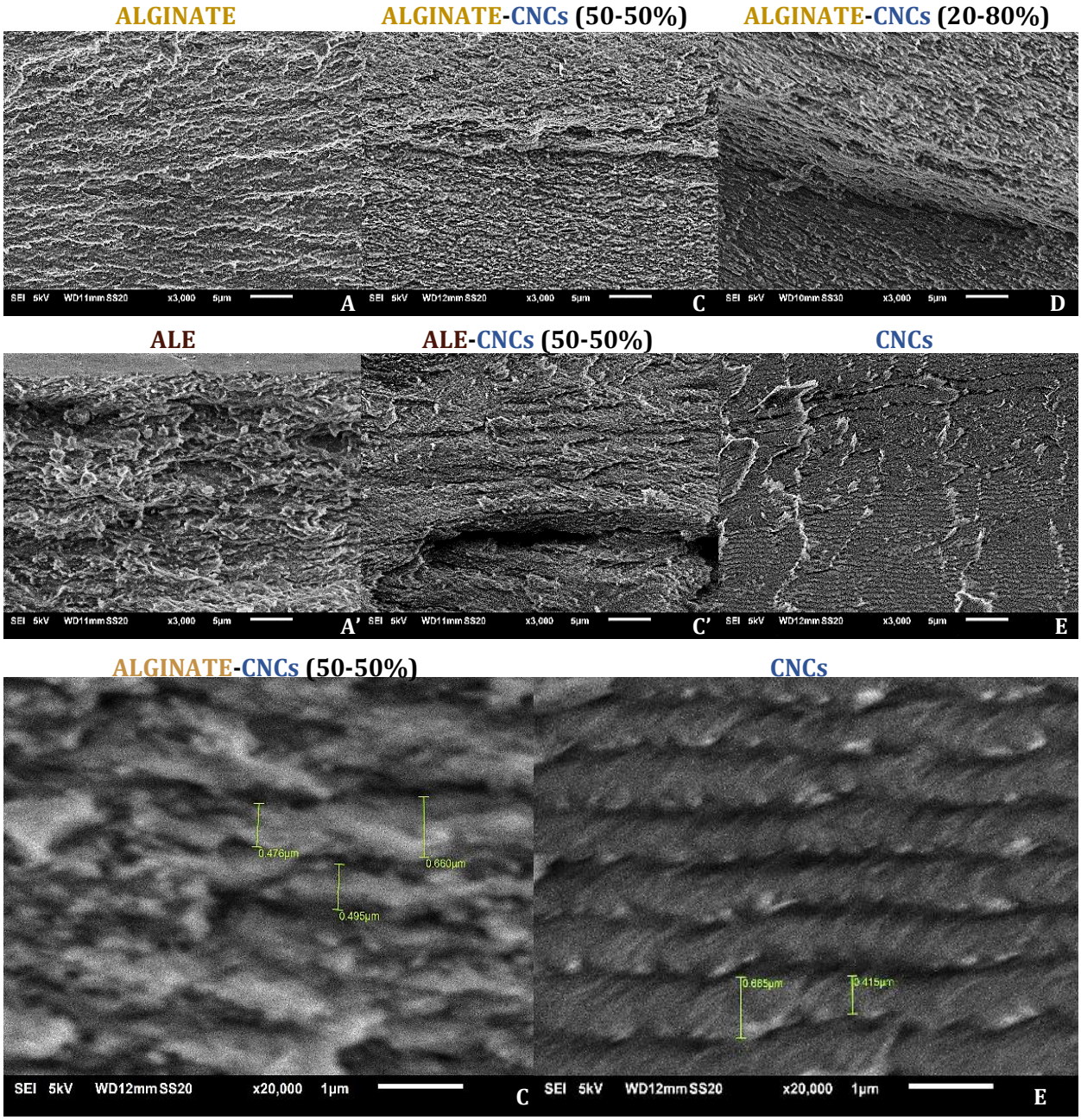


**Figure 25. SEM images of the cross-section of bionanocomposites: (A) alginate only; (C) 50% alginate and 50% CNCs; (D) 20% alginate and 80% CNCs; (E) CNCs only – ultrasonicated; (A') ALE only; (C') 50% ALE and 50% CNCs. Bottom figures are the same cross section of C and E bionanocomposites under higher magnification, showing heights of layered structured conferred to films.**

### *4.5.5 Lab-made Cellulose NanoCrystals and Commercial Alginate*

Bionanocomposites of lab-made CNCs and sodium alginate were successfully produced. Figure 26 shows these bionanocomposites with CNCs from MCC, RTP and FSF pulp in sodium alginate. The films were again opaque but translucent. In addition, the typical birefringence of CNCs, displayed in the previous Alginate- commercial CNCs 50 – 50 % film (C), is also observed.

The main goal of this experiment was to assess the reinforcement capacity of the isolated CNCs. Thus, the data on DMA of lab-made CNCs serves as an indication of product quality. All isolated CNCs increased the stiffness of alginate to a similar order of magnitude, ranging from 17 to 22 GPa (Figure 27). The wastewater-CNCs from FSF increased the modulus of alginate 1.5 times. The same was observed for other isolated CNCs (MCC, RTP), with an increase of alginate modulus of 1.4 and 1.8 times respectively. This is highly comparable to the 1.6 times increase in stiffness obtained with commercial CNCs. In detail, the modulus imparted by RTP CNCs was 11% higher than the commercial CNCs, while the reinforcement capacity of MCC and FSF CNCs was only 11 % and 6 % lower than commercial CNCs.

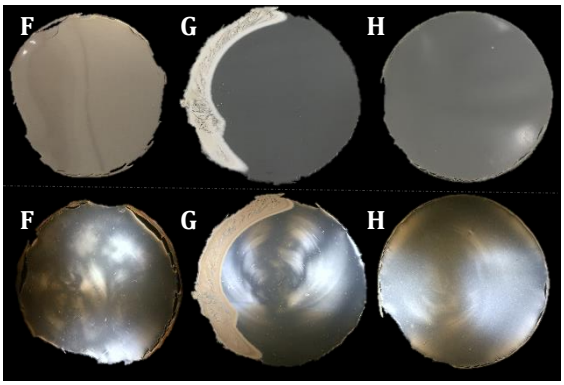


**Figure 26. Bionanocomposites with 50 % alginate and 50 % lab-isolated CNCs from MCC (F), RTP (G) and FSF (H). Upper image: normal illumination conditions. Lower image: in between cross-polarisation.**

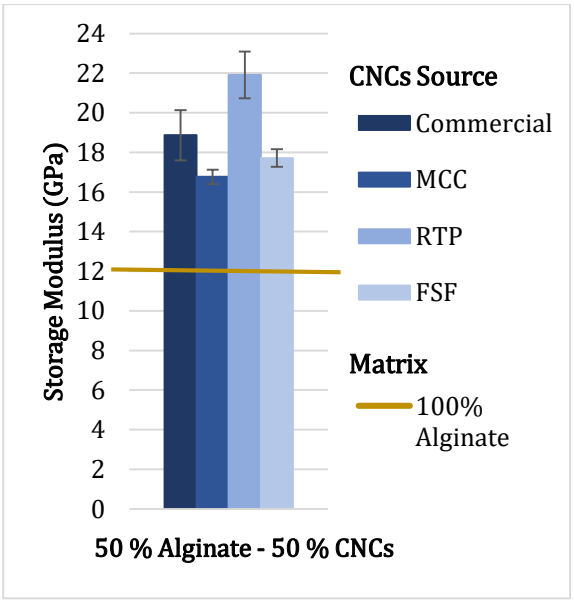


**Figure 27. Storage modulus of bionanocomposites with 50 % sodium alginate and 50 % CNCs (different sources). The storage modulus of an alginate only film (polymeric matrix) is also shown.**

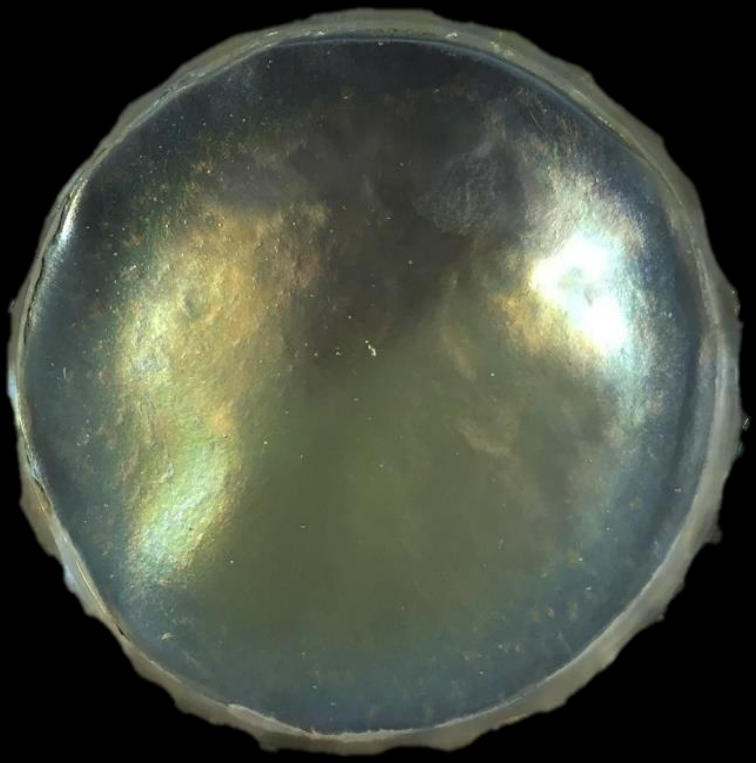

**Cellulose NanoCrystals iridescent film**

# 5. DISCUSSION

## 5.1 Cellulosic Pulp from Wastewater

### *5.1.1 Cellulose Extraction*

The proposed method shows very good recovery of the tested reference sources (FP and RTP), showing that it has a high potential of extracting cellulose from wastewater or sludge samples. For FSF, only two alkaline treatments (with NaOH under heating) were necessary to remove most sludge, EPS, and some pigments (lignin-like compounds). Moreover, the heating treatment with demi water already eliminated some turbidity and a layer of scum was formed, which indicates fat removal. This is encouraging since fewer chemicals are required during extraction.

On the other hand, for NES, at least one more alkaline step was necessary to recover cellulose fibres, mainly due to higher sludge and EPS content of this source in comparison to FSF. The alkaline treatment used is somewhat similar to the thermochemical step often applied in ALE extraction from AGS, using sodium carbonate at 80 °C (Felz et al., 2016; Lin et al., 2010). The dissolved EPS from NES could maybe also be harvested but the harsh NaOH alkaline conditions might degrade the polymers much before. Alternatively, tests with concentrated urea (8 M), well-known for causing chemical denaturation of proteins (Bennion and Daggett, 2003), were conducted. Urea quickly dissolved NES and seems to have improved the simultaneous extraction of polysaccharides in comparison with the NaOH treatment, considering the higher precipitation of the alkaline filtrate after cold acetone addition. However, the urea treatment resulted in an inefficient cellulose extraction due to incomplete removal of pigments, resulting in a greyish pulp even after successive bleaching steps. In contrast, with NaOH treatments, a gradual decolouration of the sample occurs, leaving mainly cellulosic fibres after bleaching, which are intrinsically snowy-white. Lignin-like compounds, likely conferring the colour in these samples, are well known to be solubilized in high alkaline conditions (dos Santos et al., 2016). This explains the higher pigment removal efficiency under a higher pH (13). In the delignification and pulping procedures commonly used by the paper industry or in the cellulose extraction of lignocellulosic wastes, strong alkali and heating treatments are also generally used to remove as much as possible the non-cellulosic components, i.e. hemicellulose and lignin-like compounds (García et al., 2016).

For FSF, one bleaching step was sufficient to achieve white fibres rather free of pigments. The bleaching of NES Utrecht also performed equally well. However, for the NES from Dinxperlo and Vroomshoop STPs, one and two extra bleaching steps were required respectively. The difference with NES Utrecht can be attributed to variations in the waste sludge source, which can contain different types of lignin-like compounds. The bleaching of cellulose is performed for an accurate removal of lignin-like substances and remaining hemicellulose giving a more homogeneous cellulosic pulp (dos Santos et al., 2016). The main goal behind it is to decolorize or remove the non-cellulosic colouring material existing in the mass; thus, increasing the whiteness of the product. The slightly acidic chlorite ($ClO_2^-$) bleaching can be performed in single or multiple steps, depending on the cellulose source, without considerably altering the intrinsic cellulose percentage of the sample. This allows for an optimization of the extraction process to tailored applications, even if it is only estimating the cellulose content of a sample.

However, this procedure is often not environmentally adequate, due to the formation of bleaching by-products. Other more eco-friendly (but maybe less efficient) bleaching methods, such as the use of ozone, hydrogen peroxide, and, more recently, oxygen delignification with bleach effluent recovery could be explored (dos Santos et al., 2016; García et al., 2016).

### *5.1.2 Cellulose Content of Wastewater Solids*

FSF showed a high cellulosic content, 65 % on a TS basis, in accordance with literature. Therefore, it is an interesting source for cellulose recovery in STPs (Ghasimi et al., 2015b; Ruiken et al., 2013; STOWA, 2013). On the other hand, NES samples showed a large variation in the cellulosic content (4 to 15 % on a TSS basis). It is the first time NES cellulose values are reported. Firstly, it is important to acknowledge that the AGS technology is a batch process and, therefore, NES samples are much more subjected to the initial wastewater characteristics (more domestic, industrial or rural contributions) and sporadic cellulosic discharges in the sewage line. Secondly, pre-treatment interferences could be accounting for a lower cellulose value in NES samples. For instance, it has been observed in Nereda® STPs that a grit removal of 3 mm aperture could also be removing fibres due to the accumulation of residues on the apparatus, forming a micro porous layer on the screens. Lastly, the cellulosic content in wastewaters solids can also be interfered in general by human activity and seasonal changes (Ghasimi, 2016). For instance, in autumn more leaves can enter the sewage treatment tanks, increasing the cellulose content.

Hence, the variation observed between NES values can be related to the initial raw cellulose source (wastewater), sampling and processes at STPs. Some of these differences affecting the cellulose percentage in NES are commented. The samples of NES Utrecht presented both a higher solids and cellulose fibre content when compared to NES from the other installations, what could be associated to the start-up period of this installation with internal selection for granular sludge, among other factors. In terms of wastewater composition, the AGS STPs Garmerwolde and Utrecht received mainly only domestic wastewater, which may contain higher amounts of toilet paper as the main source of cellulose. STP Dinxperlo might have had a higher rural wastewater input. STP Utrecht had no pre-treatment significantly removing fibres. However, at STP Garmerwolde there was a sand trap pre-treatment on the wastewater, while at Dinxperlo and Vroomshoop STPs it passed through a 3 mm screen. In addition, NES Vroomshoop was collected directly from the waste sludge pipeline. With this, it can be observed that more research and monitoring of NES cellulosic values is required to determine average values and draw cellulose mass balances for AGS systems.

The Van Soest method is a robust technique that fractionates fibrous lignocellulosic material into cellulose, hemicellulose and lignin. Using this method, the pulps extracted from both FSF and NES sources showed a high cellulosic content (above 86 %), and much-reduced hemicellulose and lignin values (Table 3). This validates the proposed cellulose extraction methodology. In comparison, the cellulosic content of commercial toilet paper itself is also within the range of 80 % cellulose (Table 3).

The Van Soest method as an approach for measuring the cellulosic content of wastewater samples has been recently explored. It gives reasonable values for highly cellulosic sources, such as FSF, influents, and primary sludges (Reijken, C., personal communication, 2017). However, as presented in this study, for both AS and

NES waste sludges, the values obtained with this method are controversial. The estimated cellulose values in sewage influent are within the range of 20 % per gramme of dry matter (Honda et al., 2002). The low values obtained for AS and NES (around 4 %) imply having a significant decrease in cellulosic fibre content, likely due to conversion or large dilutions in the systems by sludge addition. Thus, the method is not considered suitable as such for these samples.

Starch and proteins have been reported to interfere with the Van Soest method, with occasional use of enzymes as a pre-treatment to avoid errors when using the methodology (Chai and Udén, 1998). Thus, polysaccharides and proteins from waste sludges could be affecting the assay. Another interference in the methodology could be derived from the addition of divalent cations to wastewaters, which can be a common practice in STPs. These, could bind to the EDTA used in the analysis and overestimate the hemicellulose content of sludge samples. Remarkably, the hemicellulose content of the waste sludges was high (15 – 21 %) when compared to cellulose percentages, what supports this idea.

The limitations of this method are also related to its impracticality and the fact that at least 10 g of dry solids are required for the experiment. In addition, usually, a very specific laboratory apparatus is required for performing the hot and cold sequential extractions of this method, with samples being analysed by certified laboratories. In this sense, the newly developed alkaline-bleaching method could be an interesting alternative. However, more tests for AS and other wastewater solids are required.

Many other cellulose determination methods have been proposed but no consensus has been achieved on which methods are more suitable for wastewater and sludge samples. With regards to the alkaline-bleaching method proposed here, it is imperative that the analysis is only carried out on wastewater/sludge where the cellulose input is much higher than that of other inert solids, such as sands, plastics, seeds, among others (Cellulose >> Inert solids). This is a limitation of the method. Moreover, milling at 0.5 mm mesh size has also shown to be a good alternative to purify the extracted pulp. Cellulose fibres are light and the large material should deposit first on the bottom of the milling collector. Thus, milling releases impurities attached to the cellulosic matrix to some extent.

### *5.1.3 Cellulose from Wastewater*

Currently, the investigated wastewater solids FSF and NES are mostly incinerated, digested or even used in composting. With regards to digestion, since the conversion of cellulose as a substrate in anaerobic tanks can still be quite slow (Azman, 2016; Ghasimi, 2016), except for when an enhanced digestion is applied, fibres in STPs mainly build up as waste to be incinerated. Alternatively, in the case of FSF, some useful applications have already been shown or are proposed. Previously reported possible applications for FSF are: in soil conditioner; in the construction of roads as asphalt binder; in the production of bioenergy, since FSF is an energy-rich material and enhanced digestion can yield biogas (Ghasimi, 2016); in fermentation and production of bioethanol or bioplastics; and in textile, furniture, ceramic applications (Ghasimi, 2016; Ruiken et al., 2013; STOWA, 2016, 2013, 2010). However, the origin of wastewater solids limits reuse opportunities due to its aspect and odour.

The proposed alkaline-bleaching method for extracting cellulosic pulps from wastewater seems to recover high quality cellulose fibres. Hence, it could be applied to wastewater solids for developing different

product applications. Cellulose and derivatives have been used as engineering materials for thousands of years and there is increasing interest in their use. For instance, a large number of cellulose forest-based products is currently applied in worldwide industries, such as paper, textiles, construction, among others. Cellulose-derivatives can be produced for a large number of applications such as coatings, laminates, optical films, sorption media, additives in building materials, composites, pharmaceutical, foodstuffs and cosmetics (Poletto et al., 2014). They are attractive due to the renewable and sustainable aspect of cellulose, with low environmental, health and safety risks. This thesis investigated the use of wastewater-derived cellulosic pulps for nanocellulose production (CNCs).

## 5.2 Cellulose NanoCrystals Isolation

### *5.2.1 Conditions*

Conditions of cellulose to acid ratio, acid addition, temperature and time of reaction, centrifugation, filtration and neutralisation steps were crucial to obtaining the CNCs. The sulphuric acid hydrolysis of cellulose has been optimised by several researchers already. A common method to produce CNCs with sulphuric acid is by using 64wt.% sulphuric acid solution at 45 °C for 45 – 60 minutes with constant stirring, followed by quenching the suspension with 10X deionized water, re-concentration of the CNC through centrifugation and dialysis against demi water until a constant neutral pH is achieved. To separate the nanocrystals, the suspension has to be repeatedly sonicated as well (Börjesson and Westman, 2015).

After an extensive literature review, a table showing average values and common practices in the isolation of CNCs from paper-based sources and lignocellulosic wastes was constructed (Table 7). Some of the references used were: Börjesson and Westman (2015), Jiang and Hsieh (2015), Kallel et al. (2016), Ostiguy and Emond (n.d.), Reddy and Rhim (2014), Rhim et al. (2015), Rosa et al. (2010) and Silvério et al. (2013a). The main information that could be extracted from this review is that, although a general way to produce CNCs is present in literature, there are minor differences in the isolation of CNCs depending on the source used, especially when agricultural and industrial wastes are considered. However, in general, highly concentrated acid is often used (61 %), with a low cellulose to acid ratio, and for a relatively short time (about one hour) to obtain CNCs.

**Table 7. Average values or common practices of conditions reported for CNCs isolation based on extensive literature review.**

| **Sulphuric acid (wt.%)** | **Ratio cellulose : acid (g : mL)** | **Time (minutes)** | **Temperature (°C)** |
|---|---|---|---|
| 61 (average) | 1:20 | 40 – 75 (range) | 48 (average) |
| **Centrifugation** | **Dialysis** | **Sonication** | **Yield** |
| 10,000 rpm, 10', 2 – 5X | against distilled water minimum 4 days | 5 – 30' in ice bath | 12 – 30 % (starting material)<br>19 – 52 % (cellulose or pulp) |

As shown by results, the applied CNCs isolation methods varied per cellulose source. Comparing the common procedures (Table 7) to the processes used in the isolation of CNCs in this study, the main difference for toilet paper-based sources is the slightly higher cellulose to acid ratio used (1:30 or 1:55) but also with a reaction time shorter than 75 minutes (30 to 60 minutes). For MCC, the reaction times were higher but all other conditions used were similar to standard procedures. Moreover, for MCC, harsh 96.5 % acid addition on wet cellulose resulted in the good isolation of CNCs. These optimal conditions are in agreement with the current literature (Bondeson et al., 2006).

The term MCC is used to refer to a highly crystalline structure composed of bundles of heterogeneous cellulose microfibril aggregates, which are strongly hydrogen bonded to one another (dos Santos et al., 2016). Thus, MCCs are intrinsically harder to hydrolyse due to high crystallinity, what explains its required harsh acidic conditions and longer hydrolysis reaction time. In contrast, slightly higher acid to cellulose ratio (cold, 60 %) but shorter reaction times were more suitable for the isolation of RTP and wastewater-CNCs. The process of CNCs isolation is source-specific, and differences with MCC can be attributed to the presence of more easily degradable cellulose and hemicellulose fractions in toilet paper-based samples.

The excessive yellow-brownish impurities formed during acid reaction, observed for CNCs sample from RTP (II), can be attributed to over hydrolysis of the cellulose fibres with release of residual lignin from the raw materials and by-products formation (polymers, sugars, salts) (Reid et al., 2016; Silvério et al., 2013a). This might be related to the caramelization or browning of sugars, with the formation of C double bonds due to dehydration, also increasing the viscosity of the mixture. Even though washing and dialysis steps were performed, remaining larger sugars might attach to the fibre surface. Thus, hydrolysis conditions also determine key characteristics of isolated CNCs, such as colour. Size can also be dramatically affected by over hydrolysis, as it will lead to shorter CNCs of low aspect ratio and dispersibility (Reid et al., 2016). Even further, if extreme conditions of hydrolysis are applied, such as long times, complete hydrolysis of cellulose, yielding only unwanted sugars and salts is observed. On the other hand, if the time of hydrolysis is too much lowered, a higher degree of polymerization is obtained with no isolation of nanometer-sized particles but of longer fibrils.

The overall CNCs extraction pathway includes several post-treatment and purification steps, such as washing, centrifugation, sonication, homogenization, dialysis, neutralization. For some of the isolated CNCs, neutralisation with higher concentrations of NaOH was required due to inefficient dialysis, what could have caused more adhesion of hydrolysis by-products on the nanocrystals (Reid et al., 2016). A neutralisation step was also performed in other reported CNCs isolation protocols using 0.1 to 0.25 mM NaOH (Chen et al., 2016; Reid et al., 2016).

### *5.2.2 Yield*

The 38 % yield of CNCs from MCC is in accordance with values previously reported in literature (30 %) (Bondeson et al., 2006). For RTP and wastewater-CNCs, this yield was also around 30 % on an extracted-pulp basis, with large variation. The yield of CNCs from hydrolysis is strongly influenced by conditions, especially reaction time (García et al., 2016). It is important to note that, even though the toilet paper was highly processed and recovered from wastewater, MCC and toilet paper have a common primary

cellulose source, which is wood pulp. The yields for both MCC and toilet paper-based isolated CNCs (on a pulp basis) comply with values previously reported for papers and lignocellulosic wastes (Table 7). Nevertheless, more isolations are required to determine a constant value for these sources. This becomes even more problematic for wastewater-CNCs due to the intrinsic variation of the cellulose values and level of purity (caused by inert solids). As a reference value, for lignocellulosic wastes, CNCs preparation yield between 26 % and 77 % have been reported for aspen Kraft pulp and pineapple leaf respectively (García et al., 2016). Lower yields are usually associated with extreme treatments and presence of hemicelluloses or pectines (dos Santos et al., 2016; García et al., 2016; Reid et al., 2016). Interestingly, a recent report has shown that lower acid concentrations (57 – 58 %), higher temperature (64 – 67 °C), and longer hydrolysis times (2 h) resulted in larger CNCs yields (66 – 69 %) (Reid et al., 2016), which could be tested for toilet paper-based CNCs in a later stage.

## 5.3 Cellulose NanoCrystals Characterisation

Even though all cellulose nanocrystals were made of the same biopolymer, the use of different cellulosic materials and different extraction methods is likely to confer different characteristics to isolated-CNCs. The assessed characteristics related to visual aspect, surface morphology, chemistry and crystallinity of CNCs are discussed.

### *5.3.1 Visual Observations: Birefringence and Opalescence*

In the aqueous suspensions of isolated-CNCs, opalescence and dynamic birefringent domains were observed, what is also observed in suspensions of commercial CNCs. The birefringence was dependent on concentration and ultrasonication treatment (dispersion of nanocrystals). From many aqueous CNCs suspensions, a bluish colour was reported due to the helical chiral nematic ordering N* and length of the pitch gap (Börjesson and Westman, 2015). CNCs are able to absorb visible light and, depending on the length of the pitch gap, different wavelengths are absorbed and light gets reflected emitting different colours. Therefore, after controlled drying, different CNCs films with structural colour can be seen if the films are sufficiently thin, what was exemplified by Figure 14B for CNCs from MCC, where a bluish film is shown.

The good colloidal stability in water of the isolated-CNCs can be mainly attributed to negative hydroxyl groups from the cellulose structure and half sulphate esters groups grafted on the surface of nanocrystals during hydrolysis. This chemical structure also assists the formation of LC phases and affects CNCs' rheology.

Through freeze-drying of the isolated CNCs, thin lamellar whitish flakes that can be re-dispersed in water were produced, with aspect similar to commercial product. Overall, the visual aspects support the assumed good isolation of CNCs for all cellulose sources.

### *5.3.2 Morphology and Dimensions*

The isolated-CNCs presented a rod-like morphology, similar to configured for commercial CNCs, as observed with AFM. Nanocrystals' lengths and diameters could also be estimated and a relatively high aspect ratio (10 – 14) was observed for the isolated CNCs. This was similar to what was found for commercial CNCs (15). Typical aspect ratios for CNCs range from 1 to 100 (Börjesson and Westman, 2015; Reid et al., 2016).

Similarities were observed in the dimensions of CNCs from MCC and commercial source, but also in between toilet paper-based CNCs. For the latter, lengths were in the order of a hundred nanometres and diameters in the

order of several nanometres. Different cellulose sources are expected to give different characteristics and also different aspect ratios (Börjesson and Westman, 2015). Comparing with available literature, nanorods show typical dimensions of 5 to 20 nm in diameter and 100 to 500 nm in length for several waste-recovered CNCs (García et al., 2016). The morphology and dimensions are usually related to hydrolysis conditions, such as acid to fibre ratio and concentration, hydrolysis time, temperature, in which extremes can lead to smaller crystalline nanoparticles.

However, these results should be seen only as a first characterization of this material and not absolute. More investigation is necessary accounting for the broad heterogeneity of sizes found in CNCs suspensions. In addition, a recent report using the same source of commercial CNCs has reported lengths of 60 – 500 nm and an aspect ratio of 31(Reid et al., 2016), which is twofold higher than what was found in the present study. The high aspect ratio of CNCs can be directly related to the shear thinning behaviour observed in CNCs suspensions since particles align with the flow. Changes in particle dimensions and charge density are critical to many properties, influencing other rheological, colloidal, interfacial and reinforcing properties (Giri and Adhikari, 2012; Reid et al., 2016).

### *5.3.3 Surface Chemical Composition*

The peaks observed under FTIR can be attributed respectively to 3400 $cm^{-1}$: O-H stretching vibrations; 2900 $cm^{-1}$: C-H asymmetric and symmetric stretching vibrations of methyl and methylene cellulose groups, 1640 $cm^{-1}$: O-H bending vibration of absorbed water, 1530 $cm^{-1}$: C=C stretching of aromatic hydrocarbons of lignin or N-H vibrations of proteins, 1428 $cm^{-1}$: $CH_2$ symmetric bending, 1371 $cm^{-1}$: C-H asymmetric deformation or aromatic rings, 1315 $cm^{-1}$: $CH_2$ symmetric bending, 1245 $cm^{-1}$: stretching vibration mode of acyl-oxygen CO-OR – associated with the hemicellulose, 1160 $cm^{-1}$: C-O-C asymmetric stretching of cellulose, 1100 $cm^{-1}$: β-glucosidic ether linkages (C-O-C) of the anydroglucopyranose ring, 1050 $cm^{-1}$: C-O stretching, 898 $cm^{-1}$: C-H deformation of cellulose, 810 $cm^{-1}$: sulphonation (Chen et al., 2016; Oksman et al., 2011; Poletto et al., 2014; Rosa et al., 2010). These peaks are mainly related to the cellulose fibre and CNCs isolation procedure.

The spectra of all investigated cellulose sources was very similar. In detail, the patterns of cellulosic pulps from wastewater almost exactly matched with that toilet paper (cellulose source in wastewaters). The absence of an absorption peak at 1245 and 1530 $cm^{-1}$ in all extracted samples indicates the absence of hemicellulose and lignin-like compounds. This result supports the efficacy of the extraction procedure as non-cellulosic polysaccharides similar to lignin and hemicellulose were thoroughly removed.

For nanocellulose, strong similarities can be drawn between the commercially available and isolated CNCs. At 1640 $cm^{-1}$ region for nanocellulose, there is a narrowing of the peak in comparison with primary celluloses. This change is due to a heterogeneous environment and higher surface area of CNCs, which can absorb more water. At 3400 $cm^{-1}$ region, there is wrinkling in the spectra of the CNCs from MCC, RTP I and RTP II. This peak is related to the hydrophilic tendency of nanowhiskers but needs further systematic investigation. Furthermore, there is the appearance of a new peak at the spectra of only nanocellulose samples (810 $cm^{-1}$). It can be attributed to sulphate ester groups attached to nanocrystals due to sulphonation (hydrolysis). It is estimated that, by using 64 % sulphuric acid, around 0.5 – 2 % sulphate groups will be attached to the surface of the nanocrystals (Börjesson and Westman,

2015). Furthermore, the caramelization effect visualised in sample RTP II cannot be observed under FTIR, since the vibration of C=C bonds is not infrared active. To tackle this issue, Raman spectroscopy is indicated for further research.

Both FTIR analysis, on pulps and CNCs, suggests that cellulose and nanocellulose have been successfully produced from wastewater solids.

### *5.3.4 Crystallinity*

XRD results of the studied celluloses and CNCs is useful for comparing relative differences between samples. All cellulose samples showed reflection at equatorial peaks related to the crystal planes of native cellulose (Poletto et al., 2014). This was expected but also suggests that the primary crystal structure of the cellulosic source is preserved in the isolated CNCs.

However, the diffractograms for CNCs from wastewater-derived pulps and MCC showed other extra peaks, which were not identified for the time being. They are probably resulting from the mineralisation of compounds from acid hydrolysis or neutralisation steps, such as sodium sulphate. This tells about the purity of the isolated CNCs.

The bleached pulps showed a typical cellulose I pattern, and wastewater-CNCs were strongly similar to the commercial CNCs sample. Thus, the XRD patterns confirm the FTIR spectra results, indicating good extractions of cellulosic pulps and CNCs. After CNCs isolation, there is also clear broadening of the all the equatorial peaks for all studied sources, what suggests chemical degradation of the crystalline structure.

The crystallinity index (CrI) was similar for both celluloses and CNCs. Although most amorphous structures are expected to be broken down during hydrolysis, the components of this part still give a contribution in the XRD analysis, resulting in a similar CrI for CNCs and primary sources.

Interestingly, the CrI for toilet paper-based sources (61 – 64 %) is comparable to value obtained for the commercially available CNCs (73 %), what supports the previous product quality analysis. Moreover, the range of crystallite size values for CNCs (4 to 8 nm) is in accordance to what has been previously reported for cellulose, 5 nm (Poletto et al., 2014). This value represents a relative estimation of the crystalline portions of the isolated nanostructures, and is complementary to the dimensions obtained with AFM, showing widths of 10 to 14 for CNCs samples. Cellulose crystallites also present imperfections and, thus, a significant portion of the nanocellulose edges can still be less ordered or amorphous.

The crystallinity index of cellulose CrI has been used to describe the relative amount of crystalline material in cellulose. However, it is emphasized that numerical CrI results from the literature are much dependent on the choice of the X-ray instrument and data evaluation procedure applied to the measurement and on the distribution of the sample on the wafer. Thus, CrI values should not be compared within different literature studies.

Thus, the aspect, morphology, chemical structure and crystallinity of isolated-CNCs samples are convincingly similar to commercially available CNCs.

## 5.4 Bionanocomposites

### *5.4.1 Commercial Cellulose NanoCrystals and Alginate*

Bionanocomposites with commercial CNCs and sodium alginate could be produced using a simple film casting method. With regards the translucent aspect of films, the nanodimensional size of CNCs results in lower light scattering compared with the higher sizes of pulp fibres, making good transmittance bionanocomposites possible. Pure CNCs films, consisting of only commercial CNCs, were also produced and showed iridescence that was visible with the naked eye after ultrasonication (cover of this section). This can be explained by the formation of a well-developed chiral nematic pitch in the film (as similarly discussed for the film of CNCs from MCC). The pitch of the chiral nematic phases, hence the colour of the film, can be controlled by varying the amount of sonication applied to CNCs suspensions (Reid et al., 2016).

Several volume fractions of CNCs in alginate bionanocomposites were investigated, ranging from 20 to 80 % CNCs. The characteristic birefringence of CNCs was also visualized in this Alginate-CNCs bionanocomposite films. From this perspective, it seems CNCs has imparted their long-range order to alginate, causing layering in the bionanocomposite structure through the entire film or locally in certain anisotropic regions, what was dependent on the CNCs volume fraction. Thus, alginate was incorporated into the LC template of CNCs forming ordered structures with highly birefringent domains.

**Dynamic Mechanical Analysis**

The development of nanocellulose-reinforced matrix bionanocomposites takes advantage of the CNCs intrinsically high mechanical properties, high aspect ratio and surface area. The addition of commercial CNCs increased the stiffness of sodium alginate films up to 1.7 times, due to the increase in the ordering of the system. The modulus of a film containing 50% CNCs showing a high stiffness value (19 GPa).

Ureña-Benavides et al. (2010) investigated the effect of jet stretch and particle load on Alginate-CNCs nanocomposite fibres. They reported that CNCs addition enhanced the strength and modulus of alginate. In their investigation, there was an increase of 38 % in fibre tenacity and 123 % increase in tensile modulus with only 10 wt.% CNCs addition. They also attributed these improvements to the alignment of CNCs.

Moreover, for Alginate-CNCs bionanocomposites, achieving a good dispersion of the nanorods is key to maximising their effectiveness in altering the alginate properties. Also, slight differences between theoretical (2D-Isotropic) and experimental storage modulus in Alginate-CNCs bionanocomposites were observed, which might attributed to: (i) irregular packing of the CNCs, as figuratively showed for the 100 % loading CNCs film (Figure 18); (ii) the fact that nanocrystals' fibres, in reality, are not completely straight aligned in the 2D plane of the films (slightly wavy); and (iii) defects such as air that could have been present in the sample.

In many other studies, dramatic changes to the modulus of bionanocomposites are reported even at a low CNCs fraction (dos Santos et al., 2016). Moreover, due to the hydrophilic surface of cellulose, interactions between CNCs (filler) and hydrophilic matrices are usually satisfactory. On the other hand, adding cellulose into hydrophobic matrices usually results in poor matrix-filler interactions (dos Santos et al., 2016; Kalia et al., 2011). CNCs have proven to reinforce composites with several polymers, such as starch, polylactic acid and cellulose

acetate butyrate (Börjesson and Westman, 2015).

### *5.4.2 Phase Diagram of Cellulose NanoCrystals-Alginate suspensions*

CNCs particles formed a fully nematic liquid crystal phase in water at relatively low concentrations (>3.5 wt.%). The critical concentration for a LC suspension, which is the lowest concentration where the nanorods self-organize, depends on particle size, acidic treatment, preparation conditions, aspect ratio, and ionic strength (Börjesson and Westman, 2015). This concentration usually ranges from 2 – 10 wt.%. Reid et al. (2016) also have reported, for the same commercial CNCs, that above 3.5 wt.% the suspension showed a completely anisotropic behaviour. It was observed that low CNCs concentrations in alginate suspensions are required to induce a shift in the CNCs N critical concentration. This was also observed by Ureña et al. (2010). They reported that the LC critical concentration was noticeably reduced when CNCs final concentration was 1 wt% (for 1 wt% alginate matrix), in agreement to what was found during this study. This can be explained by the alginate-shell effect (*Appendix IV*). Good agreement was found between the proposed alginate-shell model and the phase diagram experimental results. Moreover, the biphasic stability observed in the Alginate-CNCs vials (Figure 21) can be also attributed to the anionic nature of alginate in water suspensions; since charged polymers tend to partition more evenly due to the entropy of mixing of the counterions (Risteen et al., 2017; Ureña-Benavides et al., 2010).

### *5.4.3 Alginate-Like Exopolysaccharides and Cellulose NanoCrystals*

ALE is a bio-based product that is similar to alginate from brown seaweed and can be extracted from sludges, especially in granular form. Moreover, it is a highly hydrated EPS composed of polysaccharides, proteins, nucleic acids, lipids, humics, and intracellular polymers (Felz et al., 2016). Films of pristine ALE were brittle and presented no birefringence. The addition of 50 % CNCs formed a pattern in ALE that could be observed under cross polarization. To some extent, this is similar to what was observed for commercial sodium alginate, with CNCs imparting birefringence to the polymeric matrix.

DMA of ALE-CNCs bionanocomposites was also performed. The addition of CNCs to ALE increased dramatically the stiffness of this material by a factor 3.4 (50 % filler loading, 19 GPa). This shows the good reinforcement potential of CNCs to the wastewater-extracted polymers in ALE. This experiment exemplifies the potential of wastewater-CNCs, similar to commercially available, to reinforce other wastewater-based products, what could be investigated in the future. By expanding the knowledge on nanocellulose from wastewater, and finding how to control its properties during processing, new avenues in product development can be opened. In this sense, novel biobased products with outstanding properties could be produced and used as a replacement for fossil fuel-based products.

### *5.4.4 CNCs Layers*

SEM images of the cross section of commercial CNCs and alginate bionanocomposites displayed a layered structure imparted by CNCs self-assembly, what is supported by the previous DMA data. The height of the layers is directly related to the helical pitch of the chiral N phase of CNCs. In this phase, the rods align along a director, which twists around a screw axis. The distance for a full 360 ° turn of the director is called pitch, and its height characterizes the packing and layering of CNCs. The helix has periodic layers of crystals with the same orientation. Because distance between the

developed layers in the composite of pure CNCs was uniform and within the range of visible spectra (around 400 – 600 μm), the solid presented structural colour that was visible with the naked eye, as previously mentioned (Figure 17). The charge on the surface of CNCs is also responsible for the layering effect, since it keeps the layers separated. An even more evident pattern was found in bionanocomposites with ALE. This confirms the imparting of the highly ordered CNCs template to films of alginate materials.

### *5.4.5 Lab-made Cellulose NanoCrystals and Commercial Alginate*

Bionanocomposites with CNCs from MCC, RTP and FSF pulp in sodium alginate were comparable to the films produced with commercial material, since they also displayed the characteristic birefringence of CNCs at 50 % nanofiller loading. The data on DMA of lab-made CNCs serves as an indication of product quality. With regards toilet paper-based CNCs, the increase in stiffness by the addition of RTP and wastewater-CNCs was of 1.8 and 1.5 times respectively, resulting in high final bionanocomposite modulus of 22 and 18 GPa. This is extremely similar to the commercial product reinforcement capacity at this filler loading, which was of 1.6 (19 GPa).

For CNCs loadings in composite materials, it is commonly expected that higher aspect ratios will contribute to higher self-assembly and reinforcement capacities. This was observed to some extent for RTP CNCs, which showed high aspect ratio (13) and also stiffness when in incorporated to alginate (22 GPa). Both visual and mechanical properties support the fact that the lab-made toilet paper and wastewater-CNCs have a good potential as reinforcement agents being highly comparable to a commercial product.

These results together with the previous characterization of wastewater-CNCs confirm the good quality of this potential product.

## 5.5 Nanocellulose from Wastewater: Current Scenario

Nanocelluloses are environmentally friendly materials, with relative low cost, presenting high mechanical performance, among other outstanding properties. They also allow the production of advanced materials with tuneable properties, creating possibilities for novel applications to be developed. Thus, they have become a new trend internationally. There is a current focus on the use of forest, agricultural and industrial lignocellulosic residues as cellulose sources in the production of nanocellulose. Other tertiary sources of cellulose, such as sieved toilet paper, have not been explored until this point. It is attractive to investigate the production of nanocelluloses from recovered wastewater-cellulose due to its abundance at low economical and energetic cost, and for promoting an improved waste disposal. This could be done by means of a waste treatment or management with concomitant development of high value-added products that can provide large profits. Therefore, the implementation of FSF cellulose recovery aligned to nanocellulose production steps (mechanically or chemically assisted) should be contemplated (Figure 28).

Considering the nanocellulose production as a biorefinery concept, the use of wastewater solids rich in cellulose, such as FSF, from STPs becomes a highly attractive proposal. Toilet paper is a major constituent of wastewaters in western countries. In the Netherlands, around 1 kg toilet paper is used per person in a month (Ruiken et al., 2013). The considerable production of FSF could be used for medium to large-scale production of nanocellulose products. This leads to minimization of residues by means of waste treatment or management and also to the development of high value-added products that can provide large profits.

Bionanocomposites and bio-based products that are entirely wastewater-based also could be developed.

FSF as a cellulosic source is even more attractive than lignocellulosic biomass because fewer bleaching steps are required. Chemically, wood biomass and most agricultural biomass should present higher lignin-like content than wastewater solids. Moreover, the initial cellulose percentage of these agro-wastes is on average lower than what was found for FSF, with cellulose percentages varying from 25 % for olive husks to 56.5 % for sunflower shells and lignin contents as high as 50.4 % (García et al., 2016).

Figure 28 shows a theoretical scenario for the cellulose nanocrystals production from FSF. The combined STPs production of FSF in the Netherlands is in the order of 180-kton FSF $year^{-1}$ (Holland Trade and Invest, 2016). This value is similar to the annual production of a paper mill (www.efgf.nl). This can be considered a relevant amount of feedstock for nanocellulose production.

As a starting point, the cellulosic residue should be grinded and chemically treated for extracting the cellulose fraction with alkaline and chlorite-bleaching steps. An estimation of the chemical requirements for this step would point out the requirement of about 6.7 kg NaOH, 2.2 kg $NaClO_2$ and 7.5 L of $CH_3COOH$ for alkaline-bleaching steps per kg FSF. For the CNCs isolation with sulphuric acid, the requirement would be of 7.9 kg $H_2SO_4$ per FSF pulp. Using these conditions, a yield of 217 g of CNCs per kg FSF can be expected (22 % yield). This can be translated into the potential production number of around 39-kton CNCs (FSF) $year^{-1}$ (combined STPs FSF processing).

The required technology and chemicals should be readily assumed as annexed part of the main transformation mill, leading to

interesting profitable opportunities for the wastewater sector. At the moment, the selling price for nanocelluloses is incredibly attractive, with sources selling CNCs for up to USD$ 5,000 per kg (www.celluloselab.com). Moreover, the cost of production of CNCs (FSF), related to chemicals and water, is reasonable of around USD$ 536.18 per kg CNCs (FSF) produced. This cost estimation is the equivalent to USD$ 264,416,523 per day considering the value of 180-kton FSF year$^{-1}$.

In terms of operational costs, the operation of a full-scale CNCs production facility that uses FSF as feedstock is dictated by chemical consumption. Assuming the price of USD$ 5,000 per kg of CNCs, and about USD$ 0.50 per kg for sodium hydroxide, sulphuric acid, sodium chlorite and acetic acid, it becomes obviously clear that this is a business case that deserves closer attention. This in spite of the fact that a total of 24.4 kg of chemicals is needed to produce 1 kg of CNCs (FSF).

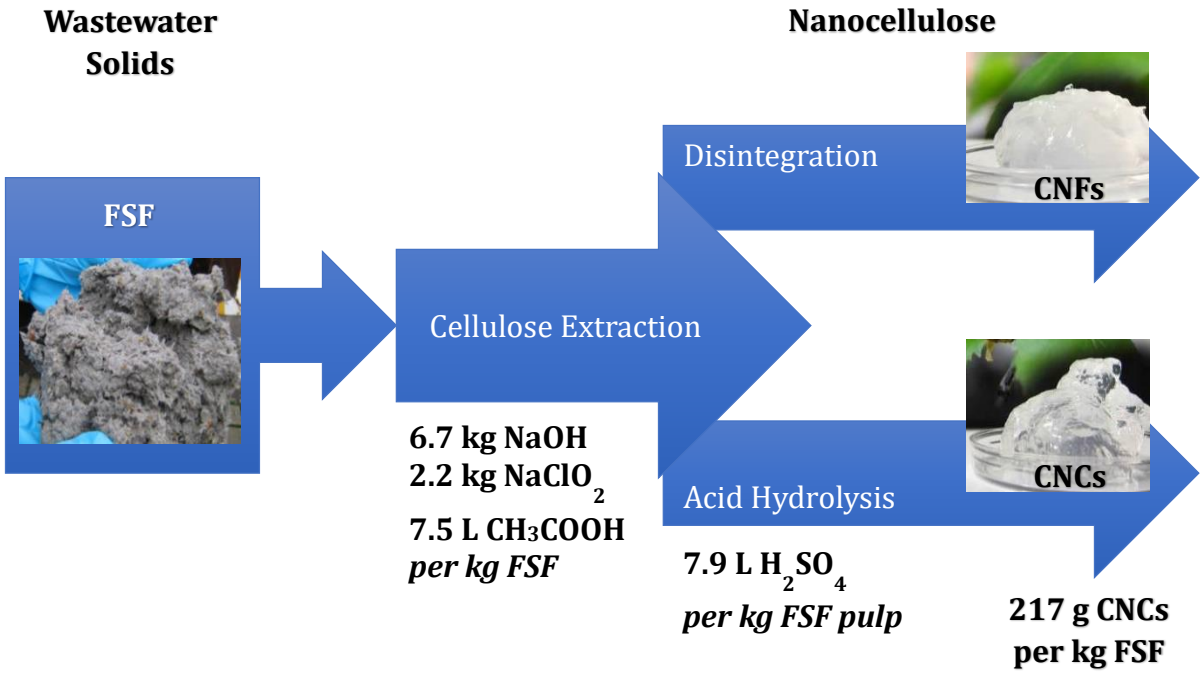


**Figure 28. A proposal of nanocellulose production scenario integrated with the cellulose recovery of FSF from STPs. Values are shown for CNCs production based on isolation data obtained in this study.**

# 6. CONCLUSIONS

An **uncomplicated cellulose extraction method** with alkaline and bleaching steps is possible for wastewater solids and sludge samples. The method is source-specific and alkaline and bleaching steps are adapted to the wastewater solid until obtaining a snowy-white cellulosic pulp. With this method, a detailed protocol for extracting and measuring cellulose in fine sieve fraction (FSF) and aerobic granular excess sludge (Nereda® Excess Sludge, NES) samples is now available.

Nanocellulose in the form of **cellulose nanocrystals (CNCs) can be isolated from toilet paper and wastewater cellulosic pulps** on a lab-scale. For that, a controlled acid hydrolysis of fibres is carried out, under which feasible conditions were first developed in this study. The wastewater-CNCs isolation needs more reproducibility and optimization but appears as a feasible process; since yields of CNCs isolation on a pulp basis can be above 30 %. **FSF is an attractive cellulose source** giving a higher overall yield of CNCs isolation (22 % g g $FSF^{-1}$) when compared to NES (4% g g $NES^{-1}$).

The suspensions of nanocrystals isolated from toilet paper and wastewater showed good water stability, with visible dynamic birefringent domains, typical of CNCs. These wastewater-CNCs present the morphology of rod-like particles, similar to a commercial sample, and are around 130 nm long and 10 nm wide (aspect ratio ranges from 10 to 14). The chemical groups on the surface of isolated nanocrystals are very much deriving from its original cellulose source and acidic hydrolysis treatment. The crystallinity of wastewater-CNCs was between 62 – 68 %, comparable to a commercial sample (73 %).

Thus, the aspect, morphology, chemical structure and crystallinity of **isolated-CNCs samples are convincingly similar to commercially available CNCs**.

Bionanocomposites of CNCs (commercial and wastewater) and alginate materials can be produced using a simple film casting method. The addition of commercial CNCs increases the stiffness of sodium alginate films up to 1.7 times, due to an increase in the ordering of the system. The resulting stiffness of Alginate-CNCs films with 50 % filler loading is high, in the order of 19 GPa. The resulting **increase in stiffness by toilet paper or wastewater-CNCs addition** ranges from 1.4 to 1.8 times. This **is extremely similar to the commercial product** reinforcement capacity. Thus, the quality of produced wastewater-CNCs is particularly good.

ALE with 50 % commercial CNCs addition results in a novel bionanocomposite with highly improved stiffness (18 GPa). This also shows a **great potential for nanocellulose as a filler**, with dramatic changes in mechanical properties even at low loadings, among other advantages. In a biorefinery perspective, this potential could also be further explored in combination with other wastewater-derived compounds.

The production of nanocellulose from FSF could be attractive due to its abundance at low economical and energetic cost. This alternative allows for an improved waste disposal with concomitant profit. Thus, the **implementation of FSF cellulose recovery aligned to nanocellulose production steps (mechanically or chemically assisted) should be contemplated**.

# 7. OUTLOOK

- The developed cellulose determination method opens doors for more research on the cellulose conversion in STPs and mass balances in AS or AGS systems.
- With regards to cellulose recovery, the effects of removing this slowly biodegradable substrate on AS and AGS treatment quality (aeration, sludge production, nutrient removal, dewaterability) is still unknown.
- The cellulose extraction method yields relatively clean, whitish fibres. Thus, new applications/products for cellulosic pulps from wastewater using this methodology could be developed. Improvements on the method and final quality of pulp can also be investigated.
- Studies over the optimal conditions for isolating CNCs from wastewater pulps at higher yields and with sound reproducibility should be carried out.
- More in depth characterization of toilet paper-based CNCs is required. The suggested key CNCs characterizations techniques are: charge density, functional groups, colloidal and thermal stability, crystallinity, morphology and self-assembly behaviour. Other extra information such as rheology, electromagnetic, and piezo-electric responsivity of CNCs, among other properties, could also be interesting depending on future applications designed for this material.
- Research on the production of CNFs from wastewater-extracted cellulosic pulps is highly recommended, since no chemicals are required for disintegrating the cellulosic pulp. Moreover, the production of CNFs from paper wastes is already a trend in Europe.
- The composition of novel, green, bio-based products when incorporating CNCs from wastewater should also be considered (CNCs-based nanoproduct development). This could even be extrapolated to the production of entirely wastewater-based products containing CNCs. This can be easily pictured by taking the example of ALE and commercial CNCs. Although not reported, a 50 % CNCs loading on Anammox EPS resulted in vivid red stiff films (19 GPa) with an interesting gelation phase.
- The complete business case for nanocellulose production from sieved toilet paper should be drawn considering other aspects not accounted for in this document (i.e. energy requirement, chemical consumption, required hardware, safety issues, etc.).

# 8. ACKNOWLEDGEMENTS

*"For beautiful eyes, look for the good in others; for beautiful lips, speak only words of kindness; and for poise, walk with the knowledge that you are never alone."*
*— Audrey Hepburn*

First, I would like to thank my primary supervisors prof. Mark van Loosdrecht and Mario Pronk (TUDelft, TNW) for all the support, freedom, inspiring talks and even the difficult talks during this 8 months journey at EBT. They were all very constructive and I surely learned a lot from you. The fact that you let me try all sort of ideas for the 'Nereda and cellulose' project was very positive to my personal development. I can definitely see now why every project related to you both blossoms. You are awesome.

I am also deeply thankful to my late-adopted supervisors from the chemical engineering side, prof. Stephen Picken and Jure Zlopasa (TNW). A special thanks to Jure Zlopasa for all the motivational talks, full of fun facts and for the precious help during all project steps (from defining and performing experiments to the interpretation of the data). The whole nanocellulose idea goes back to the first question I ever posed to you, about TGA analysis. The term nanocellulose stuck in the back of my mind and later we decided to try it for wastewater. It turned out surprisingly well! Without both of you, this project would have never been feasible. Thank you for all the excitement with the 'CNC fun stuff'.

At Waternet, I could always count on the opinion of Chris Reijken, the cellulose expert. I was very lucky I could discuss methods and test new approaches with you. Thanks for all the sharing and trips. I could build up new knowledge simply because you had already acquired quite some useful information.

Essential to this research was also the assistance of Yuemei Lin, Ben Abbas, Mitchel Geleijnse, Dimitry Sorokin, Udo van Dongen, Marc Strampaad, Linda Otten, and Stef van Hateren from TNW. I am also grateful to Merle de Kreuk (TUDelft, CiTG) for all the feedback and guidance. I also received great help from Ron Penners (CiTG), who helped with my milling and papermaking ideas. Thank you for that. At ChemE, TNW, the aid from Ben Norder, Marcel Bus, Duco Bostma, Vincent Le Sage was also imperative. Credits to Bob van Laarhoven (RUG) for teaching me his special method. For all the openness and practical support, thanks to Pascal Kamminga and Mark Stevens. Credits are also given to Richard Berry, from CelluForce™, for the material donation.

To all the friends I have made at EBT-TNW, I want to say 'Thank you very much' for the advices, moments of laugher, sharing of ideas, cakes, and coffees. During this thesis, I had to enter new fields several times without knowing if it would yield any result. I could find in you the strength to continue. Special thanks are dedicated to Ru, Cuiji, Jelmer, Laurens, Michel, Rick, Michelle, Tiago, Demi, Hugo, Bradley, Freddy, Pascalle, Stefanie, Valerie, Lenno, Danny, Ingrid, Jules, Viktor, Simon, Marissa and other MSc students, PhDs and Staff of EBT. From Wetsus, I highly appreciate the counselling given by Nelleke and friend Vanessa.

Finally yet importantly, I would like to thank my family and friends in the Netherlands and in Brazil for all the motivation and listening. Yuri for the nice times shared at the library. Special warm thanks to my mom Nereide, who always supported me so much in my educational and professional goals. Also to my father José, for being such an incredible person and my first inspiration for studying water technology. Very special thanks for all the help provided by my much-loved boyfriend David Moed, one of the most caring and enthusiastic guys on this planet, and to the Moed family.

# REFERENCES


APHA/AWWA/WEF, 2012. Standard Methods for the Examination of Water and Wastewater, Standard Methods. doi:ISBN 9780875532356

Azizi Samir, M.A.S., Alloin, F., Dufresne, A., 2005. Review of recent research into cellulosic whiskers, their properties and their application in nanocomposite field. Biomacromolecules 6, 612–626. doi:10.1021/bm0493685

Azman, S., 2016. Anaerobic digestion of cellulose and hemicellulose in the presence of humic acids. Wageningen University.

Balkom, N. Van, 2012. Energy production from fine sieve material for the benefit of the sewer mining concept. Delft University of Technology.

Bennion, B.J., Daggett, V., 2003. The molecular basis for the chemical denaturation of proteins by urea. Proc. Natl. Acad. Sci. U. S. A. 100, 5142–7. doi:10.1073/pnas.0930122100

Bondeson, D., Mathew, A., Oksman, K., 2006. Optimization of the isolation of nanocrystals from microcrystalline cellulose by acid hydrolysis. Cellulose 13, 171–180. doi:10.1007/s10570-006-9061-4

Börjesson, M., Westman, G., 2015. Crystalline Nanocellulose-Preparation, Modification, and Properties, in: Cellulose - Fundamental Aspects and Current Trends. pp. 159–191.

Camarero-Espinosa, S., Endes, C., Mueller, S., Petri-Fink, A., Rothen-Rutishauser, B., Weder, C., Clift, M., Foster, E., 2016. Elucidating the Potential Biological Impact of Cellulose Nanocrystals. Fibers 4, 21. doi:10.3390/fib4030021

CelluForce, n.d. Core properties of NanoCrystalline Cellulose | Our Products [WWW Document]. URL http://www.celluforce.com/en/products/core-properties/ (accessed 4.16.17).

Chai, W., Udén, P., 1998. An alternative oven method combined with different detergent strengths in the analysis of neutral detergent fibre. Anim. Feed Sci. Technol. 74, 281–288. doi:10.1016/S0377-8401(98)00187-4

Chen, Y.W., Lee, H.V., Juan, J.C., Phang, S.M., 2016. Production of new cellulose nanomaterial from red algae marine biomass Gelidium elegans. Carbohydr. Polym. 151, 1210–1219. doi:10.1016/j.carbpol.2016.06.083

Cirtiu, C.M., Dunlop-Brière, A.F., Moores, A., 2011. Cellulose nanocrystallites as an efficient support for nanoparticles of palladium: application for catalytichydrogenation and Heck coupling under mild conditions. Green Chem. 13, 288–291. doi:10.1039/C0GC00326C

Das, K., Ray, D., Bandyopadhyay, N.R., Ghosh, T., Mohanty, A.K., Misra, M., 2009. A study of the mechanical, thermal and morphological properties of microcrystalline cellulose particles prepared from cotton slivers using different acid concentrations. Cellulose 16, 783–793. doi:10.1007/s10570-009-9280-6

dos Santos, F.A., Iulianelli, G.C. V, Tavares, M.I.B., 2016. The Use of Cellulose Nanofillers in Obtaining Polymer Nanocomposites: Properties, Processing, and Applications. Mater. Sci. Appl. 7, 257–294. doi:10.4236/msa.2016.75026

Doucet, S.M., Meadows, M.G., 2009. Iridescence: a functional perspective. J. R. Soc. Interface 6, S115–S132. doi:10.1098/rsif.2008.0395.focus

Dufresne, A., 2013. Nanocellulose: A new ageless bionanomaterial. Mater. Today 16, 220–227. doi:10.1016/j.mattod.2013.06.004

Felz, S., Al-Zuhairy, S., Aarstad, O.A., van Loosdrecht, M.C.M., Lin, Y.M., 2016. Extraction of Structural Extracellular Polymeric Substances from Aerobic Granular Sludge. J. Vis. Exp. e54534. doi:10.3791/54534

García, A., Gandini, A., Labidi, J., Belgacem, N., Bras, J., 2016. Industrial and crop wastes: A new source for nanocellulose biorefinery. Ind. Crops Prod. 93, 26–38. doi:10.1016/j.indcrop.2016.06.004

Ghasimi, D.S.M., 2016. Bio-methanation of fine sieved fraction sequestered from raw municipal sewage. Delft University of Technology.

Ghasimi, D.S.M., Tao, Y., de Kreuk, M., Abbas, B., Zandvoort, M.H., van Lier, J.B., 2015a. Digester performance and microbial community changes in thermophilic and mesophilic sequencing batch reactors fed with the fine sieved fraction of municipal sewage. Water Res. 87, 483–493. doi:10.1016/j.watres.2015.04.027

Ghasimi, D.S.M., Tao, Y., de Kreuk, M., Zandvoort, M.H., van Lier, J.B., 2015b. Microbial population dynamics during long-term

sludge adaptation of thermophilic and mesophilic sequencing batch digesters treating sewage fine sieved fraction at varying organic loading rates. Biotechnol. Biofuels 8, 171. doi:10.1186/s13068-015-0355-3

Giesen, A., de Bruin, L.M.M., Niermans, R.P., van der Roest, H.F., 2013. Advancements in the application of aerobic granular biomass technology for sustainable treatment of wastewater. Water Pract. Technol. 8, 47–54. doi:10.2166/wpt.2013.007

Giesen, A., Loosdrecht, M. Van, Pronk, M., Robertson, S., 2017. Aerobic Granular Biomass Technology : recent performance data, lessons learnt and retrofitting conventional treatment infrastructure. Water online.

Giri, J., Adhikari, R., 2012. A brief review on extraction of nanocellulose and its application. Bibechana 9, 81–87.

Habibi, Y., Lucia, L.A., Rojas, O.J., 2010. Cellulose nanocrystals: Chemistry, self-assembly, and applications. Chem. Rev. 110, 3479–3500. doi:10.1021/cr900339w

Hentze, H.P., 2010. From nanocellulose science towards applications. VTT Tied. - Valt. Tek. Tutkimusk. 71–78.

Holland Trade and Invest, 2016. Dutch open first bike path made from toilet paper [WWW Document]. URL https://www.hollandtradeandinvest.com/latest/news/2016/september/23/dutch-open-first-bike-path-made-from-toilet-paper (accessed 4.2.17).

Holt, B.L., Stoyanov, S.D., Paunov, V.N., 2010. Novel anisotropic materials from functionalised colloidal cellulose and cellulose derivatives 10058–10070. doi:10.1039/c0jm01022g

Honda, S., Miyata, N., Iwahori, K., 2002. Recovery of biomass cellulose from waste sewage sludge. J. Mater. Cycles Waste Manag. 4, 46–50. doi:10.1007/s10163-001-0054-y

Innventia, n.d. Nanocellulose - Innventia [WWW Document]. URL http://www.innventia.com/en/Our-Expertise/New-materials/Nanocellulose/ (accessed 4.16.17).

Jiang, F., Hsieh, Y. Lo, 2015. Cellulose nanocrystal isolation from tomato peels and assembled nanofibers. Carbohydr. Polym. 122, 60–68. doi:10.1016/j.carbpol.2014.12.064

Jonoobi, M., Oladi, R., Davoudpour, Y., Oksman, K., Dufresne, A., Hamzeh, Y., Davoodi, R., 2015. Different preparation methods and properties of nanostructured cellulose from various natural resources and residues: a review. Cellulose 22, 935–969. doi:10.1007/s10570-015-0551-0

Kalia, S., Dufresne, A., Cherian, B.M., Kaith, B.S., Avérous, L., Njuguna, J., Nassiopoulos, E., 2011. Cellulose-based bio- and nanocomposites: A review. Int. J. Polym. Sci. 2011. doi:10.1155/2011/837875

Kallel, F., Bettaieb, F., Khiari, R., García, A., Bras, J., Chaabouni, S.E., 2016. Isolation and structural characterization of cellulose nanocrystals extracted from garlic straw residues. Ind. Crops Prod. 87, 287–296. doi:10.1016/j.indcrop.2016.04.060

Kim, J.H., Shim, B.S., Kim, H.S., Lee, Y.J., Min, S.K., Jang, D., Abas, Z., Kim, J., 2015. Review of nanocellulose for sustainable future materials. Int. J. Precis. Eng. Manuf. - Green Technol. 2, 197–213. doi:10.1007/s40684-015-0024-9

Koskinen, T.M., Qvintus, P., Ritschkoff, C., Tammelin, T., Pere, J., 2013. Nanocellulose materials - preparation, properties, uses 29.

Krenchel, H., 1964. Fibre Reinforcement, in: Akademisk Forlag (Ed.), . Copenhagen.

Lagerwall, J.P.F., Schütz, C., Salajkova, M., Noh, J., Hyun Park, J., Scalia, G., Bergström, L., 2014. Cellulose nanocrystal-based materials: from liquid crystal self-assembly and glass formation to multifunctional thin films. NPG Asia Mater. 6, e80. doi:10.1038/am.2013.69

Lam, E., Male, K.B., Chong, J.H., Leung, A.C.W., Luong, J.H.T., 2012. Applications of functionalized and nanoparticle-modified nanocrystalline cellulose. Trends Biotechnol. 30, 283–290. doi:10.1016/j.tibtech.2012.02.001

Lin, Y., de Kreuk, M., van Loosdrecht, M.C.M., Adin, A., 2010. Characterization of alginate-like exopolysaccharides isolated from aerobic granular sludge in pilot-plant. Water Res. 44, 3355–3364. doi:10.1016/j.watres.2010.03.019

Lin, Y.M., Nierop, K.G.J., Girbal-Neuhauser, E., Adriaanse, M., van Loosdrecht, M.C.M., 2015. Sustainable polysaccharide-based biomaterial recovered from waste aerobic granular sludge as a surface coating material. Sustain. Mater. Technol. 4, 24–29. doi:10.1016/j.susmat.2015.06.002

Liu, C., Li, B., Du, H., Lv, D., Zhang, Y., Yu, G., Mu, X., Peng, H., 2016. Properties of nanocellulose isolated from corncob residue using sulfuric acid, formic acid, oxidative and mechanical methods. Carbohydr. Polym. 151, 716–724. doi:10.1016/j.carbpol.2016.06.025

Liu, D., Chen, X., Yue, Y., Chen, M., Wu, Q., 2011.

Structure and rheology of nanocrystalline cellulose. Carbohydr. Polym. 84, 316–322. doi:10.1016/j.carbpol.2010.11.039

Lu, P., Hsieh, Y. Lo, 2012. Cellulose isolation and core-shell nanostructures of cellulose nanocrystals from chardonnay grape skins. Carbohydr. Polym. 87, 2546–2553. doi:10.1016/j.carbpol.2011.11.023

Markstedt, K., Mantas, A., Tournier, I., Martínez Ávila, H., Hägg, D., Gatenholm, P., 2015. 3D bioprinting human chondrocytes with nanocellulose-alginate bioink for cartilage tissue engineering applications. Biomacromolecules 16, 1489–1496. doi:10.1021/acs.biomac.5b00188

Oksman, K., Etang, J.A., Mathew, A.P., Jonoobi, M., 2011. Cellulose nanowhiskers separated from a bio-residue from wood bioethanol production. Biomass and Bioenergy 35, 146–152. doi:10.1016/j.biombioe.2010.08.021

Oksman, K., Mathew, A.P., Jonoobi, M., Siqueira, G., Hietala, M., Aitomäki, Y., 2013. Cellulose nanofiber isolated from industrial side-streams 187–190.

Onsager, L., 1949. The effects of shapes on the interaction of colloidal particles. Ann. N. Y. Acad. Sci. 51, 627–659. doi:10.1111/j.1749-6632.1949.tb27296.x

Ostiguy, C., Emond, C., n.d. Nanocellulose prepared by acid hydrolysis of isolated cellulose from sugarcane bagasse. doi:10.1088/1757-899X/107/1/012045

Paulsrud, B., Rusten, B., Aas, B., 2014. Increasing the sludge energy potential of wastewater treatment plants by introducing fine mesh sieves for primary treatment. Water Sci. Technol. 69, 560–565. doi:10.2166/wst.2013.737

Poletto, M., Ornaghi Júnior, H.L., Zattera, A.J., 2014. Native cellulose: Structure, characterization and thermal properties. Materials (Basel). 7, 6105–6119. doi:10.3390/ma7096105

Pronk, M., 2016. Aerobic Granular Sludge: Effect of Substrate on Granule Formation. Delft University of Technology.

Pronk, M., de Kreuk, M.K., de Bruin, B., Kamminga, P., Kleerebezem, R., van Loosdrecht, M.C.M., 2015. Full scale performance of the aerobic granular sludge process for sewage treatment. Water Res. 84, 207–217. doi:10.1016/j.watres.2015.07.011

Reddy, J.P., Rhim, J.W., 2014. Characterization of bionanocomposite films prepared with agar and paper-mulberry pulp nanocellulose. Carbohydr. Polym. 110, 480–488. doi:10.1016/j.carbpol.2014.04.056

Reid, M.S., Villalobos, M., Cranston, E.D., 2016. Benchmarking Cellulose Nanocrystals: From the Laboratory to Industrial Production and Applications. Press. doi:10.1021/acs.langmuir.6b03765

Rhim, J.W., Reddy, J.P., Luo, X., 2015. Isolation of cellulose nanocrystals from onion skin and their utilization for the preparation of agar-based bio-nanocomposites films. Cellulose 22, 407–420. doi:10.1007/s10570-014-0517-7

Risteen, B.E., Blake, A., Mcbride, M.A., Rosu, C., Park, J.O., Srinivasarao, M., Russo, P.S., Reichmanis, E., 2017. Enhanced Alignment of Water-Soluble Polythiophene Using Cellulose Nanocrystals as a Liquid Crystal Template. doi:10.1021/acs.biomac.7b00121

Römgens, B., Kruizinga, E., 2013. Wastewater management roadmap towards 2030: A sustainable approach to the collection and treatment of wastewater in the Netherlands. 36.

Rosa, M.F., Medeiros, E.S., Malmonge, J.A., Gregorski, K.S., Wood, D.F., Mattoso, L.H.C., Glenn, G., Orts, W.J., Imam, S.H., 2010. Cellulose nanowhiskers from coconut husk fibers: Effect of preparation conditions on their thermal and morphological behavior. Carbohydr. Polym. 81, 83–92. doi:10.1016/j.carbpol.2010.01.059

Ruiken, C.J., Breuer, G., Klaversma, E., Santiago, T., van Loosdrecht, M.C.M., 2013. Sieving wastewater - Cellulose recovery, economic and energy evaluation. Water Res. 47, 43–48. doi:10.1016/j.watres.2012.08.023

Rusten, B., Odegaard, H., 2006. Evaluation and testing of fine mesh sieve technologies for primary treatment of municipal wastewater. Water Sci. Technol. 54, 31–38. doi:10.2166/wst.2006.710

Segal, L., Creely, J.J., Martin, A.E., Conrad, C.M., 1959. An Empirical Method for Estimating the Degree of Crystallinity of Native Cellulose Using the X-Ray Diffractometer. Text. Res. J. 29, 786–794. doi:10.1177/004051755902901003

Silvério, H.A., Flauzino Neto, W.P., Dantas, N.O., Pasquini, D., 2013a. Extraction and characterization of cellulose nanocrystals from corncob for application as reinforcing agent in nanocomposites. Ind. Crops Prod. 44, 427–436. doi:10.1016/j.indcrop.2012.10.014

Silvério, H.A., Flauzino Neto, W.P., Pasquini, D., 2013b. Effect of incorporating cellulose nanocrystals from corncob on the tensile,

thermal and barrier properties of poly(vinyl alcohol) nanocomposites. J. Nanomater. 2013. doi:10.1155/2013/289641

STOWA, 2016. Levenscyclusanalyse van grondstoffen uit rioolwater. Rapport 22, 181.

STOWA, 2013. Vezelgrondstof uit Zeefgoed. 63.

STOWA, 2010. Influent fijnzeven in RWZI's. Stowa 110.

Ureña-Benavides, E.E., Brown, P.J., Kitchens, C.L., 2010. Effect of jet stretch and particle load on Cellulose nanocrystal-alginate nanocomposite fibers. Langmuir 26, 14263–14270. doi:10.1021/la102216v

Van Der Roest, H., Van Loosdrecht, M., Langkamp, E.J., Uijterlinde, C., 2015. Recovery and reuse of alginate from granular Nereda sludge. Water21 Mag. 21.

Van Soest, P.J.., Wine, R.H., 1967. Use of Detergents in the Analysis of Fibrous Feeds. IV. Determination of Plant Cell-Wall Constituents. J. A.O.A.C. 50, 50–55. doi:10.1016/j.ijhydene.2012.08.110

Wang, Q.Q., Zhu, J.Y., Reiner, R.S., Verrill, S.P., Baxa, U., McNeil, S.E., 2012. Approaching zero cellulose loss in cellulose nanocrystal (CNC) production: Recovery and characterization of cellulosic solid residues (CSR) and CNC. Cellulose 19, 2033–2047. doi:10.1007/s10570-012-9765-6

Wang, X.-J., Zhou, Q.-F., 2004. Liquid crystalline polymers. World Scientific.

Xu, X., Zhou, J., Jiang, L., Lubineau, G., Ng, T., 2016. Highly transparent, low-haze, hybrid cellulose nanopaper as electrodes for flexible electronics 12294–12306. doi:10.1039/c6nr02245f

Zlopasa, J., Norder, B., Koenders, E.A.B., Picken, S.J., 2015. Origin of highly ordered sodium alginate/montmorillonite bionanocomposites. Macromolecules 48, 1204–1209. doi:10.1021/ma502147m

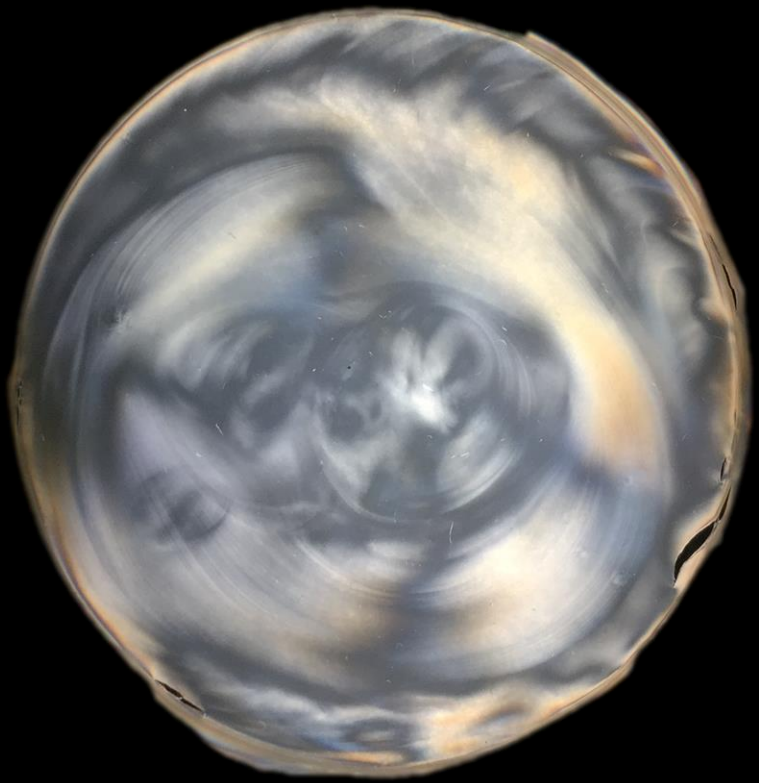

**Cellulose NanoCrystals – Alginate film**

**Cross polarisation**

# APPENDIX I – NANOCELLULOSE THEORY

This section defines nanocellulose and reviews its main properties. First, useful terms used in this thesis and for describing of nanocellulose are outlined.

## Useful terms

**Isotropy** is the property of solids to show similar physical properties in all directions.

**Anisotropy** is the property of solids to show different physical properties with different directions or crystallographic orientations.

**Biphasic regime** is the intermediary state between isotropic-anisotropic regimes.

**Chiral Nematic Liquid Crystal:** Liquid crystal is a state of matter where there are domains of order (anisotropy) within a fluid, or even, fluids that have an orientational order with no (or limited) positional order (1-D or 2-D) (Wang and Zhou, 2004). A liquid crystal is chiral nematic when it forms a helical structure with a chiral centre. Crystals organise in layers with no positional ordering within layers, but a director axis, which varies with layers (Figure 1B, Appendix I). The variation of the director axis is periodic and corresponds to the distance over which a full rotation of 360 ° is completed (known as the pitch) (Dufresne, 2013).

**Birefringence** is the optical phenomenon of an anisotropic material having a refractive index dependent on the polarisation and propagation direction of light. The optical property is responsible for the double refraction of a ray of light. When the light ray is incident upon a birefringent material, it is split by polarisation into two rays taking slightly different paths.

## Nanocellulose

Despite being the most abundant natural polymer on Earth, it is only quite recently that cellulose has gained importance as a nanostructured material, called nanocellulose. After intensive technological and process developments, nanocellulose production on a large scale is already a reality with growing interest in commercialization (García et al., 2016; Reid et al., 2016). Nanocellulose covers the range of materials derived from cellulose with at least one dimension in the nanometer range (<100 nm). Nanocellulose-based materials are sustainable, renewable and, as far as investigated, present limited toxicity (Camarero-Espinosa et al., 2016). Hence, they have the potential to be exceptional green products, with many useful and outstanding properties.

Two general classes of nanocellulose that can be obtained depending on the production method used: cellulose nanofibres (CNFs) and cellulose nanocrystals (CNCs).

### *CNFs*

CNFs are long and flexible nanoscale fibres, composed of more or less individualised cellulose microfibrils and consisting of alternating crystalline and amorphous strings (Liu et al., 2016). Cellulosic pulp fibres are generally deeply disintegrated by mechanical action under heat (homogenization at 70-80 °C) to produce CNFs (García et al., 2016). The resulting diluted dispersion is gel-like in appearance. Other mechanical processes, such as refining and homogenising, micro-fluidization, grinding, cryo-crushing, and high-intensity sonication, have

been developed to limit energy consumption during the CNFs preparation and to favour more homogenous nanomaterial (dos Santos et al., 2016; García et al., 2016). The main advantages of CNFs isolation are that no additives are required, the surface charge is the same as of the primary material, and very high yields (>90%) can be achieved (Jonoobi et al., 2015). The disadvantages are that often bundles of micro- and nano-scale materials are obtained rather than individual microfibrils, limiting its potential as a reinforcement agent. In addition, the preparation is often energy-intensive (especially in batch processes). Alternatively to traditional methods, cryo-crushing and sonication could be used although they are quite difficult to up-scale. In the last years, chemical and enzymatic treatments have been proposed to reduce the energy requirement during the disintegration process (García et al., 2016). Moreover, some plant sources or industrial crops can be more easily defibrillated and, therefore, with lower energy requirements the CNFs can be extracted (less mechanical cycles required) (Oksman et al., 2013).

***CNCs***

CNCs are the focus of this study and, therefore, described with more detail. CNCs can be isolated in an aqueous suspension with a controlled strong acid hydrolysis treatment of cellulosic fibres that allows for the selective degradation of amorphous domains and, thus, longitudinal cutting of the microfibrils (Börjesson and Westman, 2015). The individual nanocellulose crystallites are released in suspension after mechanical treatment (sonication). Different strong acids have been shown to degrade cellulose fibres successfully, but hydrochloric and sulfuric acids have been extensively used (Habibi et al., 2010). An important reason for using sulfuric acid as a hydrolyzing agent is that the reaction results in the grafting of anionic sulphate ester groups on the CNCs surface (Wang et al., 2012). These negatively charged sulphate groups induce the formation of a negative electrostatic layer covering the surface of crystals and promote their dispersion in water.

CNCs have a high aspect ratio and the morphology of highly stiff rods or needles (Börjesson and Westman, 2015; García et al., 2016). Their geometrical dimensions depend on the origin of the cellulose substrate and hydrolysis conditions (García et al., 2016). The average crystallite is usually of the order of a couple of hundred nanometers long and a couple of nanometers wide (Dufresne, 2013; Lam et al., 2012).

Acid hydrolysis is the traditional way of isolating CNCs. However, other processes allow the release of crystalline domains from cellulose have more recently been reported, including enzymatic hydrolysis treatment, TEMPO oxidation, hydrolysis with a volatile acid, and treatment with ionic liquids (Dufresne, 2013).

## Main Properties of CNCs

CNCs interact with one another based on their size, charge and shape. Since nanoparticles are at a scale where they are in constant motion, the resulting energy allows the particles to self-organise in a fluid (Liquid Crystal) (Wang and Zhou, 2004). At a critical concentration, there is a phase separation into a regime where both the anisotropic and isotropic domains co-exist (Biphasic). As the suspension is further concentrated, more CNCs becomes organised until a film with only an ordered structure remains on a given surface (Fully Chiral Nematic Liquid Crystal). When dry, this ordered structure is preserved, and it creates a hard, smooth and tightly packed film. The packing is particularly tight because the crystals contain a twist, allowing the rods to interlock efficiently.

CNCs self-assembly, states, and visual aspects are depended on concentration. At around 2% w/v, nanoparticle suspensions can be opalescent but transparent. They show some viscosity but are an indefinitely stable colloid and will readily not sink to the bottom. When observed between crossed polarizers, the CNCs dispersion shows the formation of birefringent domains due to dynamic, layered structures within the fluid (Figure 1, Appendix I.). At concentrations at least above 3.5% w/v CNCs, suspensions fully behave as an anisotropic liquid crystal having static orientation order. This chiral nematic or cholesteric structures in the anisotropic phase consist of stacked planes of CNCs rods aligned along a vector (director), with the orientation of each director vector rotated about the perpendicular axis from one plane to the other as shown in Figure 1, Appendix I. Furthermore, in an intermediate gel-like state (around 20% CNCs or less), it resembles a semi-solid.

During drying to solid state, the needle-shaped CNCs auto-assembly is preserved, and - after complete drying – they form solids with structural colour (depicted in page 29 and in the covers of this thesis between cross polarisers). Thus, iridescent films with colour variations depending on the angle of visualisation and illumination can be created. The colour is generated by the light interaction with the layered structures of CNCs. Many animals and plants use structural colour to create vibrant, iridescent and long-lasting displays (CelluForce, n.d.; Doucet and Meadows, 2009). The periodicity of CNCs is of the order of the wavelength of light, which is reflected resulting in coloured constructive interference. Because the distance of half a pitch exists in between the layers, the reflected light is polarised.

Due to its high crystallinity, CNCs are inherently strong. Each crystallite has a stiffness that is of the order of 150 GPa and a tensile strength of the order of 10 GPa (Silvério et al., 2013b). These numbers are comparable to those of Kevlar as well as hard metals and their alloys (Dufresne, 2013). Additionally, CNCs are exceptionally light relative to other nanoparticles, with density around 1.6 g $cm^{-3}$; and can be thermally stable up to 250 °C (Cirtiu et al., 2011; Dufresne, 2013).

Also, fluids containing CNC are shear thinning, which means their viscosity decreases with the application of shear. This thixotrophy property provides the basis for several types of application. The degree of shear thinning is dependent on the rigidity, charge and shape of the crystal. CNCs isolation or modification methods that alter these aspects will also affect the material's rheology (Liu et al., 2011).

A CNC is comprised of a linear glucose polymer that is rich in oxygen (hydroxyl groups). These hydroxyl groups develop the hydrogen bonds that give the CNC its inherent strength while providing a reactive surface of hydroxyl groups on two of the crystal's faces. Though not all of the hydroxyl groups are equally reactive and accessible, they adequately allow a multitude of reactions. The hydroxyl groups are also the reason why CNCs, unlike carbon nanotubes and other materials, are inherently hydrophilic. In the CNCs surface, acidic groups can also be attached, which allows for reaction with a variety of bases (Lam et al., 2012). CNCs permits the bonding of a variety of hydrophobic structures being compatible with a broad range of solvents and polymer matrices.

CNCs are anionic materials due to its negatively charged functional groups, which, in turn, transmits electromagnetic properties to the crystal and derivatives. The negative charge imparts electrical conductive properties to the suspension, which then becomes an electrolyte. This electrolyte imparts electrophoretic mobility and allows the particle to migrate in an electric field.

Moreover, as the CNC is a particle with an aspect ratio, it orients itself in electromagnetic fields even that of the Earth (CelluForce, n.d.). The charge also passes on strong dielectric properties. Solid structures also exhibit piezoelectric effects, where the application of pressure can generate an electrical charge (Kim et al., 2015; Reid et al., 2016).

With regards environmental health and safety, preliminary work on the toxicity of as-produced nanocellulose have shown minimal adverse health effects from oral or dermal studies (Camarero-Espinosa et al., 2016). Nevertheless, pulmonary and cytotoxicity studies have yielded conflicting results (CelluForce, n.d.). The toxicity of various nanocelluloses is an area of active study. Life cycle analyses have been used to assess environmental impact and for adapting manufacturing process to achieve best practices for mass production.

## Summary of Main Properties of CNCs

CNCs size, surface morphology and charge lead to a distinctive behaviour in suspensions. Hence, CNCs are considered a new super-material due to special properties. Some of these are: (a) high surface area, (b) self-assembly, (c) high inherent mechanical strength, (d) thixotropy, (e) active chemical surface, (f) thermal stability, (g) solid phase with structural colour (photonic), and (h) electro-magnetism (Börjesson and Westman, 2015; CelluForce, n.d.). Moreover, CNCs are light having a density around 1.6 g $cm^{-3}$ (Dufresne, 2013).

These properties are shortly described:

a) CNCs are rod-like and have high surface area resulting in the size of its separated crystalline particles. This is a function of the source of the cellulose and the process of extraction.
b) CNCs interact with one another to form a structured liquid crystal;
c) CNCs are strong inherently because of its high crystallinity;
d) CNCs fluids exhibit thixotropy (shear thinning), which means they decrease in viscosity with the application of shear;
e) CNCs surface is mainly comprised of hydroxyl ($OH^-$) and acidic groups ($H^+$) that are reactive and can be functionalized with other chemicals;
f) CNCs are thermally stable to 200-250°C;
g) CNCs are photonic showing structural colour as the ordered crystalline suspension solidifies. Its colour is created by the interaction of light with the layered structures that are developed;
h) CNCs are charged with anionic functional groups on its surface what results in transmitted electromagnetism to the crystals.

These core properties can be used to improve products.

## Nanocellulose Applications

Nanocellulose can be a bio-based, renewable resource instead of plastics or other fossil-fuel derived products. They can increase the stiffness and reduce the weight of materials. These characteristics are especially interesting to the automotive and aerospace industries (Azizi Samir et al., 2005). As previously mentioned, CNCs exhibit high mechanical properties. Nanocellulose young's modulus is about 150 GPa whereas that of steel is 210 and aramid Kevlar is of 124 (Börjesson and Westman, 2015). In composites, nanocellulose additions have been shown to dramatically alter the thermo-mechanical and dynamic-mechanical properties of many matrix polymers even at low filler loading (Dufresne, 2013). Such properties mainly originate from the high stiffness of crystalline cellulose, the tiny dimensions and high aspect ratio of the nanoparticles, and the high reactivity of cellulose. The high reactivity of the surface makes CNC customizable for various applications. Moreover, the nano-dimensional diameters of CNCs result in lower light scattering compared with the large sizes of pulp fibres, making good transmittance and low haze CNCs-composites possible (Xu et al., 2016). Their heat stability also allows for high-temperature applications (Hentze, 2010).

The highly ordered crystalline structure of CNCs persists after drying, resulting in interesting optical phenomena. By tailoring the CNC suspension and composite processing properties, it is possible to control the colour of the dried film. The iridescent/pearlescent optical property of films could be useful for optical, technical and decorative applications especially in the glass, automotive, and textile industries (Lagerwall et al., 2014; Silvério et al., 2013a). Other examples are the use of CNCs in security paper or mirror-less lasing (Lagerwall et al., 2014).

There are a wide variety of possible requests for nanocellulose. In the manufacture of both paper and board, nanocellulose could be used as a strengthening agent in paper with a high filler content (Koskinen et al., 2013). Other areas of application may be surface sizing and coating, e.g. as a barrier material in food packaging (against oxygen, water vapour, grease/oil) (Reddy and Rhim, 2014). There are also applications in the areas of biosensors, catalysis, photovoltaics, drug delivery, food thickeners, emulsions, dispersions, oil recovery applications, cosmetics, pharmaceuticals, and electronics (Innventia, n.d.; Lam et al., 2012).

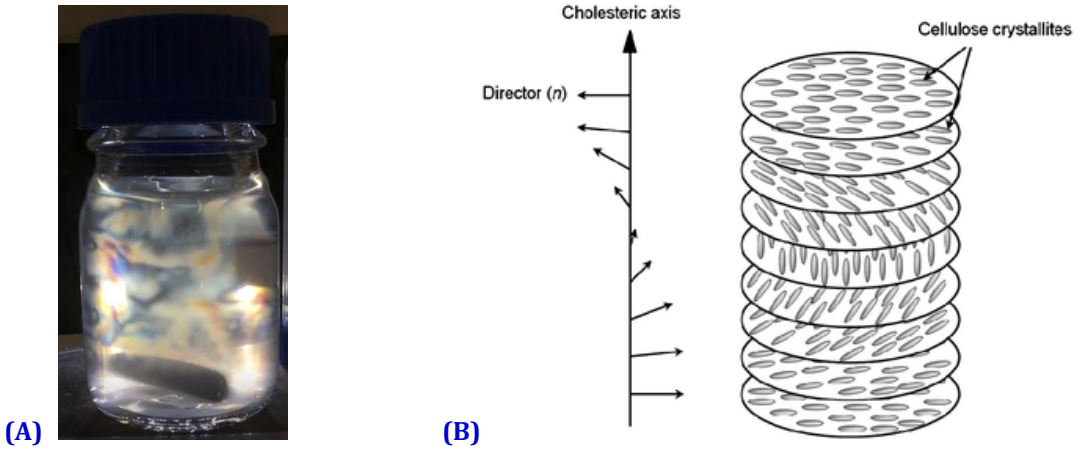


**Figure 1. (A) Birefringence of a 2% CNCs suspension observed with cross polarisation. (B) Scheme of the chiral nematic order displayed by cellulose crystallites. The director rotates along the cholesteric axis between successive layers of parallel cellulose crystals (Holt et al., 2010).**

# APPENDIX II – CELLULOSE EXTRACTION PROTOCOL

## Extraction and Measurement of Cellulose in Wastewater Solids

The following detailed protocol consists of thermal extraction steps to remove impurities covering the external surface of cellulose fibres from wastewater or sludge sources. In short, the samples are dried, blended and extracted from water-soluble compounds (carbohydrates, proteins, fats), alkaline-soluble compounds - such as most sludge, hemicellulose and some fat and lignin - and, finally, remaining hemicellulose and lignin-like compounds via bleaching. The resulting white pulp is rich in cellulose (over 86%, this thesis) and assumed to be a fair estimative of the initial cellulosic content of the wastewater solids sample. The procedure used varies per cellulose source. FSF, NES and AS samples were successfully investigated. The procedure is explained in detail for FSF and NES, which are the focus of this thesis.

### Materials & Equipment

**Chemicals:**

a) Sodium hydroxide (NaOH)
b) Sodium Chlorite ($NaClO_2$, 80% purity)
c) Glacial acetic acid (≥99.5%)

**Equipment:**

d) Blender (Kitchen) or homogenizer
e) Hot plate with temperature sensor
f) Sieves (45 µm mesh)
g) Oven at 60 °C
h) Scale (4 decimals precision)

Before the assay, ideally, estimate the cellulose content of the raw material to obtain at least around **2 g of cellulose after extraction**. This is done to promote fibre junction into a sort of pulp and avoid fibre leaks. All chemical extractions in open recipients should be performed under a fume hood.

### Protocol - Fine Sieve Fraction

The FSF end-reaction mixtures after each protocol step and filtrates can be visualised in Figure 1, Appendix II.

**Removal of water-soluble compounds**

1) Dry the FSF at 60°C for one day and weight approximately 10 grammes dry solids*;
2) Cut the dry material in in small 2x2 cm pieces and blend the FSF in a kitchen mixer at full speed with approximately 400 ml demi water (2 minutes or more). Transfer the content into a glass beaker completing the volume to 500 mL with demi water;
3) **Water**:
   Stir the pulp and water mixture at 50 ˚C for 2 hours on a hot plate with a temperature sensor. The final mixture should have a light yellow-brownish aspect;
4) Simultaneously sieve and wash the mixture with medium pressure demi water using a 45 µm mesh sieve (ideally in combination with another sieve of equal/slightly higher mesh size underneath to check for visible fibre leaks). The washing procedure should be carried out thoroughly until obtaining a clear filtrate;

5) Collect the retained material on a sieve(s) with a spoon and gently rising the sieve with demi water. Transfer it into a glass container for the next step;

**If more or fewer wastewater solids are added, the following steps of the protocol should be adjusted to keep the same weight per volume ratio of solids and chemical reagents.*

**Removal of alkali-soluble compounds**

6) **Alkaline I**:
   In the glass container mentioned above, prepare a 1 L solution of 2% NaOH. Possibly, add NaOH pearls or a more concentrated stock solution and complete the volume with demi water;
7) Heat to 80 ˚C while stirring for 2 hours in a hot plate with a temperature sensor. To keep constant the concentration of NaOH during alkaline steps, the recipient should be covered with aluminium foil. The final mixture should have a red-brownish aspect;
8) Simultaneously sieve and wash the mixture with medium pressure demi water using a 45 µm mesh sieve (ideally in combination with another sieve or equal/slightly higher mesh size underneath to check for visible fibre leaks). The washing procedure should be carried out thoroughly until obtaining a clear, pH-neutral filtrate;
9) **Alkaline II**:
   Repeat steps 6 to 8 once. The final mixture should have a much-diluted red-brownish aspect;
10) If coarse particles are still present at this point, the retained solids are blended again for 2 minutes in 400 mL demi water.
11) Collect the retained material on sieve(s) with a spoon and gently rising the sieve with demi-water and transfer it into a 1 L glass bottle;

**Bleaching**

12) Bleach the obtained pulp by preparing a bleaching solution in the glass bottle (complete to 1 L). First, prepare an acetate buffer of pH 4.6 by mixing 13.5 g NaOH (dissolved in the existing water) with 37.5 ml glacial acetic acid and diluting it to 500 mL. Secondly, prepare a 500 mL sodium chlorite solution (1.7% wt. $NaClO_2$). The bleaching solution is composed of equal parts (1:1 volume: volume) of acetate buffer and sodium chlorite stock solutions.
13) Stir the mixture on a hot plate at 70 °C for 1 hour (do not cover with aluminium foil or it will degrade), transfer the closed bottle to a 60 °C oven, and let it react for at least 6 hours in total (often overnight but never longer than 24h!). The final mixture should have a deep light yellow aspect;
14) Simultaneously sieve and wash the mixture with medium pressure demi water using a 45 µm mesh sieve (ideally in combination with another sieve or equal/slightly higher mesh size underneath to check for visible fibre leaks). The washing procedure should be carried out thoroughly until obtaining a clear, pH-neutral filtrate. Work under ventilation to avoid inhaling bleaching by-products. The final pulp should be completely white with some minimum inert debris from the source**;

**If the resulting pulp after washing is not snowy-white in aspect, the bleaching steps 12 to 14 are repeated until this is achieved. Moreover, if even after two bleaching extractions the sample still presents colour (often light red-brownish), the alkaline extraction might not have been sufficient, and the extraction should be re-started from this point.

**Drying**

15) Collect and dry the resulting FSF cellulosic pulp in aluminium containers at 60 °C and measure the dry weight (constant). The cellulose mass is obtained by subtracting the final dry weight by the weight of the aluminium dish. The initial cellulose content can be calculated in g cellulose/g FSF solids.
16) If desired, the obtained pulp can be further analysed to verify the efficiency of extraction with microscopy (for visualising the presence of remaining impurities) and/or with the method of Van Soest (gives cellulose, hemicellulose and lignin contents - section 3.2.4).

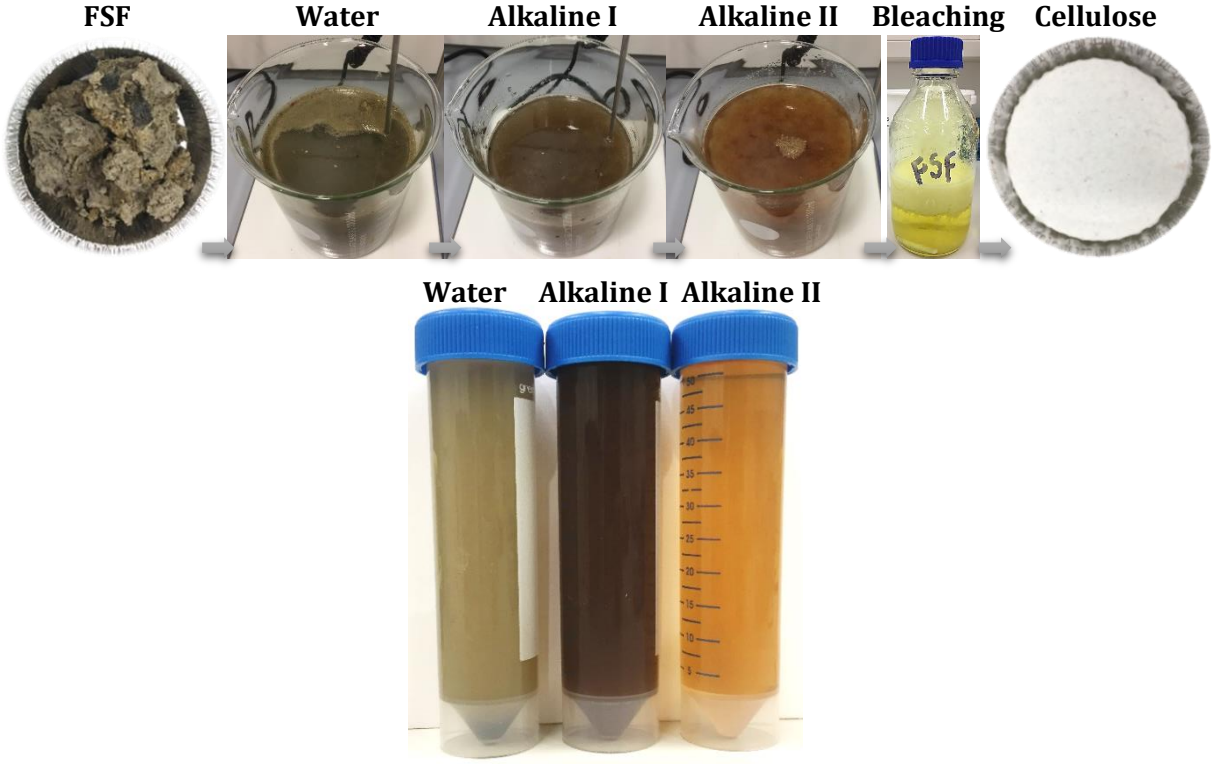


**Figure 1. Upper image: FSF extraction procedures with the initial dry matter being successively transformed for the recovery of a cellulosic pulp. Bottom image: FSF filtrates after the procedure with demi water, and first and second alkaline steps with 2% NaOH. Pictures of only the residues on sieve after each step can be found in section 4.2 of this thesis.**

## Protocol - Nereda® Excess Sludge

The NES end-reaction mixtures after each protocol step can be visualised in Figure 2, Appendix II. The filtrates of NES are relatively similar to the ones obtained during alkaline and bleaching of FSF, therefore, not shown in this report. Differently to FSF, the extraction protocol for NES and other waste sludges is performed directly on the suspended solids collected from the STPs. Thus, before the assay, the TSS of suspensions should be determined. Furthermore, due to intrinsic characteristics of NES, the initial water-soluble extraction step is not feasible (clogging).

**Removal of alkali-soluble compounds**

1) Start with a known volume of homogeneous NES in a closable glass bottle, approximately 2-6 L (considering a TSS of 1.5 $gL^{-1}$, this is the equivalent to 3-9 g starting material)*;

2) **Alkaline I**:
   Add and dissolve NaOH to obtain a final concentration of 2% (10g for 2 L initial NES). This mixture is heated to 80 °C for 1 hour on a stirring hot plate and later transferred to a 60 °C oven. The reaction is allowed to occur for around one day, and the final mixture should have a dark-brownish aspect;
3) Simultaneously sieve and wash the mixture with medium pressure demi water using a 45 µm mesh sieve (ideally in combination with another sieve of equal/slightly higher mesh size underneath to check for visible fibre leaks). Gradually pour and wash the mixture on the sieve to eliminate the viscous filtrate and avoid clogging. The washing procedure should be carried out thoroughly until obtaining a clear, pH-neutral filtrate;
4) Collect the retained material on sieve(s) with a spoon and gently rising the sieve with demi water;
5) Transfer the material to a kitchen mixer and blend at full speed with approximately 400 ml demi water (2 minutes or more). Transfer the content back into the initial glass bottle;
6) **Alkaline II**:
   In the glass bottle containing the pulp, prepare a 2 L solution of 2% NaOH again. Possibly, add NaOH pearls or a more concentrated stock solution and complete the volume with demi water;
7) Heat while stirring at 80 °C for 2 hours in a hot plate with a temperature sensor. For keeping the concentration of NaOH constant during alkaline steps, the bottles should be covered with aluminium foil. The final mixture should have a red-brownish aspect;
8) Simultaneously sieve and wash the mixture with medium pressure demi water using a 45 µm mesh sieve (ideally in combination with another sieve or equal/slightly higher mesh size underneath to check for visible fibre leaks). The washing procedure should be carried out thoroughly until obtaining a clear, pH-neutral filtrate;
9) **Alkaline III**:
   Repeat steps 5 to 7 once. The final mixture should have a very much diluted red-brownish aspect;
10) If coarse particles are still present at this point, the retained solids are blended for 2' in 400 mL demi water.
11) Collect the retained material on sieve(s) with a spoon and gently rising the sieve with demi-water and transfer it back into the initial glass bottle;

**If more or fewer wastewater solids are added, the following steps of the protocol should be adjusted to keep the same weight per volume ratio of solids and chemical reagents.*

**Bleaching**

For waste sludge, it is crucial that the bleaching step be only initiated after obtaining an already fairly pigment-free pulp (see Figure 9 at section 4.2 for reference).

12) Bleach the obtained pulp by preparing a bleaching solution in the glass bottle (complete to 1 L). First, prepare an acetate buffer of pH 4.6 by mixing 13.5 g NaOH (dissolved in the existing water) with 37.5 ml glacial acetic acid and diluting it to 500 mL. Secondly, prepare a 500 mL sodium chlorite solution (1.7% wt. $NaClO_2$). The bleaching solution is composed of equal parts (1:1 volume: volume) of acetate buffer and sodium chlorite stock solutions.
13) Stir the mixture on a hot plate at 70 °C for 1 hour (do not cover with aluminium foil or it will degrade), transfer the bottle to a 60 °C oven, and let it react for at least 6 hours in total (often overnight but never longer than 24h!). The final mixture should have a deep light yellow aspect;

14) Simultaneously sieve and wash the mixture with medium pressure demi water using a 45 µm mesh sieve (ideally in combination with another sieve or equal/slightly higher mesh size underneath to check for visible fibre leaks). The washing procedure should be carried out thoroughly until obtaining a clear, pH-neutral filtrate. Work under ventilation to avoid inhaling bleaching by-products. The final pulp should be completely white with some minimum inert debris from the source**;

**If the resulting pulp after washing is not snowy-white in aspect, the bleaching steps 12 to 14 are repeated until this is achieved. Moreover, if even after two bleaching extractions the sample still presents colour (often light red-brownish), the alkaline extraction might not have been sufficient, and the extraction should be re-started from this point.

**Drying**

15) Dry the resulting NES cellulosic pulp in aluminium containers at 60 °C and measure the dry weight (constant). The cellulose mass is obtained by subtracting the final dry weight by the weight of the aluminium dish. The initial cellulose content can be calculated in g cellulose/L or g NES solids (from the TSS value).
16) If desired, the obtained pulp can be further analysed to verify the efficiency of extraction with microscopy (for visualising the presence of remaining impurities) and/or with the method of Van Soest (gives cellulose, hemicellulose and lignin contents - section 3.2.4).

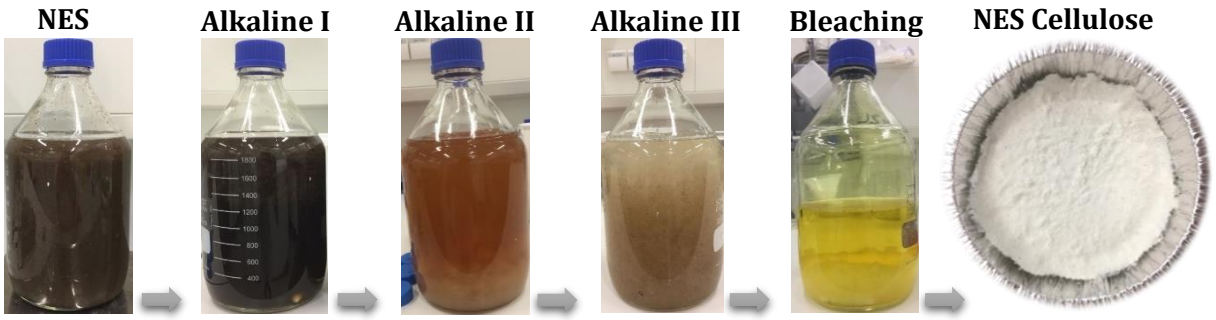


**Figure 2. NES extraction procedures with initial solids suspension being successively transformed for the recovery of a cellulosic pulp. Images of only the residues after each step can be found in section 4.2 of this thesis.**

**NOTE**

This methodology is not applicable if the cellulose content of the sample is too low compared to other rather inert solids – regarding the above-described water, alkaline and slightly acidic bleaching extractions - that are sometimes present (inert solids or impurities >> cellulose fibres). However, that is easily detectable after performing a few extractions or by analysing the resultant pulp by the Van Soest method (gives cellulose, hemicellulose and lignin content in fibrous samples, section 3.2.4 of this thesis).

**Table 1. Auxiliary protocol table for the determination of cellulose in wastewater solids.**

| Sample | Initial amount (g or L) | Blending (L) | Water (L) | Alkaline I (L) | Blending (L) | Alkaline II (L) | Alkaline III (L) | Bleaching I (L) | Drying Empty dish (g) | Dried Full dish (g) | Cellulose (g) |
|---|---|---|---|---|---|---|---|---|---|---|---|
| **FSF** | 10 g | 0.4 | 0.5 | 1 | - | 1 | - | 1 | | | |
| Temperature | | RT | 50 °C | 80 °C | | 80 °C | | 60-70°C | 60 °C | | |
| Time | | 2' | 2 h | 2 h | | 2 h | | 12 h | 1 day | | |
| **NES** | 2 L (TSS) | - | - | 2 | 0.4 | 2 | 2 | 1 | | | |
| Temperature | | | | 60 °C | RT | 80 °C | 80 °C | 60-70°C | 60 °C | | |
| Time | | | | 2 h | 2' | 2 h | 2 h | 12 h | 1 day | | |
| | | | | | | | | | | | |
| Temperature | | | | | | | | | | | |
| Time | | | | | | | | | | | |

# APPENDIX III – CNCS ISOLATION PROTOCOL

## Isolation of CNCs from Wastewater Solids (Toilet Paper)

Cellulose nanocrystals are obtained via controlled acid hydrolysis of cellulose, in which mainly amorphous regions of fibres get attacked leaving crystalline regions intact. The principle consists in promoting the hydrolytic cleavage of glycosidic bonds and thus releasing individual crystallites (Lu and Hsieh, 2012). The main steps of the isolation are dependent on the cellulosic pulp source but can mainly consist of controlled acid hydrolysis followed by centrifugation, filtration, dialysis, neutralisation and ultrasonication (Figure 6, section 3.3). The acid concentration, cellulose to acid ratio (g/mL), temperature and time of reaction are crucial to the isolation and had to be adapted to the studied cellulose sources: toilet paper (RTP) and wastewater-extracted pulps (FSF, NES). On the other hand, the isolation procedure of CNCs from microcrystalline cellulose (MCC) is well-known and can be performed as described by Bondeson et al. (2006). The following detailed protocol describes the standard procedures used for CNCs isolation from toilet paper or wastewater-derived pulps. In the section after, the main differences and optimised aspects for the different cellulose sources are pointed out.

### Materials and Equipment

a) Milling device with 0.5 mm mesh
b) Reagent grade chemicals: sulphuric acid ($H_2SO_4$, 96.5 wt. %), sodium hydroxide (NaOH)
c) Glass mercury thermometer
d) Hot plate magnetic stirrer
e) Timer
f) Centrifuge for Falcon tubes or large volumes
g) Dialysis tubing cellulose membrane (SnakeSkin™, Thermo Fisher Scientific Inc., 3.5KDa MWCO)
h) Ultrasonication equipment (microtip probe)

Optional: Cross polarisation setup (polarizer films and a source of light).

### CNCs isolation – Standard Protocol

**1.** Cut dried extracted cellulose (Appendix II) in 2x2 cm pieces and mill until passing through a 0.5 mm mesh to obtain fine cellulose fibres with uniform sizes.
**2.** Pre-heat water (200 mL in 1 L beaker) in a hot plate magnetic stirrer to 45 °C for a water-bath.
**3.** In a separate 300 mL beaker, add the desired amount of cellulosic pulp (the following numbers are with respect to 1 g). Under a fume hood, on ice, very slowly add cold 60% or 64% $H_2SO_4$ solution (around 20-50 mL) to the milled pulp while stirring with a glass rod so that no agglomerates are visible. During this step, carefully stir the reaction mixture and monitor the temperature with a mercury thermometer so that the temperature of reaction **never exceeds 20 °C**. The ratio of cellulose to acid varies per source, but as a rule, the volume of fibres have to be just submerged in acid.
**4.** Place the beaker with the reaction mixture in the warm water bath and stir vigorously for around 45' (time of reaction ranged from 30'-120' depending on source). It usually takes 5' for the solution to reach the water-bath temperature. The timer is started after the

solution reaches this temperature, which is constantly monitored with a glass thermometer.

5. Immediately following the hydrolysis, dilute the suspension 10-fold with cold water (4 °C) to stop the hydrolysis reaction (resulting in a maximum 6% acid mixture).
6. Transfer the quenched mixture into Falcon tubes (50 mL) and start washing and centrifuging cycles of 20 min at 4400 rpm 4 °C to remove the acid excess and some of the produced salts, sugars, polymers. Centrifuge as many times as necessary (usually 3X), collecting only the gel-like pellet and filling the volume with demi water until turbid supernatant.
7. Re-suspend the pellet and filtrate it with glass fibre filters under vacuum. This is a rather difficult step since the pellet forms a gel hard to filtrate at concentrated amounts. However, it is a necessary procedure due to residual larger non-hydrolysed fibres and impurities present in wastewater-derived pulps.
8. Dialyse the collected filtrate against Milli-Q water in a cellulose membrane until constant pH is obtained (4 days minimum). This step is crucial as it should adjust the pH; and remove most non-reactive sulphate groups, salts and soluble sugars. Monitor the pH of dialysis water to check process evolution. The final pH was usually around 4.
9. Due to the resultant acidic pH, carry out mild neutralisation with NaOH 0.1 M (a few drops) until pH 6-7 is reached.
10. Ultrasonicate the suspension for 5' on ice (pulse mode, 40% duty cycle, output microtip limit 3).
11. Verify the presence of CNCs in the suspension with cross polarisation. Place an aliquot in a glass phial (2 mL) and move the phial between cross polarisation films with a background source of light. If shear birefringent behaviour is observed, CNCs are present to a significant level. Other high-skilled techniques also can be readily used to verify the isolation of CNCs such as atomic force microscopy, field emission scanning electron microscopy and transmission electron microscopy.
12. Collect an aliquot of the resultant suspension (around 40 mL, write down the volume) for gravimetrically determining the CNCs concentration (60°C for 24 h in an oven or freeze-drying).
13. Calculate the yield of CNCs with the result from step 12 based on the initial amounts of pulp hydrolysed.
14. Store suspension at 4 °C until further characterization. Optional: for long time storage, other protocols also indicate chloroform to preserve the CNCs.

## Protocol Differences – Cellulose Sources

### Microcrystalline Cellulose (MCC)

Conditions used are similar to what is suggested in Bondeson et al. (2006). The MCC transformations to final CNCs hydrolysis suspension can be visualised in Figure 1, Appendix III.

Cellulose to acid ratio: 1 g: 20 mL.

Acid addition: Demi water is first added to MCC (44.3 mL). After, pure 96.5% sulphuric acid (55.7 mL) is added drop wise to the mixture in a controlled temperature environment (<50°C) in ice under vigorous mixing.

Acid concentration: 64%.

Reaction Temperature: 45 °C – 50 °C.

Time of reaction: varied from 105'-120' (deep yellow colour is developed from 70' onwards). Timer is started from the moment the reaction mixture reached 45 °C. The whole reaction mixture becomes transparent after hydrolysis.

Centrifugation and washing: 3 times of 10' at 10000 rpm 4 °C or until turbid supernatant.

Filtration: No filtration is necessary. A fourth mild centrifugation step can be used instead, collecting only the supernatant. Therefore, the resulting extraction yield is a minimum value.

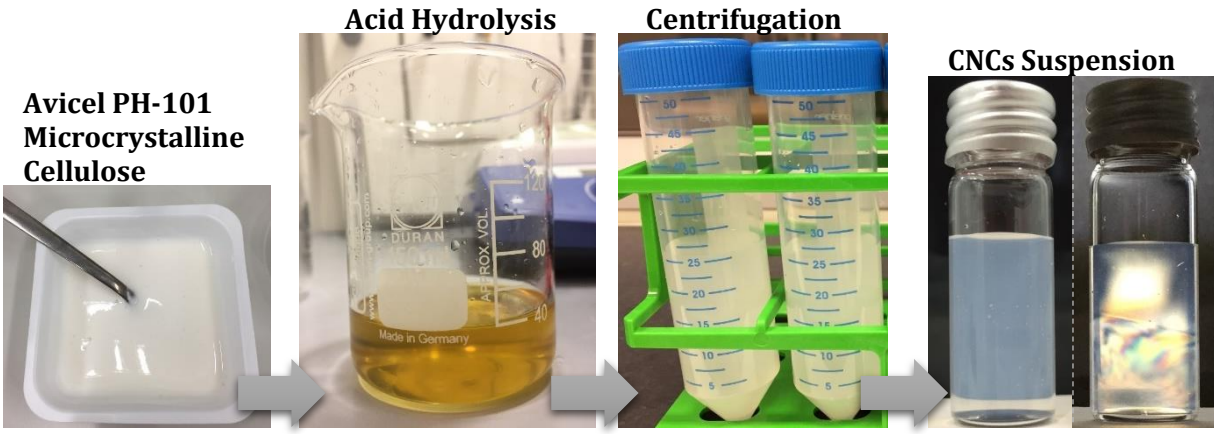


**Figure 1. MCC acid hydrolysis into CNCs and after purification steps. The final image shows the resultant CNCs suspension under normal illumination (left) and between cross polarisation (right).**

**Recycled Toilet Paper (RTP)**

The RTP transformations to final CNCs hydrolysis suspension can be visualised in Figure 2, Appendix III.

Cellulose to acid ratio: 1 g: 45 mL

Acid addition: Demi water is first added to RTP (22.2 mL). After, pure 96.5% sulphuric acid (22.8 mL) is slowly added to the mixture in a controlled temperature environment (<20°C) in ice, stirring occurs with the help of a glass rod until no agglomeration is visible. Because of the temperature limitation, acid addition can take several minutes.

Acid concentration: 60%.

Reaction Temperature: 45 °C – 50 °C.

Time of reaction: varied from 60'-120' (deep dark-yellow colour is developed very fast before 1h, after 2h the suspension becomes completely dark, indicating over-hydrolysis). Timer was started from the moment the reaction mixture reached 45 °C.

Centrifugation and washing: 4 times of 20' at 4400 rpm 4 °C or until turbid supernatant. If after centrifugation and washing steps the suspension is too diluted, small amounts of NaOH can be added to partially precipitate the CNCs with time and neutralize the mixture. The open container can be placed in a 60 °C oven for evaporation and thickening of the suspension. The resultant

precipitate is collected and further dialysed. After this step, the precipitate should become more whitish (Figure 2).

Filtration: Several filtration steps with a 90 μm sieve and glass fibre vacuum filtration are performed. Therefore, the resulting extraction yield is a minimum value.

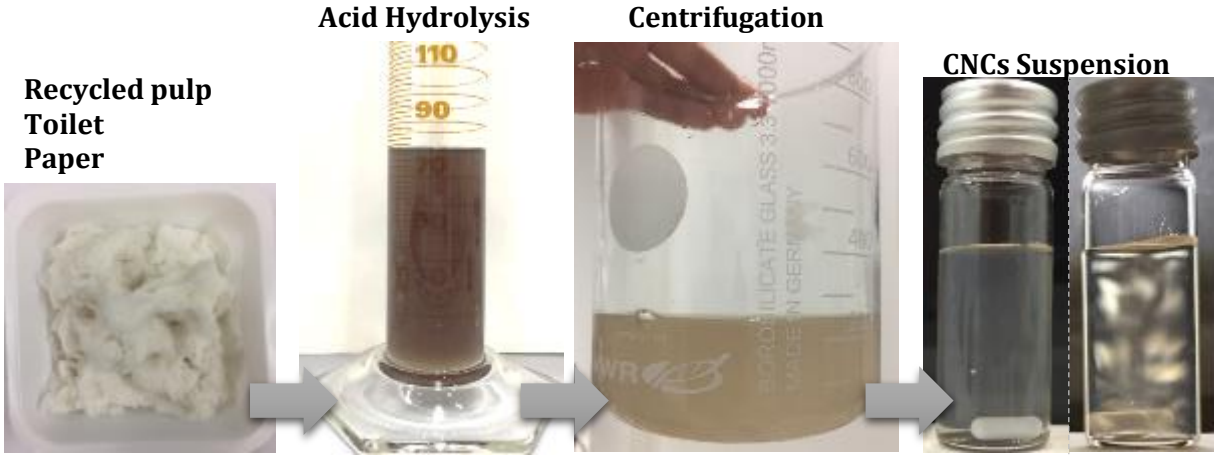


**Figure 2. RTP acid hydrolysis into CNCs and after purification steps. The final image shows the resultant CNCs suspension under normal illumination (left) and between cross polarisation (right).**

**Fine Sieve Fraction pulp (FSF pulp)**

The FSF pulp transformations to final CNCs hydrolysis suspension can be visualised in Figure 3, Appendix III.

Cellulose to acid ratio: 1 g: 50 mL.

Acid addition: Cold acid is slowly added to FSF pulp in a controlled temperature environment (<20°C) in ice, stirring occurs with the help of a glass rod until no agglomeration is visible. With this different acid addition approach, the fast digestion of fibres with formation of an unwanted dark liqueur is limited.

Acid concentration: 60%.

Reaction Temperature: 50 °C.

Time of reaction: from 45'-60' (deep brown-yellowish colour with dark dots corresponding to FSF initial impurities is developed from 40' onwards). Timer is started from the moment the reaction mixture reached 45 °C.

Centrifugation and washing: 3 times of 20' at 4400 rpm 4 °C or until turbid supernatant.

Filtration: Several filtration steps glass fibre vacuum filtration are performed. Therefore, the resulting extraction yield is a minimum value.

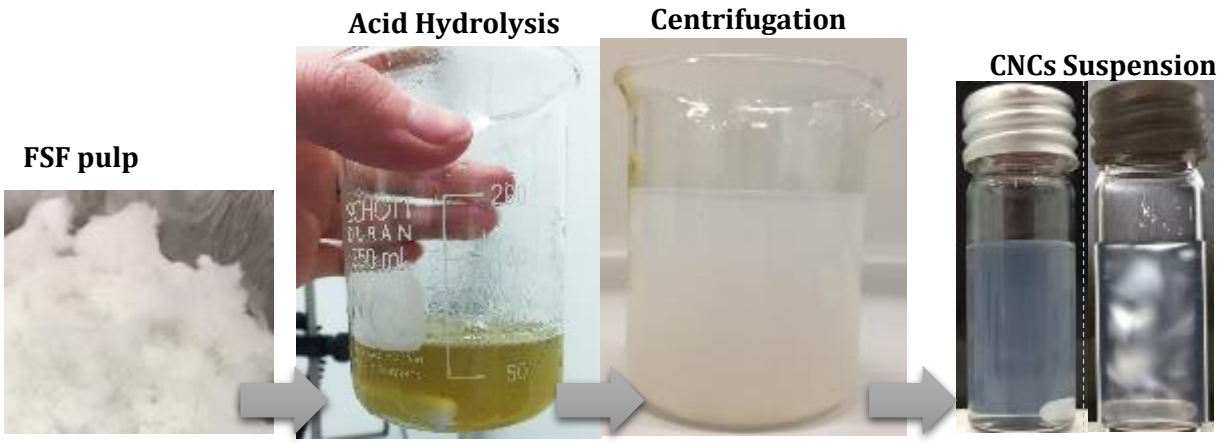


**Figure 3. FSF pulp acid hydrolysis into CNCs and after purification steps. The final image shows the resultant CNCs suspension under normal illumination (left) and between cross polarisation (right).**

**Nereda® Excess Sludge pulp (NES pulp)**

The NES pulp transformations to final CNCs hydrolysis suspension can be visualised in Figure 4, Appendix III.

Cellulose to acid ratio: 1 g: 30 mL.

Acid addition: Cold acid is slowly added to NES pulp in a controlled temperature environment (<20°C) in ice, stirring occurs with the help of a glass rod until no agglomeration is visible.

Acid concentration: 60%.

Reaction Temperature: 45 °C.

Time of reaction: 45' – 50' (deep brown-yellowish colour is developed from 40' onwards). Timer was started from the moment the reaction mixture reached 45 °C.

Centrifugation and washing: 3 times of 20' at 4400 rpm 4 °C

Filtration: Many vacuum filtration steps with glass fibre filters were performed. Therefore, the resulting extraction yield is a minimum value.

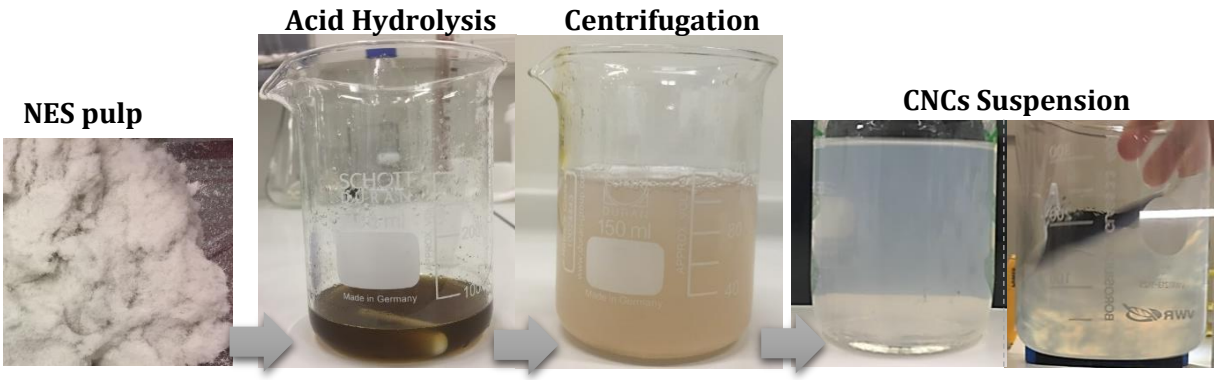


**Figure 4. NES pulp acid hydrolysis into CNCs and after purification steps. The final image shows the resultant CNCs suspension under normal illumination (left) and between cross polarisation (right).**

# APPENDIX IV – ALGINATE-SHELL MODEL

## Alginate-Shell effect:

## Decreased critical volume fraction for CNCs' Nematic phase

Let us consider a system of hard, needle-like nanocellulose fibres with diameter D and length L, where **L>D**. The Onsager theory for polydisperse rigid rod-like particles describes the critical volume fraction for coexisting nematic(anisotropic)-isotropic phases ($\Phi_{NI}$) as (Onsager, 1949; Wang and Zhou, 2004):

$$\Phi_{NI} = 4\,\frac{D}{L} = \frac{N_p\,V_p}{V} \qquad (1)$$

where N*p* is the total number of particles in a solution of volume V*p*.

If the same is assumed for alginate-covered rods with larger dimensions C (addition of thickness Δ, Figure 1, Appendix IV):

$$\Phi_{NI,C} = 4\,\frac{D+\Delta}{L+\Delta}\ \left(\approx\ 4\,\frac{D+\Delta}{L}\right) = \frac{N_{p,\Delta}\,V_{p,\Delta}}{V} \qquad (2)$$

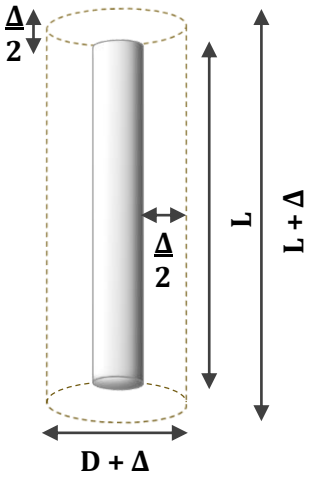


**Figure 1. Scheme of nanocellulose fiber decorated with an alginate-shell of thickness Δ.**

The required overall volume fraction $\Phi_{NI,\,C}$ increases due to loss of aspect ratio:

$$\frac{\Phi_{NI,C}}{\Phi_{NI}} = \frac{D+\Delta}{D}\,\frac{L}{L+\Delta}\ \left(\approx\ \frac{D+\Delta}{D}\right) = \frac{N_{p,\Delta}\,V_{p,\Delta}}{N_p\,V_p} = \frac{N_{p,\Delta}\,(L+\Delta)\,(D+\Delta)^2}{N_p\,L\,D^2} \approx \frac{N_{p,\Delta}\,(D+\Delta)^2}{N_p\,D^2} \qquad (3)$$

$$\rightarrow\ \frac{N_{p,\Delta}}{N_p} = \frac{(D+\Delta)^2 D^2}{D\,(D+\Delta)^2} = \frac{D}{D+\Delta}\ \text{(Particle matter is reduced!)}$$

To calculate the number of required particles:

$$\frac{N_{p,\Delta}}{N_p} = \frac{D+\Delta}{D}\,\frac{L}{L+\Delta}\,\frac{L\,D^2}{(L+\Delta)\,(D+\Delta)^2} = \frac{D}{D+\Delta}\,\frac{L^2}{(L+\Delta)^2} \qquad (4)$$

From the modified equation 3, the number of particles is reduced. The volume grows faster than the loss of aspect ratio (volume fraction function is quadratic while aspect ratio is linear). Thus, the critical CNCs concentration to form N phase is reduced in the presence of alginate. The relationship between critical volume fraction for a nematic-isotropic transition and alginate concentration ([Alg]) is:

$$\Phi_{NI\,([alg])} = \Phi_{NI}\,\frac{1}{1+\alpha[Alg]}\,\left(\frac{1}{1+\beta[Alg]}\right)^2 \qquad (6)$$

where α, β, with α>>β, are related to aspect ratio and alginate-shell layer thickness.

The model is currently under development by prof. Stephen Picken. If it doesn't work, it was developed by Jure Zlopasa. If it does, it will be claimed by prof. Mark van Loosdrecht.

# Confidentiality (Checkboxes)

Please, after reading this thesis, check for confidentiality issues regarding:

☐ **TU Delft IP**

☐ **CelluForce Information**

☐ **RHDHV Information**

☐ **Waternet Information**